FERNANDO SARAIVA ROCHA DA SILVA

# INTENSIFICATION OF ALKALINE WATER ELECTROLYSIS USING FORCED ELECTROLYTE FLOW AND PULSED VOLTAGE

Santos
2019

FERNANDO SARAIVA ROCHA DA SILVA

# INTENSIFICATION OF ALKALINE WATER ELECTROLYSIS USING FORCED ELECTROLYTE FLOW AND PULSED VOLTAGE

Undergratuate thesis presented to the Polytechnic School of the University of São Paulo for obtaining the degree of Petroleum Engineer.

Santos
2019

FERNANDO SARAIVA ROCHA DA SILVA

# INTENSIFICATION OF ALKALINE WATER ELECTROLYSIS USING FORCED ELECTROLYTE FLOW AND PULSED VOLTAGE

Undergratuate thesis presented to the Polytechnic School of the University of São Paulo for obtaining the degree of Petroleum Engineer.

Supervisor:
Joris Proost

Head of the Defense Committee:
Silvia Maria Leite Agostinho

Santos
2019

Catalogação-na-publicação

Rocha, Fernando
Intensification of alkaline water electrolysis using forced electrolyte flow and pulsed voltage / F. Rocha -- São Paulo, 2019.
97 p.

Trabalho de Formatura - Escola Politécnica da Universidade de São Paulo. Departamento de Engenharia de Minas e de Petróleo.

1.pulsed potential 2.water electrolysis 3.hydrogen production I.Universidade de São Paulo. Escola Politécnica. Departamento de Engenharia de Minas e de Petróleo II.t.

Dedicated to the memory of my aunt, Cristina Terribas, who inspired me to be who I am. Her dreams are still alive in me like an eternal flame. Amor e luta, sempre!

# ACKNOWLEDGMENTS

I would first like to thank my thesis advisor Prof. Joris Proost who guided me whenever I had a question about my research or writing and oriented me in the right direction. He gave me the technical support I needed and his comments were extremely important in the construction of this thesis.

I would also like to thank Quentin who was involved from the outset of the design of the experiments. He introduced me in detail to the laboratory and techniques which were at my disposal. Furthermore, without his active participation, the validation of the survey could not have been successfully conducted. Lastly, I am grateful for his attentive reading and invaluable comments on this thesis. Thank you.

Besides, I would like to express my gratitude to Prof. Silvia for all the long discussions where she taught me so much and for the careful review of this work. She is an inspiration for me, thank you for that.

Furthermore, my thanks to Prof. Tomi, who believed in me since my first year at the University. With his active support, my academic journey became richer and I got many experiences that allowed me to do what I did.

Moreover, my deep gratitude to my family for their continuous support during my years living on the other side of the Atlantic, in special to my father, Alex, who supported me in all the decisions I made and taught me to face the adversities of life and to fight against oppression and tyrannies; to my mother, Cecília, which gave her life on behalf of her children and motivated me to have thirst for knowledge and for all the Sundays she called me and gave me love; and last but not the least, to my sister, Marina, which was for so long the target of my judo's coup and is bonded with me not only by blood, but by heart and soul, being a close friend and sharing with me the same old dreams. This journey would not be possible without them and for that, I will always be grateful.

Finally, my thanks to Paloma, my partner in life who made countless efforts to assist me while I was far away from my home country. The Science Fair I met her changed forever my life. Her sensibility and indignation are an example for me and life is much better with her.

Fernando Saraiva Rocha da Silva

*"Urge preveni-los do muito que se poderia fazer, com apoio no saber científico, e do descalabro e pequenez do que se está fazendo"*

-- Darcy Ribeiro

# ABSTRACT

Hydrogen is considered to be the fuel of the future. It is the fuel with the highest specific enthalpy and produces only water and heat when it is burned. There are different ways to produce hydrogen, but the most sustainable is by water electrolysis. In this case, electricity is used to split water molecules, producing hydrogen and oxygen. The big issue of this production method is the cost. To reduce the cost, the process needs to be improved, increasing efficiency and production rate. Some studies indicate that, if instead of applying a constant potential between the electrodes (DC electrolysis) a pulsed potential is used, electrolysis is improved.

The study presented here investigated the effects of a pulsed voltage in alkaline water electrolysis with Nickel electrodes. The electrolyzer was operated with a solution of 1M of KOH, at room temperature and atmospheric pressure. The pulses had a square shape and widths of 100ut, 10ut, and 1ut, where ut means unit of time. Voltage varied from a base value of 1.23V to a peak value between 1.33V-2.23V. Two main parameters were investigated: hydrogen production rate and energy efficiency. The former was measured using a graduated cylinder, which stored the produced hydrogen, while the latter is the ratio between the recoverable energy by hydrogen burning and the consumed energy to produce it. During a pulse, there is the on-time defined as the time at which voltage is at peak value and the off-time, defined as the time when the voltage returns to the baseline value of 1.23V. It was observed that when the pulses were applied, the current at on-time was higher than the current of the DC electrolysis. During off-time, a change in polarization was observed, which indicates a reversible reaction going backwards or the discharge of the electrical double layer. The introduction of pulses has decreased the hydrogen production rate and efficiency. The lower the pulse width, the lower the production rate and efficiency. The effect of electrolyte flow was also observed. An increase in flow has increased mass transfer, promoting an increase in current, production rate, and efficiency. Finally, a mathematical model was proposed to predict pulse behavior.

**Keywords** – pulsed potential, water electrolysis, hydrogen production.

# RESUMO

O gás hidrogênio é considerado o combustível do futuro. É o combustível com maior entalpia específica e produz apenas água e calor quando é queimado. Existem diferentes maneiras de produzi-lo, mas a mais sustentável é através da eletrólise da água. Nesse caso, a eletricidade é usada para dividir moléculas de água, produzindo hidrogênio e oxigênio. O grande problema desse método de produção é o custo. A fim de reduzi-lo, o processo precisa ser aprimorado, aumentando a eficiência e a taxa de produção. Alguns estudos indicam que se em vez de aplicar um potencial constante entre os eletrodos (eletrólise DC), for usado um potencial pulsado, a eletrólise pode ser melhorada.

O estudo aqui apresentado investigou os efeitos de pulsos de tensão na eletrólise alcalina da água. Os eletrodos eram de Níquel puro e a célula foi operada com uma solução de KOH 1M, à temperatura ambiente e pressão atmosférica. Os pulsos tinham uma forma quadrada e larguras de 100 ut, 10 ut e 1 ut, onde ut significa unidade de tempo. A tensão variou de um valor base de 1,23 V a um valor de pico entre 1,33 V - 2,23 V. Dois parâmetros principais foram investigados: taxa de produção de hidrogênio e eficiência energética. O primeiro foi medido usando um cilindro graduado, que armazenava o hidrogênio produzido, enquanto o último é a razão entre a energia recuperável pela queima do hidrogênio e a energia consumida para produzi-lo. Durante um pulso, há o tempo on definido como o tempo em que a tensão atinge o valor de pico e o tempo off, definido como o tempo em que a tensão retorna ao valor de base de 1,23 V. Observou-se que, quando os pulsos foram aplicados, a corrente no tempo on era maior que a corrente da eletrólise DC. Durante o período off, foi observada uma mudança na polarização, que indica uma reação reversível retrocedendo ou a descarga da dupla camada elétrica. A introdução de pulsos diminuiu tanto a taxa quanto a eficiência da produção de hidrogênio. Quanto menor a largura do pulso, menor a taxa e a eficiência da produção. O efeito do fluxo de eletrólitos também foi observado. Um aumento no fluxo aumentou a transferência de massa, promovendo um aumento na corrente, na taxa de produção e na eficiência. Finalmente, um modelo matemático foi proposto para prever o comportamento do pulso.

**Palavras-chave** – pulsos de potencial, eletrólise da água, produção de hidrogênio.

# LIST OF FIGURES

# CONTENTS

# 1 INTRODUCTION

Hydrogen is the most abundant element in the universe, representing 92% of the atoms in the cosmos. It is present in many compounds such as water, living matter, fossil fuels, etc. By contrast, hydrogen gas, $H_2$, is not abundant on earth, since the gravitational field of our planet is not high enough to hold such a light substance (LEE, 2008). Most of the hydrogen atoms on earth are presented as water molecules (ATKINS; JONES, 2009). As a result, hydrogen must be produced by several chemical reactions.

Half of the hydrogen gas produced worldwide is used for the manufacture of ammonium from the reaction with nitrogen, in the so called Haber-Bosch process: $N_2 + 3H_2 \rightleftharpoons 2NH_3$. The other half is mainly used for: a) the hydrogenation of unsaturated organic compounds (eg. hardening of fats and oils); b) for the methanol production: $CO + 2H_2 \rightarrow CH_3OH$; c) and for welding and cutting of metal by hydrogen burning: $2H_2 + O_2 \rightarrow 2H_2O$ (LEE, 2008) (ATKINS; JONES, 2009).

Besides all those applications, hydrogen can also be used as an energy carrier. Fossil fuels are being depleted, they undergo important price variation and they cause serious environmental impacts (WILBERFORCE et al., 2018). By contrast, hydrogen is widely considered to be the fuel of our future. It has the highest specific enthalpy of any known fuel: 142KJ.$g^{-1}$, against 55KJ.$g^{-1}$ for methane, 48KJ.$g^{-1}$ for octane and 32.8KJ.$g^{-1}$ for coke (ATKINS; JONES, 2009). Liquid hydrogen is already used as fuels in space rockets and shuttles. Car engines have been modified to run on hydrogen. Unlike burning fossil fuels, burning hydrogen does not produce $SO_2$ nor $NOx$ nor $CO_2$, responsible for acid rain and the latter, for global warming. Burning hydrogen produces only water and liberates a significant amount of energy (LEE, 2008). In the future, hydrogen can replace natural gas in existing facilities such as gas turbines and engines for power generation. In addition, it can be transported in the same pipelines that at present transport natural gas (BREEZE, 2017).

Nowadays, hydrogen is mainly produced by steam reforming, where methane reacts with water to produce hydrogen and carbon dioxide: $CH_4 + 2H_2O \rightarrow 4H_2 + CO_2$. This is an endothermic reaction, so, generally uses fossil fuels as a source of heat. The second most used process is the partial oxidation of hydrocarbons, where hydrogen is produced as a by-product from oil refining. In this case, hydrocarbons (such as heavy oil or petroleum refinery residual oil) reacts with oxygen and steam: $2C_nH_m + H_2O + 23/2O_2 \rightarrow nCO + nCO_2 + (n+1)H_2$. A third method is the reaction of steam with coke: $C + H_2O \rightarrow 2H_2 + CO_2$. All of these methods present a severe disadvantage: the production of significant amounts of $CO_2$. Hopefully, there is a clean method that produces very pure hydrogen (99.99% pure) without emission of greenhouse gases: water electrolysis. In this method, water is split into hydrogen and oxygen by the application of an electrical potential difference between two metals, called electrodes, immersed in an electrolytic solution. The overall reaction is given by: $H_2O \rightarrow 2H_2 + O_2$ (LEE, 2008) (KOTHARI; BUDDHI; SAWHNEY, 2008). Water electrolysis was discovered in 1800 by Nicholson and Carlisle, in the context of the first industrial revolution. A hundred years later, 400 industrial electrolyzers were operating (KREUTER; HOFMANN, 1998). Nowadays, commercial low-temperature electrolyzers have system efficiencies of 56—73% (MONK; WATSON, 2016). In 2003, the worldwide hydrogen production was estimated at 500 $Nm^3$ (normal cubic meters) per year, 96% coming from fossil fuels and, despite its advantages, only 4% from water electrolysis as can be seen in table 1. This small share in the total hydrogen production is a consequence of the production cost, which remains a key issue for water electrolysis (LIPMAN, 2004). While, in 2018, hydrogen from steam methane reforming with carbon capture and storage had a total cost of 2.46\$/Kg($H_2$), hydrogen from electrolysis powered by windmills cost 3.50\$/Kg($H_2$) and if the power source was photovoltaic cells, 8.03\$/Kg($H_2$). Almost 75% of the cost of hydrogen production comes from the electrolyzer, from both capital and operation cost (NEWMAN; BONINO; TRAINHAM, 2018).

Production of hydrogen from water electrolysis allows the integration of renewable energy sources. As an example, one can imagine a photovoltaic solar panel (or a windmill) linked to a fuel cell. During day-time, part of the energy is used by customers and the surplus is used to produce hydrogen. During the night, hydrogen is consumed, supplying uninterrupted electricity. Combining water electrolysis with renewable sources is important because water electrolysis is only as clean as the method used to produce the electricity used to split water molecules (MARBÁN; VALDÉS-SOLÍS, 2007). If coal was

Table 1: Annual Worldwide Hydrogen Production Share by Source

| Source | $Nm^3$ (billions)/Year | Share |
|---|---|---|
| Natural gas | 240 | 48% |
| Oil | 150 | 30% |
| Coal | 90 | 18% |
| Electrolysis | 20 | 4% |
| Total | 500 | 100% |

Source: U.S. DOE, 2003, cited by (LIPMAN, 2004)

Note: $Nm^3$ are normal cubic meters of hydrogen

burned to produce electricity and this electricity was used in an electrolyzer, the produced hydrogen cannot be considered clean, since in the overall process, $CO_2$ was produced. A schematic representation of a renewable and sustainable energy system with hydrogen playing an important role is seen in figure 1 (ZENG; ZHANG, 2010).

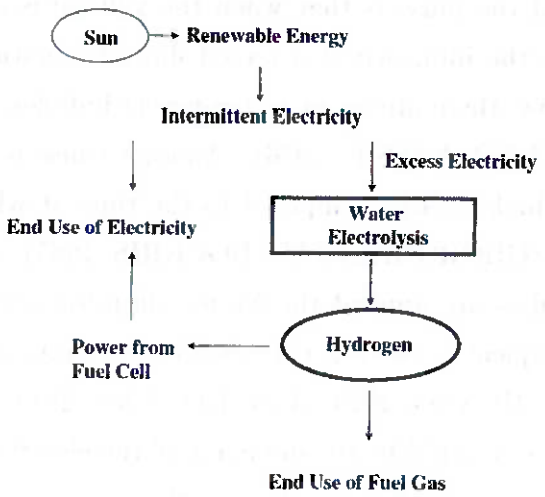


Figure 1: Schematic illustration of a conceptual sustainable distributed energy system (ZENG; ZHANG, 2010)

The way to reduce electrolysis cost is to achieve better electrolyzer performance. Recent and encouraging studies achieved an improvement in water electrolysis efficiency by the substitution of DC (direct current) power supply by a pulsed power supply. Demir, Kaya & Albawabiji (2018), for example, improved the efficiency of water electrolysis using potential pulses. This recent research confirms the conclusions of Shimizu, Hotta, Sekiya, & Oda, (2006), which succeeded in improving the hydrogen production rate and efficiency with potential pulses. These two researches were carried after the pioneering work of Ghoroghchian & Bockris (1985) and Tseung & Vassie (1976). The former achieved

a hydrogen production rate two times greater than DC, while the latter showed that when a potential pulse is applied, the resulting current is increased 2-10 times the value of the DC current. Furthermore, recently, Dobó & Palotás (2016) studied the effects of voltage fluctuations in water electrolysis. A voltage average value was set and sinusoidal variations were applied with different frequencies and amplitudes. In specific conditions, efficiency was improved (DOBÓ; PALOTÁS, 2016b). Vincent et al. (2018) used current pulses instead of potential pulses. It was discovered that at constant current density, the voltage is reduced if pulses are applied (VINCENT et al., 2018). These results are the main motivation of this Undergraduate thesis, as they show pulses as a hope to achieve a more efficient electrolyzer performance, reducing cost and helping to create a more sustainable future.

Furthermore, there are theoretical arguments to support these conclusions. The first argument is that, as the reaction occurs, bubbles are formed, which decreases the current. The idea of the pulse is that when the voltage is cut, the bubbles have time to detach thanks to the influence of a forced flux or a natural convection. Hence, when the voltage returns, there are no more (or fewer) bubbles, thereby increasing the resulting current (TSEUNG; VASSIE, 1976). Another cause is that if the time at which the voltage is cut is high enough compared to the time at which voltage is on, bubbles do not appear at all (GHOROGHCHIAN; BOCKRIS, 1985). Another possible reason would be that when pulses are applied the Nernst diffusion layer will not have time to form completely, consequently, the concentration of reactants at the surface of the electrodes will be enhanced (HUANG, 2013) (LIN; HOURNG, 2014) (VINCENT; BESSARABOV, 2018). Another cause could be the discharge of the electrical double layer when the pulse is off, which would conduct electrolysis without resistive losses (PUIPPE; IBL, 1980) (VANAGS; KLEPERIS; BAJARS, 2012) (SHIMIZU et al., 2006).

This work was developed in the Université Catholique de Louvain with the supervision of Prof. Joris Proost within the framework of a double-degree program between the Universidade de São Paulo and the Université catholique de Louvain. The publication presented here aims the obtainment of the degree of Petroleum Engineer. The main goal of this work is to investigate the effects of potential pulses in the efficiency and hydrogen production rate of a specific electrolyzer set-up, using an alkaline solution of 1M KOH. Three pulse widths were analyzed: 100ut, 10ut, and 1ut, where ut means unit of time. The corresponding value in seconds will not be shown due to confidentiality

reasons. This work begins from a theoretical background, where some important theories will be explained, starting from water electrolysis and finalizing with the state of the art of pulsed water electrolysis. There, concepts such as electrical double layer and the Nernst diffusion layer, cited before, will be explained in detail. Then, materials and methods will be presented and every choice justified. Two main experiments were carried out: pulsed chronoamperometry varying potential, and pulsed chronoamperometry with fixed potential and hydrogen collection. Different electrolyte fluxes were applied, going from natural convection (no forced flow) to maximum pump flow. Following the presentation of the materials and methods comes the results and discussion, where two main parameters will be analyzed: efficiency and hydrogen production rate. With the data collected in experiments, a model fitting was made and its fitting parameters analyzed. Lastly, the conclusions will be presented together with recommendations.

# 2 OBJECTIVES

Hydrogen gas produced from water electrolysis plays an important role in the storage of energy coming from sustainable sources such as windmills and solar panels. It has the highest specific enthalpy of any known fuel and does not produce $CO_2$ when it is burned. However, in order to be competitive, the water electrolysis technology needs to reduce its costs. Many efforts has been done to achieve this goal, but still much needs to be done. This work analyses one method of intensification.

## 2.1 General objective

As stated before, the main objective of this work is to investigate the effects of potential pulses in the efficiency and hydrogen production rate of a specific electrolyzer set-up, using an alkaline solution of 1M KOH and Nickel electrodes.

## 2.2 Specific objectives

1. Analyse the relation between the applied voltage and the energy efficiency;
2. Analyse the relation between the applied voltage and the current;
3. Determine the minimum voltage value for the hydrogen production to occur;
4. Analyse the relation between the pulse width and the resulting current;
5. Analyse the relation between the pulse width and the energy efficiency;
6. Analyse the effects of the electrolyte flow in both the energy efficiency and the production rate;
7. Verify if the resulting current can be approximated to the faradaic current. In other words, to verify if the capacitive current can be neglected.

# 3 STATE OF THE ART

## 3.1 Water electrolysis

The kinetics for reactions on the surface of the electrode can be seen in Appendix A. The focus here will be the specific case of water electrolysis. In this case, the reaction at the cathode in an alkaline medium is given by:

$$2H_2O_{(l)} + 2e^- \rightarrow H_{2(g)} + 2OH^-_{(aq)}; E^o_R = -0.83V \quad [A]$$

While in an acid medium it is:

$$2H^+_{(aq)} + 2e^- \rightarrow H_{2(g)}; E^o_R = 0V \quad [B]$$

In the case of the anode, the reaction in an alkaline medium is given by:

$$2OH^-_{(aq)} \rightarrow \frac{1}{2}O_{2(g)} + H_2O_{(l)} + 2e^-; E^o_R = +0.40V \quad [C]$$

While in an acid medium it is:

$$H_2O_{(l)} \rightarrow \frac{1}{2}O_{2(g)} + 2H^+_{(g)} + 2e^-; E^o_R = +1.23V \quad [D]$$

Therefore, the global reaction is given by (BUTTLER; SPLIETHOFF, 2018):

$$H_2O_{(l)} \rightarrow H_{2(g)} + \frac{1}{2}O_{2(g)}; E^o = -1.23V \quad [E]$$

Between these electrodes, there is a membrane to prevent gas mixing and electron migration (VINCENT; BESSARABOV, 2018). The membrane only allows ions to pass through (ZENG; ZHANG, 2010). The mechanisms for each half-reaction in alkaline water electrolysis (reactions [A] and [C]) is presented in the Appendix B. Considerations about acid water electrolysis will not be presented, since they are not the relevant mechanisms for this work.

### 3.1.1 Electric double layer - EDL

When there is charge transfer from the electrode to the solution, the process is said to be faradaic. In other words, Faradaic current is a current corresponding to the reduction or oxidation of some chemical substance (MCNAUGHT; MCNAUGHT, 1997). However, there are processes in which even if there is no charge transfer in the metal/solution interface, there is an electric current flowing. This may happen due to processes such as adsorption and desorption, which changes the properties of the interface or due to the formation of an electrical double layer, which will be explained in this section (BARD et al., 1980).

When no charge transfer occurs but a difference in potential is applied between two electrodes, ions are attracted to the surface of the electrode as a consequence of the force of the resulting electric field. As the ions arrive at the impenetrable surface of the electrode, they accumulate there. This accumulation of counterions reduces the field felt by the ions further away from the surface of the electrode, reducing the attraction force felt by these ions. This reduction continues until there is no more electrical field in the bulk, creating a free-charged bulk (OLDHAM; MYLAND; BOND, 2011). Because of this behavior, the electrode/solution interface works as a capacitor: current flows and charge accumulated in the interface until the following relation is satisfied (BARD et al., 1980):

$$C = \frac{Q}{E} \tag{3.1}$$

Where Q is the accumulated charge (C), E the electrical potential (V) and C the capacitance (farads, F) (BARD et al., 1980). As a capacitor, the non Faradaic current is calculated as (VANAGS; KLEPERIS; BAJARS, 2012):

$$i_{NF} = C\frac{\partial \eta}{\partial t} \tag{3.2}$$

With $\eta$ the overpotential; and t the time. However, unlike capacitors, the capacitance here is often dependent on the voltage. Its value is typically between 10-40 $\mu F/cm^2$. The current that flows during the charging process is known as charging current. If the electrode is connected to a more negative potential, electrons will accumulate at the metal surface and cations will accumulate on the solution side of the electrode/solution interface. If it is connected to a more positive potential, holes accumulate at the electrode and anions on the solution. The charge accumulated in the electrode is the same in absolute number as the charge in the solution, but with opposite sign. This region of charge accumulation is called Electric Double Layer - EDL (BARD et al., 1980). To illustrate it, one can imagine that if the electrolysis is made in a KOH solution, potassium ions accumulate in the cathode while hydroxide ions accumulate in the anode.

There are different models of EDL, here the Stern model will be presented. For information about the other models, the Appendix C may be consulted. In the Stern model, the ions closer to the electrode form a rigid Helmholtz plane and outside this plane, there is a dispersed Gouy-Chapman layer (ATKINS; PAULA; KEELER, 2018). Its thickness depends on the electrolyte concentration. For concentrations higher than $10^{-2}$M, the thickness is lower than $100\mathring{A}$ (BARD et al., 1980). In this model, the capacitance can be calculated assuming that the capacitances of the two other models are in series (OLDHAM; MYLAND; BOND, 2011):

$$\frac{1}{C_S} = \frac{x_H}{\epsilon_H} + \sqrt{\frac{RT}{2F^2\epsilon_{GC}C_O^*}}\left(\frac{1}{A\cosh(\frac{F}{RT}(E - E_{zc}))}\right) \tag{3.3}$$

A representation of the Stern model of EDL and the change in the electrical potential from metal to bulk can be seen in figure 2. Increasing even more the level of sophistication, there is the Grahame model, which includes an inner Helmholtz plane to the Stern model. In this case, there is an IHP of specifically adsorbed ions followed by a rigid OHP formed by ions in their hydration spheres and after that, a dispersed phase (ATKINS; PAULA; KEELER, 2018).

The EDL causes changes in the kinetics of the reactions. As an example, imagine that the reactant is only non specifically adsorbed. This means that the closer it can get to

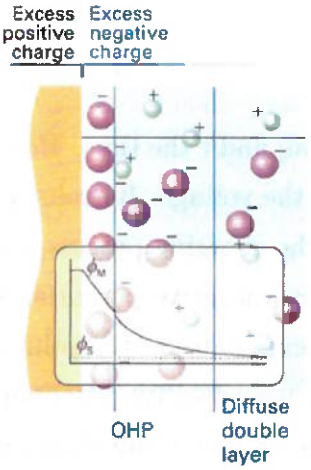


Figure 2: Schematic representation of the Stern model of EDL and the changes in potential (ATKINS; PAULA; KEELER, 2018)

the surface of the electrode is at the OHP. The potential experienced there is lower than the potential at the surface, as can be seen in figure 2. In addition, the presence of the charging current cannot be neglected in electrochemical experiments (BARD et al., 1980).

If, independently of the imposed potential, there is no charge transfer across the metal-solution interface, the electrode is called ideal polarized electrode (IPE). Even if no real electrode can have this behavior, some electrode-solution systems can have it over limited potential ranges, notably, in an interval where no reaction occurs (BARD et al., 1980).

If a potential step is applied to an IPE, the current behaviour with time can be approximated as follows (BARD et al., 1980):

$$i(t) = \frac{E}{R_s} exp\left(\frac{-t}{R_s C_D}\right) \tag{3.4}$$

Where $R_s$ is the solution resistance between the electrodes, t is the time, and $C_D$ is the differential capacitance of the EDL (BARD et al., 1980). This concept will be reviewed in the section 3.2.

### 3.1.2 Diffusion and concentration

Consider the classical redox reaction:

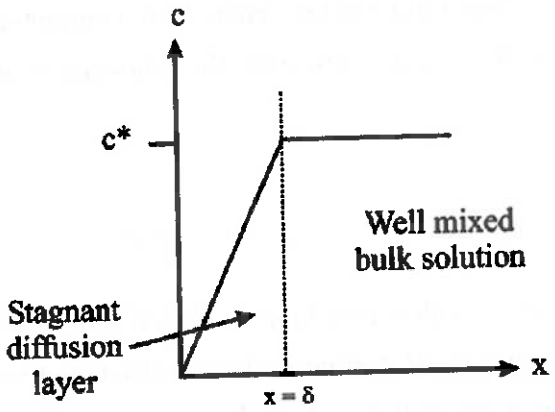


Figure 3: Schematic representation of the Nernst diffusion layer. $C^*$ is the concentration at the bulk and $\delta$ is the thickness of the diffusion layer (COMPTON; BANKS, 2011)

$$O + ne^- \rightleftharpoons R \qquad \text{[F]}$$

In the beginning, t=0, the concentration of O on the surface of the electrode is the same as the concentration in the bulk, $C_O = C_O^*$. As the reaction starts, O is consumed and R is formed, reducing the concentration of O at the surface. Beyond a critical distance, $\delta$, the solution is well mixed and the concentration of O is the same as in the bulk. This mixing can occur by natural convection or by a forced electrolyte flow. Natural convection is induced by a difference in density. On the surface of the electrode, convection is negligible, due to the rigidity of the solid electrode and friction forces. The zone at which $C_O < C_O^*$ is called Nernst diffusion layer and it is represented in figure 3. In the Nernst model, the change in concentration is linear. Since in this zone there is a concentration gradient, diffusion occurs (following Fick's laws), and the current response is given by (COMPTON; BANKS, 2011):

$$i = \frac{nFA(C_O^* - C_O)D_O}{\delta(t)} = nFAm_t(C_O^* - C_O) \qquad (3.5)$$

Where $m_t$ is the so-called mass transfer coefficient, given by the ratio between the diffusion coefficient and the thickness of the diffusion layer, $\delta$. According to Compton & Banks (2011), this thickness is in the order of 10-100 $\mu$m, which is much higher than the thickness of the electrical double layer (100 $\AA$, as seen in section 3.1.1). Using the Butler-Volmer formulation (equation A.20), one should expect that an infinite increase in voltage would lead to an infinite increase in current. In practice, however, the current

arrives at a limit. This limit occurs when O is completely depleted at the surface of the electrode ($C_O = 0$), and it is given by the following equation (COMPTON; BANKS, 2011):

$$i_{lim} = nFAm_t C_O^* \tag{3.6}$$

When the voltage is sufficiently high so the current reaches this limit, the cell is said to be in the diffusion-limited regime and no further increase in the current is possible. In other words, when the voltage applied is high enough to deplete the reactants from the surface of the electrode, the reaction rate is no more limited by the charge transfer and Butler-Volmer is no more applicable. Instead, kinetics is limited by the diffusion of reactants, hence, current is governed by Fick's Law and can be calculated using equation 3.6. The value of $C_O$ is function of the electrode potential. In addition, the thickness of the diffusion layer grows with time (COMPTON; BANKS, 2011) (BARD et al., 1980):

$$\delta(t) = 2\sqrt{D_O t} \tag{3.7}$$

Hence, equation 3.5 becomes:

$$i = \frac{nFA(C_O^* - C_O)\sqrt{D_O}}{2\sqrt{t}} \tag{3.8}$$

It can be seen by equations 3.7 and 3.8 that while $\delta$ increases with $t^{1/2}$, current decreases with $t^{-1/2}$. Nevertheless, equation 3.7 predicts an infinite $\delta$ for an infinite time. In practice, there is a maximum value, $\delta_{max}$, given by convection. The time for the diffusion layer to reach this steady-state value is given by (BARD et al., 1980):

$$t = \frac{\delta_{max}^2}{4D_O} \tag{3.9}$$

The profile of concentration at different times and the increase in the thickness of the diffusion layer is seen in figure 4 (BARD et al., 1980).

### 3.1.3 Losses

There are different resistances in electrode reactions which create energy losses. To start, there is the electric resistance of the conductor, which can be calculated as follow

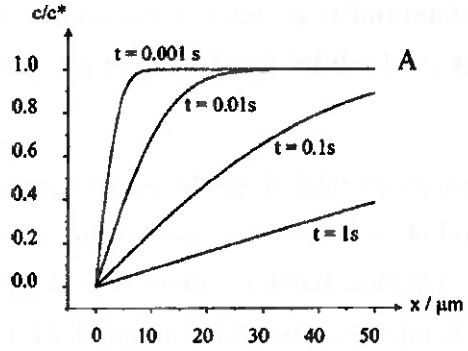


Figure 4: Concentration profile near the electrode surface as a function of time (BARD et al., 1980)

(ZENG; ZHANG, 2010):

$$R_{el} = \frac{L}{kA} = \frac{E}{i} \tag{3.10}$$

With $L$ the conductor's length, $k$ the specific conductivity, A the cross-sectional area, E the potential, and i the electric current. In addition to this resistance, there are resistances related to ion transport. Their causes are the formation of bubbles in the electrode/solution interface, and the resistances to ions transfer of the solution and of the membrane. Together, the resistance related to ions transport and the electric resistance are called ohmic resistances. They cause losses as thermic energy. In between these resistances, the one which creates more losses is the bubble's resistance. Therefore, a special attention will be given to this resistance in section 3.1.5. Minimizing bubble effect is extremely important for the improvement of electrolyzer efficiency, as we will se further (ZENG; ZHANG, 2010).

Another factor that increases the potential is the junction potential. It exists when there is an interface between two solutions containing or different concentrations and/or different ions. In this case, ions will flow from the more concentrated solution to the less concentrated one. However, since the ions have different mobilities, an electric field will be developed at the interface. To illustrate one can imagine two solutions of HCl connected by a membrane. The ions $H^+$ and $Cl^-$ will flow from the more concentration solution to the less concentrated one. As $H^+$ flows much faster than $Cl^-$, the dilute solution will become positively charged due to the gain of protons while the concentrated side will become negatively charged. The correspondent electric field will accelerate the $Cl^-$ and slow down the $H^+$, until both ions cross the junction with equal rate. The ef-

fect of the junction potential is no more than some tens of mV and can be minimized by the use of a concentrated salt bridge (BARD et al., 1980) (COMPTON; BANKS, 2011).

Finally, the last factor is related to the overpotential needed to reach the activation energy of the cell and it is called electrochemical resistance (ZENG; ZHANG, 2010). It is related to the activation barrier. The cell voltage needed to initiate the reaction can be calculated as being the standard voltage (1.23 V for water electrolysis) more the overpotential due to all the resistances:

$$E_{\text{real}} = \Delta E^0 + iR_{\text{cell}} + E_j + \sum \eta \tag{3.11}$$

Where $\Delta E^0$ is the standard cell potential, calculated as the difference between the standard electrode potential at the cathode and the standard electrode potential at the anode (for more details check Annex A.0.2); $\sum \eta$ is the sum of the electrochemical overpotentials from the cathode and anode; $R_{\text{cell}}$ is the sum of the ohmic resistances; and $E_j$ is the junction potential.

### 3.1.4 Theoretical and thermo-neutral voltage for water electrolysis

As seen in equation A.8, the standard cell potential of an electrolytic cell is defined as the difference between the highest standard electrode potential and the lowest one. On the other hand, the theoretical cell potential is calculated using the Nernst equation (equation A.24). The theoretical cell potential is also proportional to the Gibbs free energy:

$$E_{cell}^{th} = \frac{-\Delta G}{nF} \tag{3.12}$$

Where $\Delta G$ is the variation in the Gibbs free energy. The theoretical cell potential can be interpreted as the thermodynamic requirement needed to drive a reaction. In water electrolysis, an increase in the temperature of the cell reduces the change in the Gibbs free energy. As a consequence, the theoretical cell potential in equation 3.12 is reduced. Consequently, the electrical power demand is also reduced. Considering standard conditions, the value of $E_{cell}^0$ begins at 1.25V when the temperature is 0°C and decreases until 0.91V at 100°C (BUTTLER; SPLIETHOFF, 2018). At 25°C, $E_{cell}^0$=1.23V and $\Delta G$=+237.2kJ.mol$^{-1}$ (ZENG; ZHANG, 2010). However, the reduction in the stan-

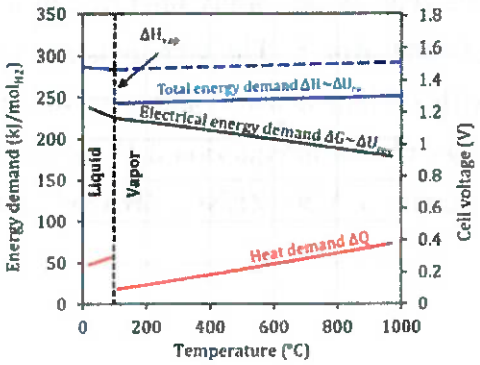


Figure 5: Total, electric and calorific energetic demand as a function of temperature(BUTTLER; SPLIETHOFF, 2018)

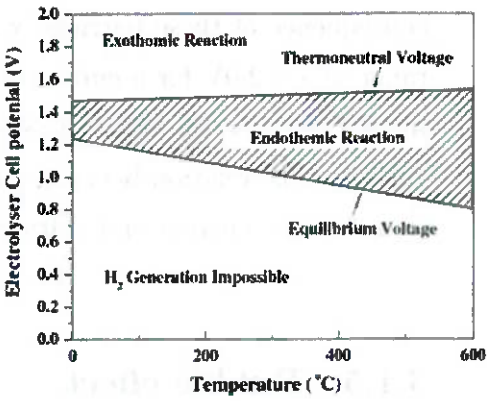


Figure 6: Cell potential as a function of temperature (liquid water)(ZENG; ZHANG, 2010)

dard cell potential also makes the reaction more endothermic, hence, there is an increase in the heat demand. Combining the change in the electric demand with the change in heat demand, an increase in temperature slightly increases the total energy demand. It is important to notice that the enthalpic variation of the reaction is higher for liquid water than for water vapor. As a consequence, at temperatures higher than 100°C, the heat demand will decrease abruptly. This can be seen in figure 5 (BUTTLER; SPLIETHOFF, 2018).

Another important concept is the one of thermo-neutral voltage. It is defined as the voltage below which the reaction is endothermic and above which it is exothermic (TARASCON, ). It is given by:

$$E_{\text{thermo}} = \frac{\Delta H}{nF} \tag{3.13}$$

Where $\Delta H$ is the variation in entalphy. For liquid water, the $E_{thermo}$ value is between 1.47-1.48V while for water vapour it is between 1.26-1.29V from 100-1000 °C (BUTTLER; SPLIETHOFF, 2018). Its value increases slightly with temperature, as shown in figure 6 (ZENG; ZHANG, 2010).

As seen in section 3.1.3, there are some kinetic barriers that need to be overcome for a reaction to proceed at a measurable rate. In water electrolysis, the overpotential needed to overcome this barrier associated with the oxygen evolution is generally higher than that the one from the hydrogen evolution (WHITE; BOCKRIS; CONWAY, 1983). As a

consequence of these barriers, water elecrolysis cells are generally operated in a voltage range of 1.8-2.0V for a current density of 1000-3000 $Am^{-2}$. The voltage is not increased further because the ohmic losses increases with current density, and consequently with voltage. The relation between current and losses is seen in equation 3.11, while the relation between current and voltage is given by equation A.30 (ZENG; ZHANG, 2010).

### 3.1.5 Bubble effect

During electrolysis of water, hydrogen bubbles are formed at the cathode and oxygen bubbles at the anode. To detach from the electrode, these bubbles need to grow until reaching a critical volume, at which, through buoyancy forces, they detach and rise. The growing process of bubbles takes some time. De Jonge, Barendrecht, Janssen, & van Stralen (1982) reported that after the interruption of the current, all oxygen bubbles immediately leave the surface (JONGE et al., 1982). Matsushima, Iida & Fukunaka (2012) used a high-speed camera to calculate the time needed for the bubbles to detach from the surface of the electrode. The result indicates a detaching time in the order of 0.15s. The authors also estimate a void fraction of 0.5 in the anode's vicinity and 0.4 in the cathode's (MATSUSHIMA; IIDA; FUKUNAKA, 2012). Studies have shown that the gas fraction at electrode strongly increases with current density (JONGE et al., 1982). During the period at which the bubbles are at the electrode, they block the arrival of new reactants to the surface of the electrode, thus reducing the active surface of the electrode. This will create an increase in the ohmic resistance and in the overpotential needed to maintain the same current and is called bubble effect. The consequence of the decrease in the active area of the electrode is that in order to maintain a constant hydrogen production rate, the current density needs to be increased. To do that, the overpotential needs to increase, following the Tafel law (equation A.13) and equation A.30. To account for bubble effect, the Tafel equation should be modified as follows (WANG et al., 2014):

$$\eta = a + b.log\left(\frac{i}{A}\right) + b.log\left(\frac{1}{1-\theta}\right) \tag{3.14}$$

Where $\theta$ is the bubble coverage ratio at the surface of the electrode, i is the total current and A is the geometrical surface area (WANG et al., 2014). Alternatively, according to White, Bockris & Conway (1983), the overpotential resulting from bubble effect is given by:

$$\eta = \frac{l}{AF(z_+ + \mu_+ + c_+ + z_- + \mu_- + c_-)} i \tag{3.15}$$

Where l is the space between electrodes; A is the electrode area; i is the current; and z, $\mu$, and c are the charge, the mobility, and the concentration of ions in the electrolyte, respectively. The index + indicates cation and the index -, anions (WHITE; BOCKRIS; CONWAY, 1983).

Following their detachment, the bubbles do not follow a vertical path. This happens due to the difference of concentration which pushes the bubbles in the bulk's direction. This means that the thickness of the bubbles' layer increases with height. The dispersion of bubbles in electrolyte leads to a poor conductivity, increasing electrolyte resistance and overpotential (WANG et al., 2014). A method to calculate the void fraction in a froth layer is to measure the electrolyte resistance with and without the presence of bubbles, as given by the Bruggeman equation (ROBERT; TOBIAS, 1959):

$$\frac{R_b}{R_e} = (1 - \theta)^{-3/2} \tag{3.16}$$

With $R_b$ the electrolyte resistance in the presence of bubbles, $R_e$ the gas-free electrolyte resistance, and $\theta$ the void fraction. Alternatively, the effect caused by the presence of bubbles in the electrolyte is given by:

$$k_g = k(1 - 1.5\theta) \tag{3.17}$$

Where k stands for the specific conductivity of the electrolyte solution without the presence of bubbles, and $k_g$ the specific conductivity with bubbles (ZENG; ZHANG, 2010).

The bigger the bubbles, the lower will be the surface and the more difficult it will be for the reactants to arrive at the surface, thus, the overpotential rises even more. Departure radius of hydrogen is small and decrease slightly with current density. Oxygen radius is large and increases with current density (JONGE et al., 1982).

Hydrogen bubbles have a small contact angle with the electrode, therefore, during growth, bubbles have almost no contact area with the electrode. With the increase of current density, this angle decreases due to the decrease in the surface tension in the

metal-electrolyte interface. The oxygen bubbles have a large departure radius at low current density. Increasing current density, one should expect a decrease in this radius as a consequence of the decrease in the surface tension of the metal-electrolyte interface, as it is for hydrogen. Experimentally, the opposite happens: an increase in bubbles radii (JONGE et al., 1982).

The method most commonly used to accelerate the detachment of bubbles is the introduction of a forced electrolyte flow. This recirculation of electrolyte mechanically accelerate the departure of gas bubbles by drag force. It is also helpful to reduce the electrolyte difference in concentration, which would increase overpotential. Finally, recirculation is also useful for heat distribution in the cell (WANG et al., 2014) (ZENG; ZHANG, 2010). The effects of electrolyte flow when potential pulses are applied will be analyzed in the work presented here.

### 3.1.6 Efficiencies

The voltage efficiency of water electrolysis is defined as the ratio between the theoretical energy consumption to produce $1m^3$ of hydrogen (considering voltage=1.23V) and the practical energy consumption for the same hydrogen volume. Since Energy=E.Q (E the cell voltage and Q the charge), voltage efficiency can also be calculated as a ratio between the experimental cell voltage and the theoretical voltage value (WANG et al., 2014):

$$\eta_e = \frac{Energy_{theoretical}}{Energy_{real}} = \frac{E^0 Q}{E_{cell} Q} = \frac{E^0}{E_{cell}} \tag{3.18}$$

The physical meaning of this efficiency is the proportion between the effective voltage used for the reaction and the applied voltage. Thermodynamically, a way to improve voltage efficiency is to reduce the energy needed to split water by the increase in temperature or pressure, as seen in section 3.1.6. In addition, efficiency can be improved by the reduction of losses, which decreases $E_{cell}$. Another definition of efficiency is the thermal efficiency. It is related to the enthalpic change and to the thermo-neutral voltage, seen in equation 5. A thermal efficiency of 100% means no heat produced nor absorbed (ZENG; ZHANG, 2010). If the reaction occurs endothermically, the thermal efficiency will be superior to 100%. The equation for thermal efficiency is given by:

$$\eta_{Thermic} = \frac{E_{thermo}}{E_{\text{cell}}} = \frac{1,48V}{E_{cell}} \tag{3.19}$$

Efficiency can also be determined by means of current: Faraday efficiency, also known as current efficiency. It is defined as a ratio between the actual and the theoretical hydrogen volume produced, given by:

$$\eta_{Faraday} = \frac{V_{H_2}}{V_{H_2}^{th}} = \frac{V_{H_2} nF}{V_{molar} Q} = \frac{\dot{V}_{H_2} nF}{V_{molar} i} \tag{3.20}$$

With $V_{H_2}$ the actual volume, $V_{H_2}^{th}$ the theoretical volume, $V_{molar}$ the molar volume of gas in the experiment's conditions, n the stoichiometric electron's coefficient, F the Faraday constant, Q the charge, $\dot{V}_{H_2}$ the hydrogen volumetric production rate, and i the current. The theoretical hydrogen production is calculated using Faraday's law of electrolysis, which assumes that the mols produced is equal to the electrical charge divided by nF. Faraday efficiency has commonly a value between 98-99.99% (BUTTLER; SPLIETHOFF, 2018). Deviations from 100% are caused by parasitic current losses. A significant decrease in Faraday efficiency was observed by Ulleberg (2003) below a current density of 50-100mA/cm$^2$ for alkaline electrolysis. The decrease of Faraday efficiency was attributed to parasitic current losses along the gas and electrolyte ducts in the cell, which increases with the decrease of current density. The same was observed by Hug, Bussmann & Brinner (1993), with a decrease in Faraday efficiency for current densities below 150 mA/cm$^2$ (ULLEBERG, 2003).

Another way to calculate efficiency is to see how much of the input energy can be recuperated by hydrogen burning. It is calculated multiplying the hydrogen's production rate, $\dot{V}$ $(Nm^3/h)$, by the hydrogen Lower Heating Value - LHV ($H_{H_2}^l$), and dividing it by the consumed electric power $P_{el}$:

$$\eta_{LHV} = \frac{\dot{V}_{H_2} . H_{H_2}^l}{P_{el}} \tag{3.21}$$

The LHV is defined as the heat that can be produced by the complete combustion of an organic substance, considering that as product one has steam and not liquid water. If in the product one has liquid water, one should use the High Heating Value - HHV. The LHV value for hydrogen is 3 kWh/Nm$^3$, meaning that 3KWh of energy can be produced by burning 1Nm$^3$ of hydrogen, considering that the water will evaporate. The physical

meaning of this efficiency is the maximum quantity of energy that can be recovered as heat compared with the inserted energy.

Finally, another way to compare efficiencies of different cells is to use the curve current density versus voltage, also known as polarization curve. The cells that at the same voltage produce more current density are better.

### 3.1.7 Alkaline water electrolysis

There are different technologies for water electrolysis: alkaline electrolysis (AEL), polymer electrolyte membrane or proton exchange membrane electrolysis (PEM), and solid oxide electrolysis (SOEL). Since the technology chosen in this study was AEL, the efforts will be concentrated on this one. Good and recent reviews and book chapters about alkaline water electrolysis can be found in (ZENG; ZHANG, 2010), (DAVID; OCAMPO-MARTÍNEZ; SÁNCHEZ-PEÑA, 2019), (ITO; LI; HAO, 2016), (RASHID et al., 2015), and (GUILLET; MILLET, 2015). AEL was chosen for many reasons. First, it is a mature technology, with hundreds of years of industrial production. Second, it has the highest industrial production rate, with active cell area one or two orders of magnitude higher than other technologies. Third, it has the longest lifetime, up to 30-50 years. Fourth, it also has the lowest specific investment and maintenance costs. Lastly, it s the only that nowadays is used in an industrial scale. A comparison between the technologies can be seen in figure 7. AEL has the highest nominal stack and system LHV efficiency (BUTTLER; SPLIETHOFF, 2018). In addition, alkaline electrolysis avoids corrosion losses presented in acid electrolysis (PEM). Commonly, alkaline electrolysis is operated at a current density of 200-500 mA $cm^{-2}$, temperatures of 70-90°C, cell voltage in the range of 1.85-2.2V (ZENG; ZHANG, 2010), and an electrolyte composed of 25-30% KOH (VINCENT; BESSARABOV, 2018).

A disadvantage of alkaline electrolysis is that KOH solution is very sensitive to the carbonic gas, present in the air. When in contact, they react:

$$CO_2 + 2KOH \rightarrow K_2CO_3 + H_2O$$

The formation of potassium carbonate reduces electrolysis performance, since it pre-

| | AEL | PEMEL | SOEL |
|---|---|---|---|
| **Operation parameters** | | | |
| Cell temperature (°C) | 60–90 | 50–80 | 700–900 |
| Typical pressure (bar) | 10–30 | 20–50 | 1–15 |
| Current density (A/cm$^2$) | 0.25–0.45 | 1.0–2.0 | 0.3–1.0 |
| **Flexibility** | | | |
| Load flexibility (% of nominal load) | 20–100 | 0–100 | −100/+100 |
| Cold start-up time | 1–2 h | 5–10 min | hours |
| Warm start-up time | 1–5 min | < 10 s | 15 min |
| **Efficiency** | | | |
| Nominal stack efficiency (LHV) | 63–71% | 60–68% | 100%[a] |
| ...specific energy consumption (kWh/Nm$^3$) | 4.2–4.8 | 4.4–5.0 | 3 |
| Nominal system[b] efficiency (LHV) | 51–60% | 46–60% | 76–81% |
| ...specific energy consumption (kWh/Nm$^3$) | 5.0–5.9 | 5.0–6.5 | 3.7–3.9 |
| **Available capacity** | | | |
| Max. nominal power per stack (MW) | 6 | 2 | < 0.01 |
| $H_2$ production per stack (Nm$^3$/h) | 1400 | 400 | < 10 |
| Cell area (m$^2$) | < 3.6 | < 0.13 | < 0.06 |
| **Durability** | | | |
| Life time (kh) | 55–120 | 60–100 | (8–20)[c] |
| Efficiency degradation (%/a) | 0.25–1.5 | 0.5–2.5 | 3–50 |
| **Economic parameter** | | | |
| Investment costs (€/kW) | 800–1500 | 1400–2100 | (> 2000)[c] |
| Maintenance costs (% of investment costs per year) | 2–3 | 3–5 | n.a. |

[a] Operating at thermoneutral voltage.
[b] Including auxiliaries and heat supply (SOEL).
[c] High uncertainty due to pre-commercial status of SOEL.

Figure 7: Comparison between main technologies for water electrolysis (BUTTLER; SPLIETHOFF, 2018)

cipitates in the pores of the electrode, reduces electrolyte concentration, and reduces ionic conductivity due to modification in electrolyte composition (VINCENT; BESSARABOV, 2018).

In alkaline electrolysis, Nickel is used as electrode material due to its high catalytic activity and high corrosion resistance in alkaline mediums (WHITE; BOCKRIS; CONWAY, 1983). Platinum and palladium are not used because of its high cost, as seen in section B.0.1.

### 3.1.8 Potential step electrochemical methods

Now that conventional water electrolysis was seen, the discussion will continue with pulsed water electrolysis. Nevertheless, before that, the use of potential pulses for electrochemical analysis will be introduced. Using once again the general electrode reaction

[F] and considering n=1, one has:

$$O + e^- \rightleftharpoons R \qquad [G]$$

In a potential pulse, there is a baseline potential, $E_{off}$, and a peak voltage value, $E_{on}$. The first electrochemical method that will be presented here is known as chronoamperometry. In this experiment, at the beginning there is just O, $E_{off}$ has a value at which no reaction can occur and $E_{on}$ has a value at which the reduction reaction is in the diffusion limited region (current given by equation 3.6). In chronoamperometry, voltage starts at $E_{off}$ and then is increased to $E_{on}$, and the resulting current is recorded as a function of time. When $E=E_{on}$, there is no O in the surface of the electrode, since all the O was reduced to R. This creates a depletion zone of O. By diffusion, there is a flux of O from the bulk to the surface, as seen in section 3.1.2 (BARD et al., 1980). Observing the first Fick's law, one can see that the diffusion depends on the derivative of concentration by distance. As the depletion zone gets thicker with time (equation 3.7), the flux of reactants O is reduced and consequently, the measured current. The fashion at which the current decreases with time gives information about the reaction e.g. the estimation of the mass-transfer coefficient, $m_t$ (BARD et al., 1980).

The second experiment is called double potential step chronoamperometry. This experiment starts in the same way as the chronoamperometry, however, after a time $t=\tau$, the voltage returns to $E_{off}$. When it happens, no R can exist at the surface of the electrode since at $E_{off}$, equilibrium establishes no R. Since before the decrease to $E_{off}$ there was just R, all of it needs to be oxidized. Hence, there is the flow of a counter current. The magnitude of this current reduces with time as R is consumed. A representation of the current response in this experiment is shown in figure 8 (BARD et al., 1980). This experiment is very similar to the one presented in the Material and Methods of this work, however, instead of applying just one step, multiple steps were applied.

Imagine now that the value of $E_{off}$ is fixed, but the value of $E_{on}$ goes from a value at which no reaction happens to a value in the mass-transfer-limited region. The current is measured at a fixed time ($\tau$) for each one of the different $E_{on}$ values. This method is known as sampled-current voltammetry. The fashion of the curve current (at time $\tau$) versus $E_{on}$ is a sigmoid, starting from zero for small $E_{on}$ and reaching a maximum which

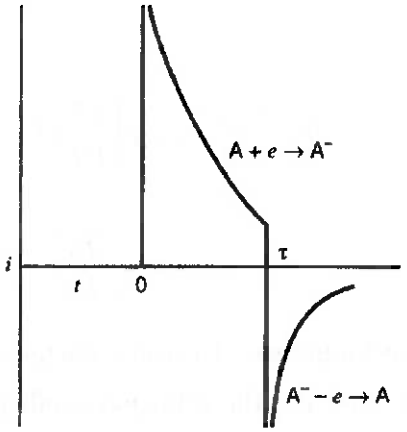


Figure 8: Double potential step, in the first step , reduction occurs, and second, oxidation (BARD et al., 1980)

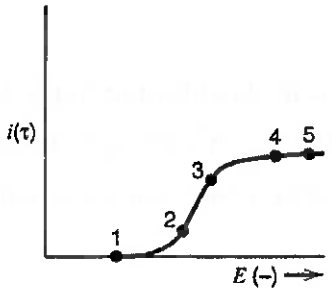


Figure 9: Current value at a time $\tau$ versus $E_{on}$ in sampled-current voltammetry (BARD et al., 1980)

is limited by the diffusion. This curve is represented in figure 9 (BARD et al., 1980).

For the specific case of a reversible reaction in a planar electrode, the half-wave potential seen in the sampled-current voltammetry (potential at which the current is half of the maximum value) is the standard potential of the electrode, $E^0$. In the case of a non-reversible reaction, the curve will be shifted some mV. Thus, the value obtained for the half-wave potential can be used to infer the reversibility of the reaction (BARD et al., 1980).

In chronoamperometry, the current versus time response can be described by the following equation (BARD et al., 1980):

$$i(t) = \frac{nFA\sqrt{D_O}C_0^*}{\sqrt{\pi t}(1+\xi\theta)} \tag{3.22}$$

With:

$$\theta = \frac{C_O}{C_R} = exp\left[\frac{nF}{RT}(E - E^0)\right] \tag{3.23}$$

$$\xi = \sqrt{\frac{D_0}{D_R}} \tag{3.24}$$

Where n is the stoichiometric electron's coefficient; F is the Faraday constant; A the electrode's area; $D_O$ and $D_R$ the diffusion coefficients for O and R (in reaction [F]), respectively; $C_0^*$ the concentration of the substance O in the bulk; t is the time; $C_O$ and $C_R$ the concentrations of O and R at the surface of the electrode and time t; R is the gas constant; T the temperature; E the electrode potential; $E^0$ the standard potential.

When the voltage $E_{on}$ is in the diffusion-limited regime, the concentration of O at the surface is always zero during $t_{on}$, where $t_{on}$ is the time during a pulse at which E=$E_{on}$. This means that $\theta$ is also zero, hence, the equation 3.22 can be re-written as (BARD et al., 1980):

$$i_d(t) = \frac{nFA\sqrt{D_O}C_0*}{\sqrt{\pi t}} \tag{3.25}$$

This equation, known as the Cottrell equation, predicts very high currents at short times. Nevertheless, the actual maximum current may depend on the current and voltage output characteristics of the potentiostat.

When pulses are applied, the concentration profile at the surface varies with time according to the following equations (BARD et al., 1980):

$$C_O = C_O^*\left[1 - \frac{i(t)}{i_d(t)}\right] \tag{3.26}$$

$$C_R = \xi C_O^* \frac{i(t)}{i_d(t)} \tag{3.27}$$

Where $i_d(t)$ is the Cottrell current defined in equation 3.25.

Cottrell equation works well for reversible reaction. For a quasireversible, one electron,

one step reaction, in semi-infinite linear diffusion with current being governed by both mass transfer and charge-transfer kinetics, the current-time response can be given by (BARD et al., 1980):

$$i(t) = FA(k_f C_0^* - k_b C_R^*) \exp(H^2 t)\, \mathrm{erfc}(H\sqrt{t}) \tag{3.28}$$

With:

$$k_f = k^0 exp(-\alpha f(E - E^0)) \tag{3.29}$$

$$k_b = k^0 exp[(1-\alpha) f(E - E^0)] \tag{3.30}$$

$$f = \frac{F}{RT} \tag{3.31}$$

$$H = \frac{k_f}{\sqrt{D_0}} + \frac{k_b}{\sqrt{D_R}} \tag{3.32}$$

erfc is the error function complement of x, defined as:

$$\mathrm{erfc}(x) = 1 - \frac{2}{\sqrt{\pi}} \int_0^x e^{-y^2} dy \tag{3.33}$$

Where $k^0$ is the standard rate constant; $\alpha$ the transfer coefficient; F the Faraday constant; A the electrode's area; $k_f$ and $k_b$ the rate constant for the forward (reduction) and backward (oxidation) reactions, respectively; $C_0^*$ and $C_R^*$ the concentration of the reactant O and the product R in the bulk, respectively; t is the time; R the gas constant; T the temperature; E the potential; $E^0$ the standard potential; $D_0$ and $D_R$ the mass transfer coefficients for specimens O and R, respectively. Further in this work, this equation will be used to predict pulse's behaviour and to fit the obtained data.

Finally, when the potential is high enough for a reaction to take place but below the mass transfer regime, the measured current is a combination of the kinetic current given by the Butler-Volmer equation and the mass transport current, given by the setup and level of stirring. This is given by the Koutecky-Levich equation (BARD et al., 1980):

$$\frac{1}{i} = \frac{1}{i_k} + \frac{1}{i_{mt}} \tag{3.34}$$

Where $i_k$ represents the current in the absence of any mass transfer effect, such as the concentration on the electrode surface is always equal to the concentration at the bulk; and $i_{mt}$ is the current at the totally mass-transfer-limited regime and depends in the level of the forced flux. The higher the electrolytic flux, the higher will be $i_{mt}$ and higher the total current.

## 3.2 Pulsed water electrolysis

A good and recent review about the use of pulsed power for hydrogen production can be seen in (MONK; WATSON, 2016). As seen in section 3.1.1, when a potential is applied to an electrode, the EDL is formed. During EDL charging/discharging, the current is the sum of two parts: a capacitive current, $i_C$, which charges/discharges the EDL, and a Faradaic current, $i_F$, which conducts chemical reactions (PUIPPE; IBL, 1980). If potential pulses are applied, the current versus time behavior will be as shown in figure 10. It can be seen that even if the total current decreases with time, Faradaic current increases, due to the decrease in the charging current (WENDT; KREYSA, 2013). It was seen that the EDL works as a capacitor. Hence, the behaviour of the charging current with time is given by the equation 3.4. It can be seen that the charging current decays exponentially with a cell time constant: $R_s C_D$, where $R_s$ is the solution resistance and $C_D$ is the double-layer capacitance (WENDT; KREYSA, 2013). The charging time, $t_c$, is the time needed for the Faradaic current to be equal to the total current.

Puippe and Ibl (1980) studied the rate of charge and discharge of the EDL using current pulses in electric plating. If charging time is longer than pulse time, Faradaic current never reaches its maximum value. A similar process occurs att off-time: EDL discharge, creating a discharge current, which takes some time to be equal to zero. Again, if the discharge time is longer than $t_{off}$, current never drops to zero. Following the same logic as $t_{on}$, $t_{off}$ is the time during a pulse when E=$E_{off}$. Figure 11 shows some possible cases for potential pulses (PUIPPE; IBL, 1980).

The first one is when the double layer charging time is negligible. In this case, Faradaic

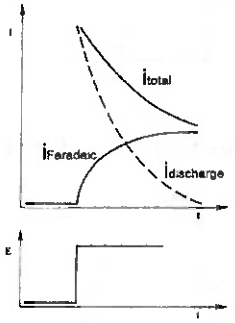


Figure 10: Schematic representation of a potential pulse and its current response (WENDT; KREYSA, 2013)

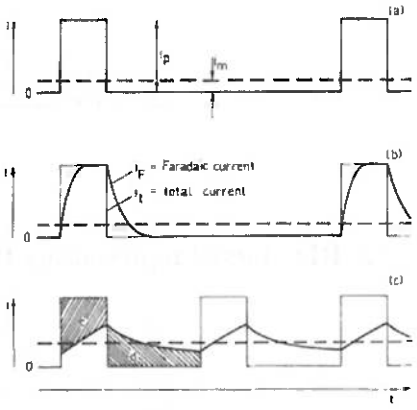


Figure 11: Schematic representation of a Faradaic current behaviour (a) $t_c ¡¡ T$ ; (b) $t_c ¡ T$ ; (c) $t_c ¿¿ T$ and $t_d ¿¿ T$. Where $t_c$ and $t_d$ are the EDL charging and discharging time, respectively. T is the pulse time. (PUIPPE; IBL, 1980)

current is equal to total current, hence, this case is similar to an interrupted DC electrolysis without the effects of the charge/discharge of the EDL. Case b is when the charging time is lower than $t_{on}$, but not negligible. Hence, at the beginning of the pulse the Faradaic current is lower than the total current, but after some time it reaches its maximum value. Finally, there is the case where the charging time is higher than $t_{on}$ and the discharging time is higher than $t_{off}$. As a consequence, the current neither returns to zero nor reaches maximum value. According to the authors, this damping does not change the Faraday efficiency, since the charge accumulated during the pulse application is recuperated during $t_{off}$ (PUIPPE; IBL, 1980). The authors claim that the damping decreases losses, since reducing Faradaic current also reduces ohmic losses (FERRERO et al., 2012). When the pulse is switched off, there is a Faradaic current, but none ohmic drop in the solution. The authors also studied the capacitance of the EDL. The results have shown a capacitance in the range 10-100$\mu$Fcm$^{-2}$, depending on the electrode. For rough nickel (Ni/$H_2SO_4$ 1 N) it was 80 $\mu$Fcm$^{-2}$. Still according to this study, 50$\mu$Fcm$^{-2}$ is a good approximation if the real value of the capacitance is unknown 11 (PUIPPE; IBL, 1980).

Mazloomi K. et al (2003) proposed a second order RLC equivalent circuit to be the best representation of a water electrolysis cell. The proposed circuit can be seen in figure 12, where $R_{leak}$ is equal to the internal resistance of the electrolyte; C is the cell capacitance; ESR and ESL come mainly from the cabling and external connections of the

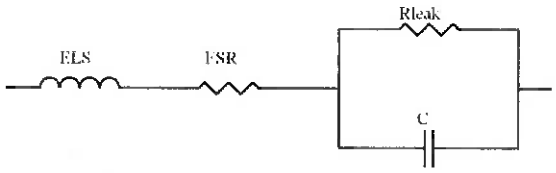


Figure 12: RLC model representing the water electrolysis cell (MAZLOOMI et al., 2013)

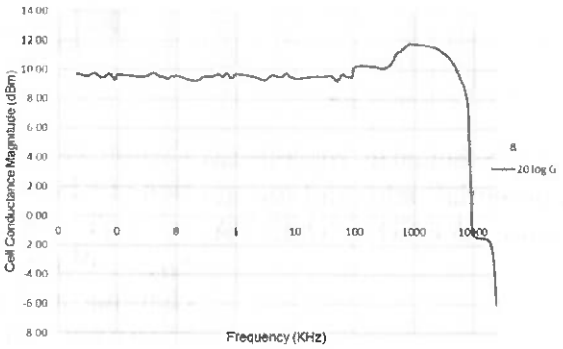


Figure 13: Plot of the cell conductance magnitude versus pulse frequency (MAZLOOMI et al., 2013)

system. The experimental set-up consisted of two Aluminium plate electrodes immersed in a KOH solution. The authors applied AC sinusoidal pulses with amplitudes between 0-10V. The cell reached a minimum impedance value at a certain pulse frequency, interpreted as the resonance frequency of the cell's electrical equivalent circuit. Its value went from 0.8 MHz to 12.2 MHz, depending on the cell's conditions. The value for the resonance frequency increased with increasing electrodes' sizes, the distance between electrodes, and the electrolyte's molarity. As a result of this analysis, if the applied pulse has the same frequency as the resonance frequency, conductance is maximized (minimum impedance). An example of a curve frequency versus conductance can be seen in figure 13. It can be seen that at a frequency of 1000 KHz, conductance is increased (MAZLOOMI et al., 2013).

Vanags et al (2012) used a 1$\mu$s high-voltage ($\approx$600V) pulse in alkaline medium (KOH concentration between 0.1-3 mol/Kg). It was concluded that when this short voltage pulse is applied, the cell behaves as a capacitor with a high Q factor, indicating that it approaches an ideal capacitor. Furthermore, it was shown that it is possible to separate the charging of the double-layer from electrochemical reactions using short pulses. When the voltage pulse is on, EDL is charged, when it is off, the energy is discharged and electrolysis occurs. The electrolyte concentration had no effect on the rate of EDL charge, just on the rate of EDL discharge: higher for more diluted solutions. Another conclusion

was that oxygen can be produced at the cathode during $t_{off}$ if the solution is deionized water or very low concentrated solutions. The authors obtained a Faraday efficiency of 50%, meaning that only half of the average current was used for hydrogen production. This is an indicator that in pulsed electrolysis we cannot assume a Faraday efficiency of 100%, as in DC electrolysis. Bearing that in mind, in the experiments presented in this work, Faraday efficiency will be calculated. In addition, an LHV efficiency between 59-85% was obtained, which is a great achievement, since the maximum LHV efficiency that can be obtained is 85.7%, corresponding to a HHV efficiency of 100% (VANAGS; KLEPERIS; BAJARS, 2012).

Now that the effects of the pulses in the EDL were seen, we will see their effects in the Nernst diffusion layer. Still according to Vanags et al (2012), in pulsed electrolysis, the diffusion layer is characterized by pulsed concentrations of active ions on the electrode surface and a normal diffusion layer far from the surface (as in DC). The time needed for the concentration at the surface to fall to zero after a pulse is applied is given by equation 3.8, with $C_O = 0$. In addition, the thickness of the pulsed diffusion layer is obtained substituting t in equation 3.7 by $t_{on}$ (VANAGS; KLEPERIS; BAJARS, 2012) (IBL, 1980):

$$t_{C_O=0} = \frac{D_O C_O^{*2} (nF)^2}{2i^2} \tag{3.35}$$

$$\delta_{pulsed} = 2\sqrt{D_O t_{on}} \tag{3.36}$$

One of the first studies using potential pulses was made by Tseung & Vassie (1976). To study the effects of bubbles in porous electrodes, the authors compared the value of the current at a) DC power b) pulsed power with a width of 100 $\mu$s. The pulse width was chosen in order to be much higher than the EDL charging time, and therefore, not be influenced by it, but to be lower than the time for bubble formation. The current at the pulse case was considered to be the current value when bubbles are not present. The result was that the pulsed power presented a current value between 2-10 times higher than the DC current value at the same voltage. Nevertheless, in their research, only one pulse was used. The next step would be to see how much time the bubbles need to detach in presence of a forced flux and then, apply the following pulse after this time, always maintaining a high current density. The authors also argued that at low current densities, the hydrogen produced by electrolysis can be dissolved in the electrolyte and

escape the pores of the electrode by diffusion. However, at higher current density, bubbles are formed. The creation of bubbles pushes the electrolyte far from the surface of the electrode and reduce the active surface area and the performance of the electrode. Under this condition, the reaction can still occur at the entrance of the pores, but not in their interior. Bubbles detach from the surface just when the pressure is equal to (TSEUNG; VASSIE, 1976):

$$P = 2\sigma cos\theta / r \tag{3.37}$$

With $\sigma$ the electrolyte's surface tension; $\theta$ the contact angle; and r the radius of the pores (TSEUNG; VASSIE, 1976).

Ghoroghichian & Bockris (1985) carried out some experiments in water electrolysis with triangular pulses on a rotation disc in a magnetic field. The pulses width was 600$\mu$s and the mean potential was of 2.6V. The double layer charging time was estimated to be approximately 140$\mu$s. Hence, the pulse lasted for five times the charging time. The authors discovered that the formation of bubbles depends on the duty cycle. Duty cycle is defined as the time at which the pulse is on divided by the total period of the pulse. For a $t_{off}/t_{on}$ ratio higher than 10, no bubbles were observed, while for ratios lower than 2, bubbles were visible. Furthermore, a model to calculate the current due to a triangular potential pulse was proposed (GHOROGHCHIAN; BOCKRIS, 1985):

$$i_p = i_{max} exp(-kt) \tag{3.38}$$

Where $i_p$ is the actual pulse current, t is the time, k is a time constant, and $i_{max}$is the current peak value. Comparing with equation 3.4, $i_{max} = E/R_S$ and $k = 1/(R_S C_D)$. In addition, if there is a succession of n pulses:

$$i_p = i_{DC} + \frac{i_{max}}{k\tau}[1 - exp(-k\tau)] \tag{3.39}$$

With $i_{DC}$ the DC current value and $\tau$ the pulse width. The ratio obtained in their experiment was two, meaning that a pulsed power was able to produce hydrogen twice as fast as DC electrolysis (GHOROGHCHIAN; BOCKRIS, 1985).

Shaaban (1994) applied potential pulses to 3D electrodes made of a dispersion of

spherical ultramicroelectrodes. 3D electrodes were used because they caused an increase in hydrogen production rate per cell volume within 1 or 2 orders of magnitude greater than 2D electrodes. In this case, frequencies varied from 10Hz to 40KHz and the duty cycle went from 10-80%. Duty cycle is the ratio between $t_{on}$ and the pulse period. To illustrate, a duty cycle of 50% means that the time at which $E = E_{on}$ is equal to the time at which $E = E_{off}$. The electrolyte was a solution containing 10wt% sulfuric acid. A change in the current polarity during $t_{off}$ was noticed, which was attributed to a reversible reaction going backward. To prevent this counter current, the authors used a diode, nevertheless, the diode maintained the potential during the $t_{off}$ at 2.3V instead of 0V. $E_{on}$ went from 3.5-14V. A phase difference between current and potential was observed, which indicates an inductive system, agreeing with the conclusions of Mazloomi K. et al (2003). There was also a high voltage drop between the applied voltage and the cell's voltage, caused by inductive reactance. This voltage drop was given by (SHAABAN, 1994) (MAZLOOMI et al., 2013):

$$\Delta V = -L_w \frac{di}{dt} \tag{3.40}$$

Where $L_w$ is the wire inductance. Since $\frac{di}{dt}$ was high, the voltage drop was also high. This voltage drop also changed the shape of the potential pulse, going from a square in the power supply to a sinus curve in the cell. Contrary to the previous works, the charging EDL current was not observed. Furthermore, it was found that non-pulsed DC power presented better efficiency than pulsed power and that increasing frequency increases efficiency. In addition, efficiency was better for higher duty cycles. Finally, when the diode was used, current continued to flow during $t_{off}$, but this phenomenon was not attributed to the EDL discharge, but to the collapse of magnetic fluxes around the leads that connects the cell to the power supply (SHAABAN, 1994).

Shimizu, Hotta, Sekiya, & Oda (2006), studied pulses with a width of 300ns in alkaline water electrolysis. The pulse width was chosen in order to be significantly lower than the time for the formation of the EDL and of the Nernst diffusion layer. The time for the formation of the diffusion layer was given by (SHIMIZU et al., 2006):

$$t = \frac{1}{4D_O}\left(\frac{X_{ad}}{X}\right)^2 \tag{3.41}$$

Which is exactly equation 3.9 with $\delta_{max} = \frac{X_{ad}}{X}$. $D_O$ is the diffusion coefficient; $X_{ad}$

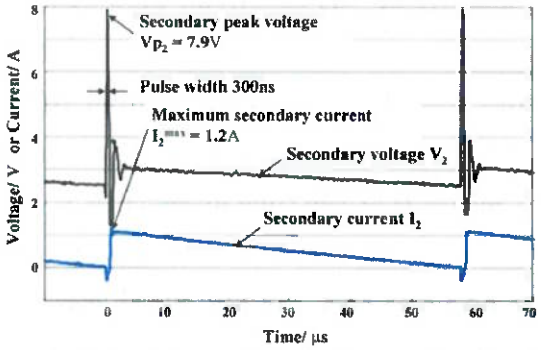


Figure 14: A typical example of pulse waveforms for the experiment of Shimizu, Hotta, Sekiya, & Oda (2006) (SHIMIZU et al., 2006)

is the density of hydrogen ions on the cathode ($cm^{-2}$); X is the concentration of hydrogen ions in the bulk ($cm^{-3}$). For proton diffusion ($D_O$=2.3x$10^{-5}$ $cm^2$ $s^{-1}$), 1M of KOH (X=6.$10^{20}$$cm^{-3}$), and platinum electrode ($X_{ad}$=$10^{15}$$cm^{-2}$); the diffusion layer formation time is equal to 3$\mu$s. Any pulse with a width below this value will not give time for the complete formation of the diffusion layer (SHIMIZU et al., 2006). According to Vincent et al. (2018) the time for the formation of the Nernst diffusion layer is in the order of 2s for 3D nickel hydroxide (anode)/Metal hydride (cathode) electrodes in a solution of 6M KOH. Returning to Shimizu, Hotta, Sekiya, & Oda (2006), the time for the formation of a stable EDL was considered to be several tens of milliseconds. DC power was also applied as a control. The $E_{on}$ voltage varied from 7.9-140 V with a frequency between 2—25 kHz. A typical pulse with $E_{on}$=7.9V can be seen in figure 14. The results have shown that at DC power, the increase in voltage also increases current and production rate, but decreases efficiencies. Nevertheless, contrary to DC, in the pulsed power case, the production rate was decreased when $E_{on}$ was increased. In the case of low $E_{on}$ (7.9V and 9.7V), the efficiency increased with the increase of the pulse frequency (maintaining pulse width=3$\mu$s), as can be seen in figure 15. In the case of pulses with $E_{on}$=7.9V and frequency of 17KHz, the efficiency was higher than DC. At DC. the reduction in efficiency with the increase of voltage occurs because a more energetic electron can reduce only one hydrogen. The surplus of energy between the applied voltage and the decomposition voltage is dissipated as heat, reducing efficiency. In addition, the electrons that do not participate in the reaction also lost energy as heat. This logic is not applied in pulsed electrolysis, because, as the authors proposed, while DC electrolysis is based on electrical double layer formation and is a diffusion-limited process, pulsed power electrolysis is an electron transfer limited process. As a consequence, production rate and power can be increased (increasing frequency) without a decrease in efficiency (SHIMIZU et al., 2006).

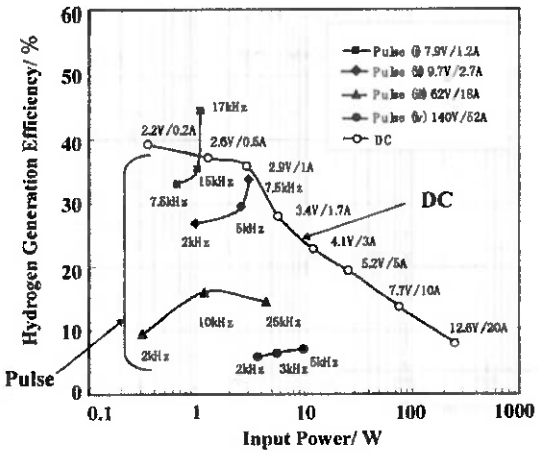


Figure 15: Hydrogen generation efficiencies as a function of power for the experiment of Shimizu, Hotta, Sekiya, & Oda (2006) (SHIMIZU et al., 2006)

Demir, Kaya & Albawabiji (2018) also conducted experiments with pulses in alkaline water electrolysis. The authors used 10wt% and 15wt% KOH solution. The $E_{on}$ values applied were 6V, 8V and 10V. Two duty cycles were used: 10% and 50%. The frequencies varied between 0.1Hz-500KHz for 10% duty cycle ($t_{on}$: 0.2$\mu$s-1s) and between 0.1Hz-1200KHz for 50% duty cycle ($t_{on}$: 0.43$\mu$s-5s). The authors concluded that the energy consumption to produce one mole of hydrogen could be decreased between 20-25% if the pulses were applied. Another conclusion was that, at 50% duty cycle, hydrogen production rate may be improved with frequency. This improvement was attributed to the relaxation time of the bubbles on the surface of the electrode (which enhanced diffusion of dissolved gases), and to the pumping effect created by the pulse potential in the bubbles. The authors claim that the method also improves the electrode's lifetime since it reduces the contact with oxygen bubbles at the anode. Another result was that the hydrogen flow rate has always decreased when pulses were applied. Furthermore, lower duty cycles presented lower energy consumption per mole and a lower production rate (DEMIR; KAYA; ALBAWABIJI, 2018). Some of the results can be seen in figure 16, where it is clear that the pulses increased efficiency and reduced production rate.

Huang (2013) studied the effects of pulses in the electrolysis of ammonium sulfite solution. As in water electrolysis, hydrogen is produced at the cathode, which changes, however, is that oxygen is not produced at the anode, but $SO_4^{2-}$, from the oxidation of $SO_3^{2-}$. He noticed that at the microsecond scale, the rate of DC electrolysis was not constant. This observation indicated that the rate of electrolysis was controlled by electrolyte

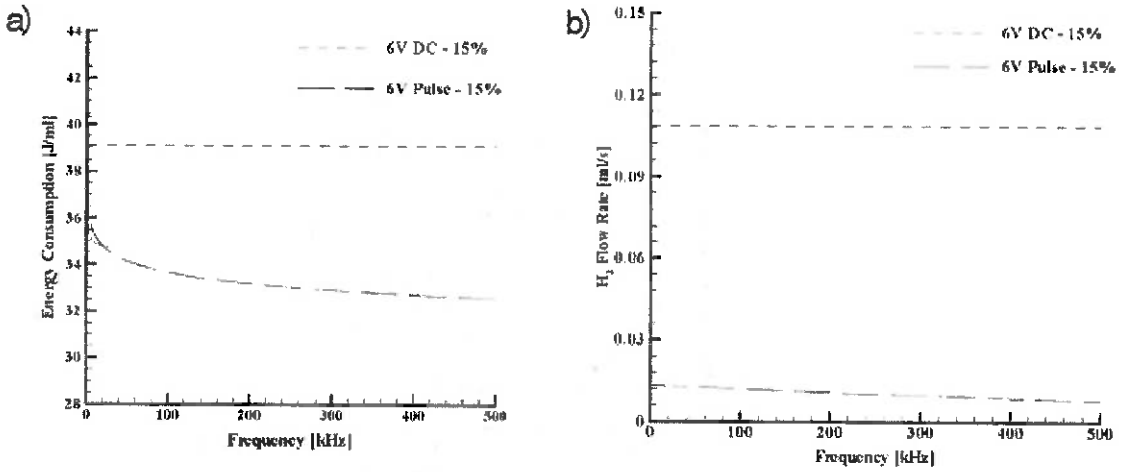


Figure 16: 15% KOH solution in 6 V 10% Duty Cycle a) Energy consumption (J/ml) b) Hydrogen production flow rate (ml/s). Modified from (DEMIR; KAYA; ALBAWABIJI, 2018)

transfer rate, as a consequence, pulses were applied to try to improve this transfer. In his experiment, the pulse width was 10ms and the duty cycle was between 12.5% and 50%. $E_{off}$ was zero and $E_{on}$ changed between 0.6-1.2V. The conclusion was that if pulses are applied, the voltage $E_{on}$ can be lowered to achieve the same current density from DC. As an example, to reach a current density of 180 mA/$cm^2$, DC electrolysis needed a cell potential of 1.26V. In the case of pulses with 50% duty cycle and a frequency of 50Hz, an average current of 180mA/$cm^2$ was obtained with a $E_{on}$ of only 1.2V, meaning an average voltage value of 0.6V. It also means that for the same hydrogen production, one consumes half of the power, showing an energy saving of 50% and a significant increase in electrolysis efficiency. This example can be seen in figure 17. The improvement in electrolysis was attributed to mass transfer since when voltage is interrupted, the $SO_3^{2-}$ reactant migrates to the anode's surface and its concentration builds up to its initial value, and just then, another pulse is applied. Thereby, electrolysis occurs always at maximum reactant's concentration on the surface of the electrode, minimizing the overpotential of the electrolysis (HUANG, 2013).

Lin & Hourng (2014) studied the effects of pulsed potential and magnetic field in water electrolysis. Regarding the pulses, their width varied from 10-90ms with a duty cycle between 10-90%, $E_{on}$ between 3.5-4.5V, and $E_{off}$ between 0-4.5V. It was argued that when voltage is on, the reaction occurs and creates a difference in concentration. During the $t_{off}$, diffusion replenishes ions that were consumed in electrolysis. This argument justifies the results obtained: increase in current density and in efficiency. Part of the results

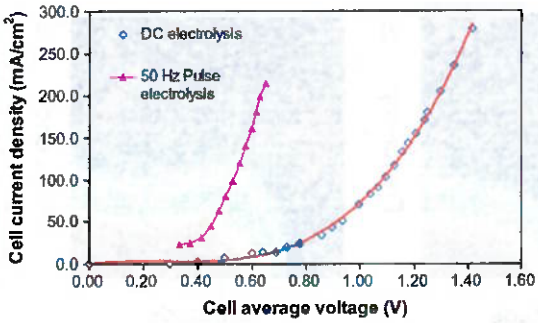


Figure 17: Polarization curves for DC and 50 Hz pulse electrolysis (HUANG, 2013)

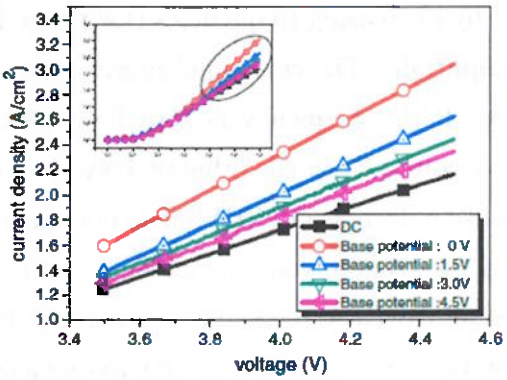


Figure 18: Polarization curve for pulse width=10ms and different $E_{off}$ (base potential) (LIN; HOURNG, 2014)

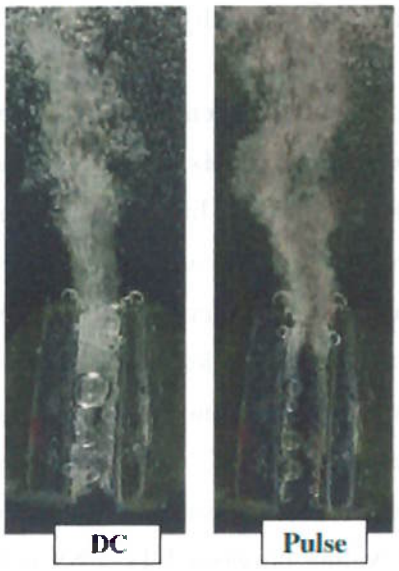


Figure 19: Bubbles produced with electrode distance=2mm, $E_{on}$=4.0V, and $E_{off}$= 0V (LIN; HOURNG, 2014)

can be seen in figure 18, where it is noticed that at the same voltage, pulsed electrolysis obtained higher currents, especially for low $E_{off}$. In addition, with the help of a video camera, it was observed that the pulses caused: (a) an increase in the concentration of gas in both electrodes, (b) a decrease in the thickness of the gas diffusion layer, (c) a faster bubble rise from the surface of the electrode. These results are shown in figure 19 (LIN; HOURNG, 2014).

Dobó & Palotás (2016b) studied the effects of the fluctuations in DC power in alkaline water electrolysis. The voltage varied in a sinusoidal shape around an average value. The average voltage (DC component) was between 1.4-2.8V, while the ripple amplitude went from 0-2V. The pulse frequency varied between 1-5000Hz. The results show that the

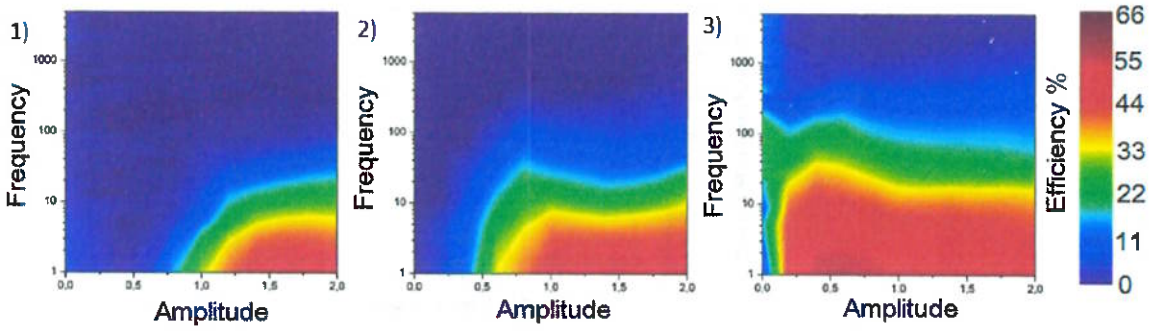


Figure 20: Cell efficiency as a function of signal parameters (frequency (f), amplitude (a), and DC offset). Average voltage value 1) 1.4V 2) 1.6V 3) 1.8V. Adapted from (DOBÓ; PALOTÁS, 2016b)

produced hydrogen flow can be improved by decreasing frequencies (for ripple frequencies lower than 1000Hz) and by increasing amplitude. The consumed power increases mainly with amplitude, but also with frequency. If the frequency is kept low, LHV efficiency increases by increasing amplitude, up to a voltage average value of 1.8V. For voltage average values higher than 2V, all pulses cause a decrease in LHV efficiency. As can be seen in figure 20, efficiency could be improved for average voltage values between 1.4V-1.8V, low frequencies and high amplitudes. For all the cases, consumed power was increased in comparison to DC power. The production rate was increased for low frequencies and high amplitudes. To sum up, the study has shown that sinusoidal pulses with average voltage values between 1.4V-1.8V can improve efficiency for frequencies lower than 30-200Hz, corresponding to a pulse width higher than 33-5ms (DOBÓ; PALOTÁS, 2016b).

Still in the domain of power fluctuations, the same authors studied the effects of current fluctuations in water splitting. The applied current varied around a mean value in different shapes: sinusoidal, triangular, saw-tooth, and square. The mean current density went from $1000A.m^2$ to $5000A.m^2$ (corresponding voltage between 2.1-2.9V), with frequencies going from 1Hz to 10kHz. Amplitude went from zero to twice the average value. The main conclusion was that any change from steady DC power causes a decrease in energetic efficiency. According to the authors, this decrease happened because the current fluctuations increased the consumed power while the hydrogen production rate was the same (DOBÓ; PALOTÁS, 2016a).

Vincent et al. (2018) carried out experiments with alkaline pulsed electrolysis using three-dimension electrodes. This time, instead of potential pulses, current square pulses were applied going from zero to a value between 0.1-0.6$Acm^{-2}$, which promoted a voltage

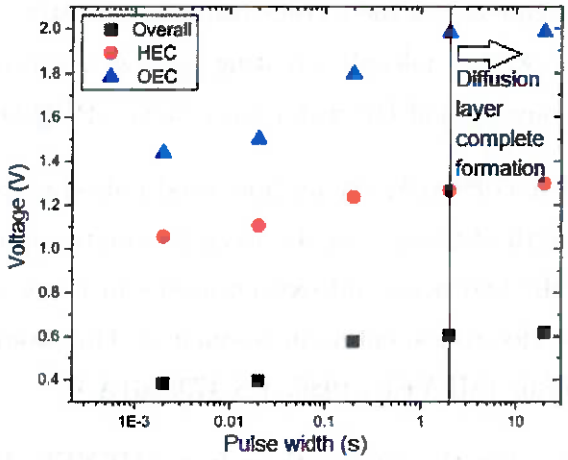


Figure 21: Pulse width-voltage profile for anode (blue); cathode (red); and total reaction (black) for a current density of 0.1 A.$cm^{-2}$. There is a decrease in the voltage for pulse widths lower than 2s. Adapted from (VINCENT et al., 2018)

in the range of 1.4-3.2V. The frequency varied from 0.05-500Hz (pulse width: 2ms-20s). The results have shown that the potential could be lowered by the use of pulses. The efficiency was increased with pulse frequency. The ohmic resistance was also calculated and the conclusion was that it was higher for lower frequencies. These results were attributed to the reduction in the thickness of the pulsed diffusion layer, caused by the fast pulses (equation 3.7). As a consequence, ions had time to diffuse back at the surface of the electrode, restoring the concentration to its value from before the pulse's application, and in this way, reducing the diffusion layer losses and the cell overpotential. The results can be seen in figure 21, where it can be seen that when $t_{on}$ is lower than 2s the voltage, at constant current, is reduced (VINCENT et al., 2018).

In the domain of patents, there are some related to the application of pulses:

- Patent US 3954592 for alkaline water electrolysis with pulsed DC at a frequency between 83-667Hz, duty cycle of 0.6%, and $E_{on}$=3V. The authors claimed to have achieved a more efficient hydrogen production due to the creation of a strong magnetic field during the pulse application. The anode was a cylinder and it was surrounded by the cathode. The magnetic field created between these two electrodes would increase the mobility of ions (HORVATH, 1976. US 3954592.).
- In the patent US 4394230A, the authors claim to have shifted the bond angles of water molecules from 104° to 109.28° by the application of pulses with the same

resonance frequency of the tetrahedral form of water. Then, by resonance, the pulse shatters the water molecule, creating hydrogen and oxygen gas in a more efficient way than conventional DC water electrolysis (PUHARICH, 1983. US 4394230A.).

- In patent US 4798661A, the authors used pulsed power with a frequency matching the wavelength of the spacing between two plates oppositely charged. The physical motion of the hydrogen and oxygen atoms in the water molecule, being attracted by different electrodes, enters in resonance. This would enhance the dissociation of water molecule (MEYER, 1989. US 4798661A.).

- Three years later, the same authors from (MEYER, 1989. US 4798661A.) obtained the patent US 5149407A. They put a capacitor in water and applied a pulsating voltage to induce resonance within water molecules and exceed the bonding forces of water (MEYER, 1992. US 5149407A.).

- In the case of patent US 6419815B1, the authors used a pulsed signal with a frequency between 10-250KHz in a solution with tap water, $E_{on}$=12V, and 10% duty cycle. They claim to have achieved a more efficient process (CHAMBERS, 2002. US 6419815B1.).

# 4 MATERIALS AND METHODS

Two main experiments were carried out: pulsed chronoamperometry varying potential, and pulsed chronoamperometry with fixed potential and hydrogen collection. Different electrolyte fluxes were applied, going from natural convection (no forced flow) to maximum pump flow. Three pulse widths were analyzed: 100ut, 10ut, and 1ut, where ut means unit of time. With the data collected in experiments, a model fitting was made and its fitting parameters analyzed.

The setup used in the experiments is seen in figure 22. There were two pumps (in blue in figure 22), one for the cathode and the other for the anode, to promote a forced electrolyte flow. The power of each pump and consequently the flux was controlled by the shifters highlighted in yellow. The electrolyte solution was stocked in two drums (in red). The volume of solution in each drum was 1 liter. The electrolytic solution consisted of potassium hydroxide 1 mol/L and was prepared by adding 56.11 g of KOH pellets in 1 liter of de-ionized water. The potassium hydroxyde was chosen because it is the most commonly used salt for water electrolysis (ZENG; ZHANG, 2010). Furthermore, the purity of water is crucial, since impurities can accumulate in the porous of the electrode and ions like magnesium, calcium and chloride can cause side reaction. In our 1M KOH solution, concentrations of $Mg^{2+}$ higher than 1.8 x $10^{-11}$ M or $Ca^{2+}$ higher than 5.5 x $10^{-6}$ M are sufficient for their hydroxyle salts to precipitate. For that it is important that there are no such ions in the composition of the salt. Nevertheless, there are some chloride ions, which can be oxidised at the anode forming the corrosive chlorine gas. Since its concentration is very low, this reaction can be neglected (ZENG; ZHANG, 2010).

The electrolytic cell can be seen inside the green circle. The details of the cell is seen in figure 23, where it can be seen that the cell was prepared stacking different components. The outer layers (1 and 15 in figure 23) consist of supports where two ducts were placed, connecting the reservoir containing the electrolytic solution with the electrolytic

cell. These tubes were connected to the pumps to force a flow, which enters in each side of the cell, going upwards. This flux was used to drag gas bubbles from the electrode surface and to stir the solution.

After this outer layer, there is a metal plate to connect electrically the system (3 and 13). It contains a socket where an external circuit from a potentiostat (power supply) was connected. Then, comes a plastic support (5 and 11) to create a space where the metal electrode (6 and 10) was put. In the middle, there was a membrane, which only permits the passage of ions. The membrane was used to prevent mixing between oxygen and hydrogen as well as to separate the electrodes, creating a barrier for electron migration. In between each of these layers, there was a rubber layer (2, 4, 7, 9, 12, and 14) to prevent friction and deterioration. The electrodes were made of pure Nickel. Nickel electrodes were chosen because they have good alkali corrosion resistance, electrochemical activity for hydrogen and oxygen evolution and price. The inconvenience of Nickel is that it can be deactivated at the cathode in the presence of $H_2$ due to the formation of NiH (ZENG; ZHANG, 2010). The total surface area of each electrode was 353.97 $cm^2$. Before and after every cell assembly, the components were washed three times with de-ionized water.

Figure 22: Eexperimental setup


Figure 23: Components of the electrolitic cell

Even trace quantities of impurities as low as $10^{-10}$ mol/L and the formation of oxides on the electrode's surface can compromise reproductibility in the measurement of electrode

potential (BOCKRIS; POTTER, 1952). Knowing that, before running the experiment, a galvanostatic run at 2A was performed to initiate the cell. During the galvanostatic experiment, nitrogen gas was circulated in the cathode, to remove the remaining oxygen present in the cathode's drum and to avoid explosions. The galvanostatic test was also performed to evaluate the stability of the membrane and to check the maximum voltage value, since the potentiostat is limited to a maximum current of 2A. It can be seen in figure 24a that the maximum voltage values were close to 2.3V. The results also show that there was no increase in potential during the galvanostatic experiment, showing an absence of membrane degradation in the experiment time-scale. After the galvanostatic run, a Cyclic Voltammetry - CV - was applied to guarantee that the only reaction occurring was the water electrolysis. The CV was done at a rate of 0.1V/s from 1.23V to 2.23V. The results can be seen in figure 24b. There were no side reactions and the water electrolysis reaction began at a voltage close to 1.7V. After the galvanostatic and the CV, the power supply imposed potential pulses in the form of squares, as shown in figure 25. A reference electrode was not used since in the chosen electrode the potential and current presents spacial variations. As a consequence, depending on the location where the reference electrode is put, the result is different. To avoid that, it was decided to work with the total current and total voltage between the cathode and the anode, which, at the end of the day, is how the companies measure their consumed electricity and how their electricity bill is calculated. All the experiments were performed at room temperature (~21°C) and all the necessary algorithms and codes were developed using MATLAB ©.

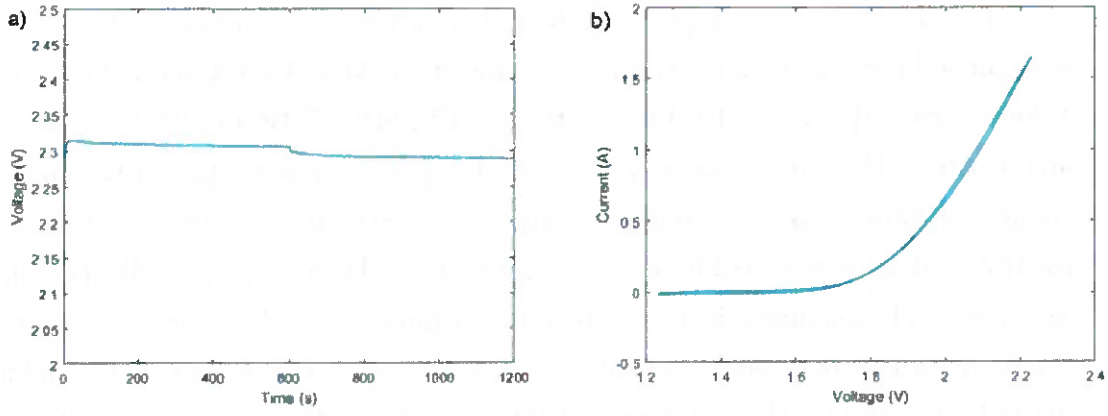


Figure 24: Galvanostatic and CV from water electrolysis 1M KOH, C10A10. a) Galvanostatic 2A; b) Cyclic Voltammetry (scan rate=0.1V/s).

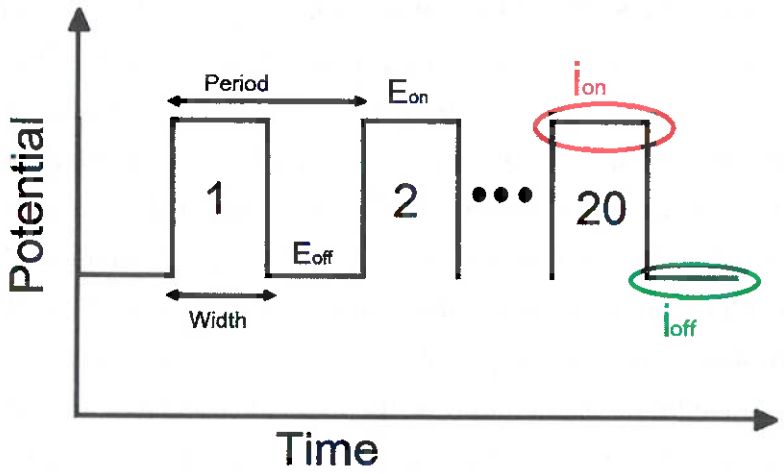


Figure 25: Representation of the applied voltage pulses, showing: $E_{on}$; $E_{off}$; Pulse period; Pulse width. The currents' average was calculated in the last $E_{on}$ and the last $E_{off}$, as represented here.

## 4.1 Pulsed chronoamperometry varying potential

In this first experiment, $E_{off}$ was fixed at 1.23 V, which is the standard potential for water electrolysis, and $E_{on}$ started at 1.33 V (overpotential of 0.1 V) and 20 pulses were applied. Then, $E_{on}$ was increased to 1.43 V and 20 subsequent pulses were produced. This process continued in steps of +0.1V until reaching an overpotential of 1 V ($E_{on}$=2.23 V). Here, overpotential is defined as the difference between the actual potential and the standard cell potential of 1.23 V. The power supply limited the maximum voltage at 2.23 V, since it was incapable of giving 2.33 V neither at 100 ut pulses nor at 10 ut. This took place because the power supply is limited at a current maximum of 2 A, as previously seen. In addition, the nominal voltage for commercial AEL electrolyzers is between 1.7-2.1 V for a current density of 0.4 A.cm$^{-2}$ (BUTTLER; SPLIETHOFF, 2018), so it is reasonable to study $E_{on}$ within this range. Then, the process was re-started two more times, completing three loops. Two different pulse periods were tested: 100 ut and 10 ut. Three electrolyte flows were tested for each electrode: natural convection, middle flux, and maximum flux. The maximum is defined by the maximum power the pump could provide. All the combinations of cathode and anode flux were tested, this means: nine combinations per pulse frequency. The terminology C0A5 indicates natural convection in the cathode and middle velocity in the anode, while C10A10 indicates maximum flow in both. The values for the flows were measured calculating the time needed to fill a graduated cylinder.

The first time the experiment was made, inadvertently, a wrong membrane was used.

The wrong membrane was not adapted for the environment of 1 M KOH, but for an a environment much more alkaline. Consequently, the membrane imposed a very high resistance so the recorded current values were far below the expected, as shown in figure 26. When there was no forced flux in either the cathode or the anode (figure 26a), the current was very low, in the order of $10^{-3}$ A, while it increased a hundred times when a forced electrolyte flow was imposed (figure 26b). The values obtained with the good membrane were much higher, thus, they are the values that will be presented in the results. Nevertheless, the results obtained using the incorrect membrane already gave some hints regarding the behaviour of the electrolitic cell when pulses are applied. Most of the results were replicated when the good membrane was used. Even if the order of magnitude was different when the appropriated membrane was used, the fashion of these curves and the best results for forced flux were similar, as will be shown in detail in the following chapter.

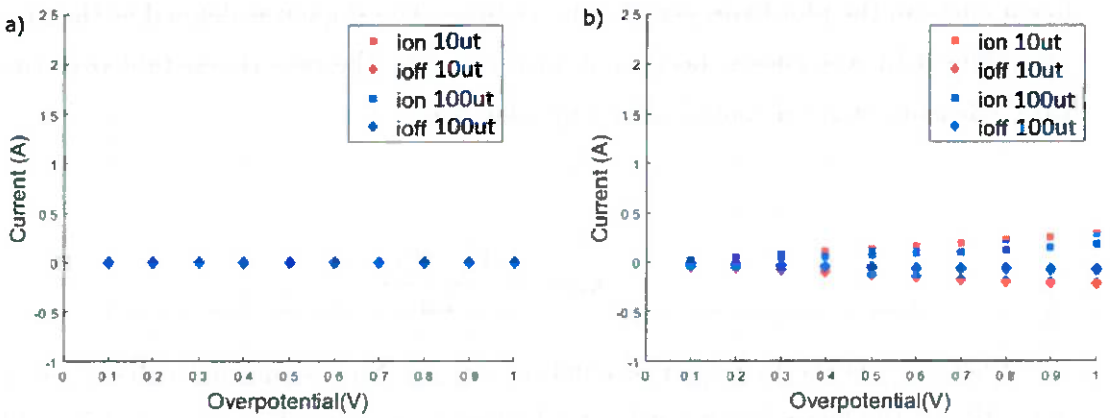


Figure 26: Polarization curves for the wrong membrane for the case of a) natural convection b) forced flux C5A5

## 4.2 Pulsed chronoamperometry with fixed potential and hydrogen collection

The setup used for this experiment was the same as in pulsed chronoamperometry varying potential. The only difference was that in this case a graduated cylinder (purple in figure 22) was used to measure the volume of hydrogen produced. Even though the setup was more or less the same, the method was different. Here we kept $E_{off}$=1.23 V, however, $E_{on}$ was fixed at 1.93 V. Furthermore, this experiment took more time. To evaluate the efficiency of hydrogen production, pulses were applied for 20min. The variables that were changed were: the electrolyte flow and pulse frequency. The hydrogen volumetric pro-

duction was measured. For that, at each increase of 5 ml in the total hydrogen volume, the time was recorded, up to a maximum volume of 30 ml. The same combinations of fluxes as in the latter experiment were tested, going from natural convection to maximum pump power, passing through middle power. Here, three pulse widths were evaluated: 100 ut, 10 ut, and 1 ut. These pulses were compared with the results obtained from an experiment using direct current, DC, at 1.93 V. Again, the combination of flows which will be presented are: C0A0, C5A5, and C10A10.

## 4.3 Analysis factors

Three main factors were used for the analysis: hydrogen production rate, LHV efficiency and Faraday efficiency. The hydrogen production rate was calculated fitting a linear curve in the plot hydrogen volume vs time. The slope was defined as the production rate. Linear fit was chosen because it was seen that the rate is constant over time. The LHV efficiency was calculated using equation 3.21:

$$\eta_{LHV} = \frac{\dot{V_{H_2}}.H^l_{H_2}}{P_{el}}$$

Where $\dot{V_{H_2}}$ is the hydrogen production rate, in $Nm^3/s$ (normal cubic meter per second); $H^l_{H_2}$ is the lower heating value for hydrogen, meaning the amount of heat liberated in the combustion of one normal cubic meter of hydrogen gas [1.08x$10^7$ J/N$m^3$ (joule per normal cubic meter)]; and $P_{el}$ is the average electrical power consumed (W). The latter was calculated in the same form as in (DOBÓ; PALOTÁS, 2016a), (DOBÓ; PALOTÁS, 2016b), (SHAABAN, 1994), and (SHIMIZU et al., 2006):

$$P_{el} = \frac{1}{T}\int_0^T U.idt \tag{4.1}$$

With T the pulse period, U the instantaneous voltage and i the instantaneous current. Faraday efficiency was calculated dividing the volume of hydrogen produced, measured in the graduated cylinder, by the theoretical value, given by the Faraday's Law of electrolysis: Volume=($V_{molar}$.Charge)/(nF), with charge the integral of current by time, n the stoichiometric electron's coefficient, F the Faraday constant, and $V_{molar}$ the molar volume in the normal conditions of temperature and pressure (22.4 L/mol).

## 4.4 Model fitting

With the results from the experiment of pulsed chronoamperometry varying potential, a curve fitting was made. As we saw in chapter 3, for a quasireversible one electron, one step reaction, in semi-infinite linear diffusion with current being governed by both mass transfer and charge-transfer kinetics, the current-time response is given by the equation 3.28:

$$i(t) = FA(k_f C_0^* - k_b C_R^*) \exp(H^2 t) erfc(H\sqrt{t})$$

Where the coefficients are described in equations 3.29, 3.30, and 3.32. The fitting was performed using this equation with the curve current vs time as the input and $k_f$ and H as output. However, the equation is for analysis in just one electrode. As in the experiment presented here, there is not a reference electrode, it is not possible to separate the reaction in the cathode from the reaction in the anode and so, adaptations were made. The coefficients $k_f$ and $k_b$ are the rate constant for the forward (reduction) and backward (oxidation) reactions, respectively, and are described by equations 3.29 and 3.29. In the adapted model, since there is no reference electrode and the potential was measured between the two electrodes, it was considered that $k_b$ was zero and $k_f$ is now representing an equivalent equilibrium constant related to the rate limiting reaction. $D_O$ is also representing an equivalent diffusion coefficient. H is the ratio between the rate constant and the square of the diffusion coefficient, as shown in equation 3.32. The hypotheses used in the model presented here are the following:

1. All the electrodes have the same area and A is the total surface area of just one electrode;
2. The electrolyte concentration is the same for both cathode and anode, in a way that $C_0^*$=1M;
3. $\eta$ is equal to the potential difference between the electrodes and 1.23V;
4. The rate limiting step is a one electron reaction;

5. The experiments were carried out under isothermal conditions.

An example of a pulse and the correspondent fitting is shown in figure 27. The effect of the change in the fitting parameters can be seen in figure 28. An increase in $k_f$ increases equally all the values of current in the curve current vs time. Increasing H changes the shape of this curve.

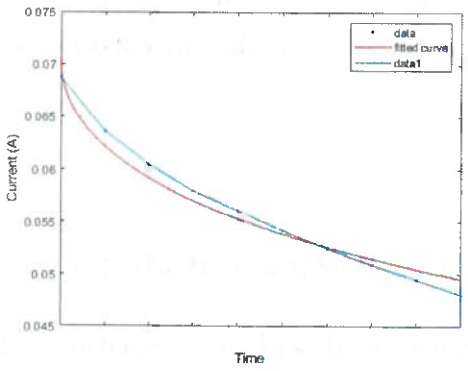


Figure 27: Example of a fitting for pulsed chronoamperometry varying potential C5A5, $E_{on}$=1.5V, f=10ut

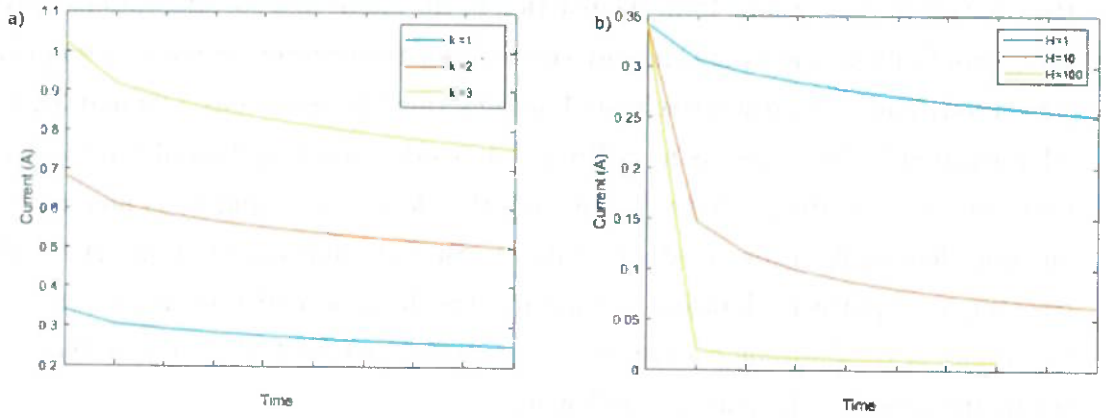


Figure 28: Effect of the change in fitting parameter a) changing $k_f$, in blue $k_f = 1.10^{-4}$, red $k_f = 2.10^{-4}$, and yellow $k_f = 3.10^{-4}$, b) changing H, in blue H=1, red H=10, and yellow H=100

# 5 RESULTS AND DISCUSSION

## 5.1 Pulsed chronoamperometry varying potential

In this section, it will be seen that the results of this experiment indicate that 100ut pulses have a higher LHV efficiency and hydrogen production rate than 10ut pulses. Nevertheless, both the efficiency and the production rate were lower than DC electrolysis. LHV efficiency was calculated using the formula 3.21. In addition, we will see that efficiency increases with $E_{on}$ in pulsed electrolysis. This phenomenon is the opposite of the behaviour of DC electrolysis, where an increase in voltage decreases efficiency.

Figures 29 shows some plots of the mean current versus voltage. The mean current was calculated as a current average at the $20^{th}$ pulse for each $E_{on}$ at the third (and last) loop, as seen in figure 25, with $i_{on}$ the mean current during on-time and $i_{off}$ the mean current at off-time. The existence of a counter current $i_{off}$ confirms the results of Shaaban (1994), where a change in current polarity was also observed during the $E_{off}$ period. $i_{total}$, shown in figures 29b, 29d, and 29f, is the average between $i_{on}$ and $i_{off}$. No difference in the value of the pulse was observed between the loops. In figure 30a one can see that the first pulses at $E_{on}$=1.3V presented different values than the others. After five pulses, the value was stabilized and the fashion of the curve current versus time remain constant. That is why the $20^{th}$ pulse was chosen, as it has been proved to be the most stable and so, representative of the series. For $E_{on}$ higher than 1.3V, the 20 pulses shown the same behaviour, as can be seen in figure 30b. Three electrolyte flows are shown here: C0A0; C5A5; and C10A10.

At natural convection (figure 29a), $i_{on}$ is twice as high for 10ut than for 100ut, however, the absolute value of $i_{off}$ is also much higher. Yet, looking at $i_{total}$ in figure 29b, it can be seen that for overpotentials higher than 0.7V, $i_{total}$ is higher for 10ut. The overpotential is defined as the difference between $E_{on}$ and 1.23V. At lower overpotentials

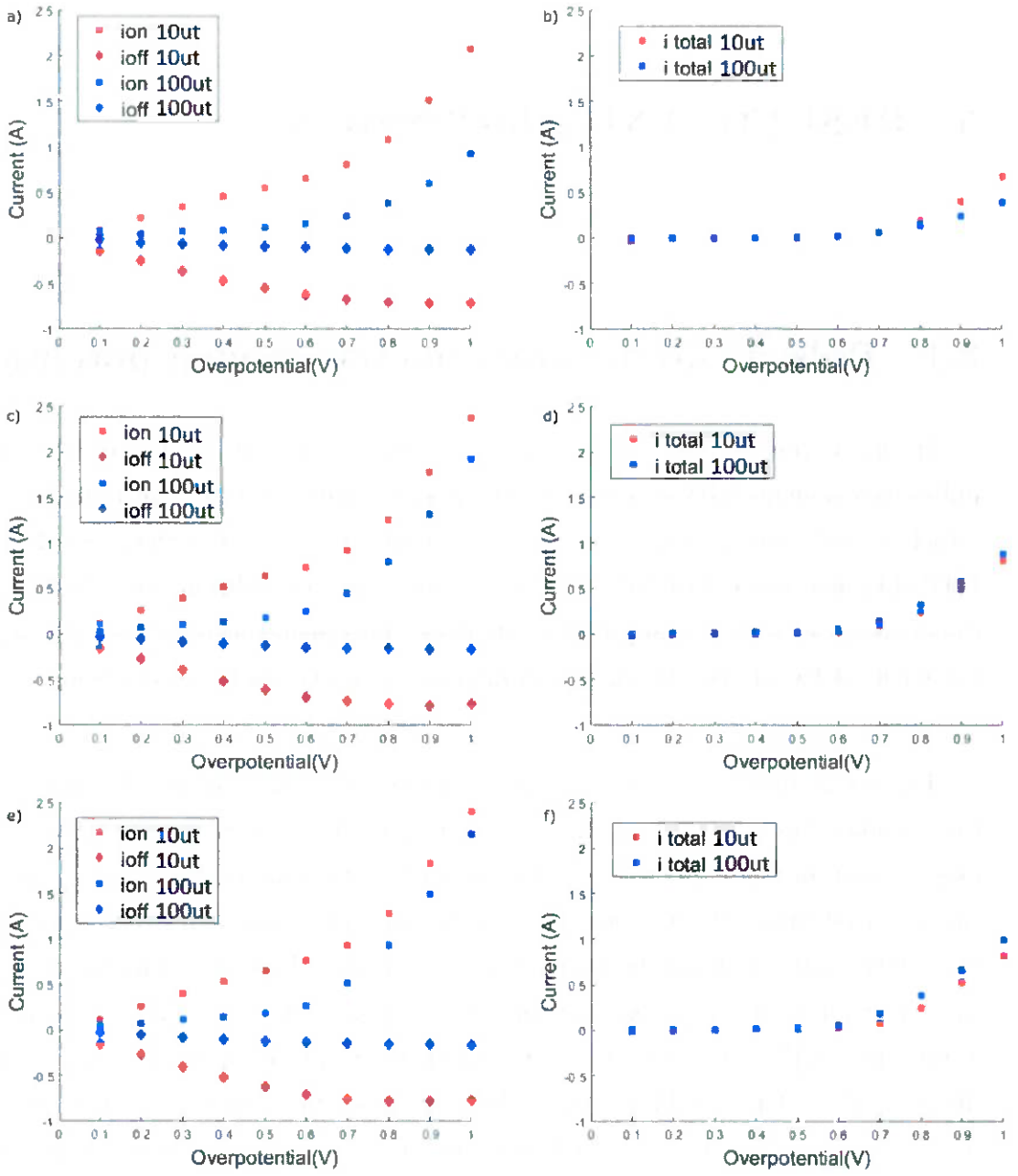


Figure 29: Polarization curves for 100ut pulses (blue) and 10ut pulses (red). The current displayed here is the average in a pulse for each overpotential. a) C0A0 average $i_{on}$ (square) and $i_{off}$ diamond; b) C0A0 average $i_{total}$; c) C5A5 average $i_{on}$ (square) and $i_{off}$ diamond; d) C5A5 average $i_{total}$; e) C10A10 average $i_{on}$ (square) and $i_{off}$ diamond; f) C10A10 average $i_{total}$;

and natural convection, $i_{total}$ is higher for 100ut, as can be seen in figure 31. However, the principal interest here is not for overpotentials lower than 0.7V, as the total current is negligible (figure 29b). It can be stated that for $\eta > 0.6V$ and natural convection (C0A0), pulses at 10ut presented the higher average current. This result, however, was

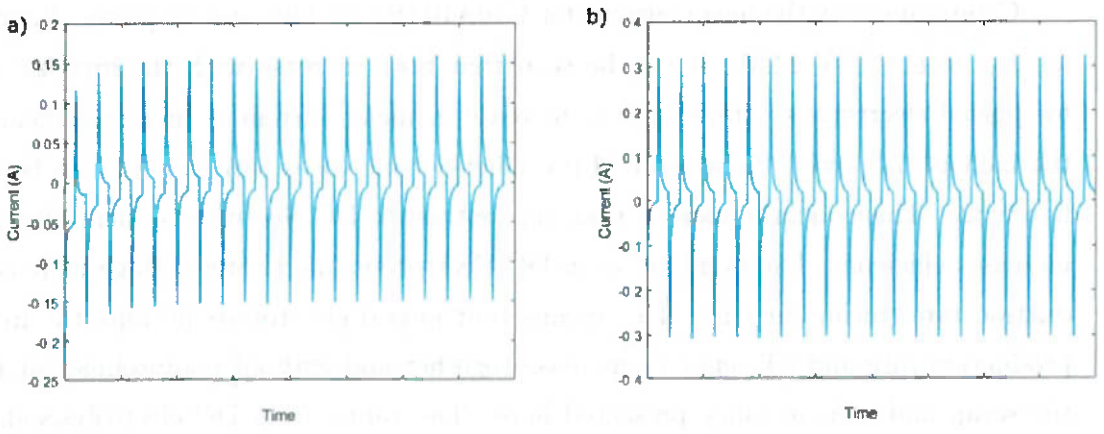


Figure 30: Pulses with a width of 100ut a) $E_{on}$=1.33V; b) $E_{on}$=1.4V. The values in the x-axis were purposely removed due to confidentiality reasons

not replicated in the experiment of pulsed chronoamperometry with fixed potential and hydrogen collection, as we will see further.

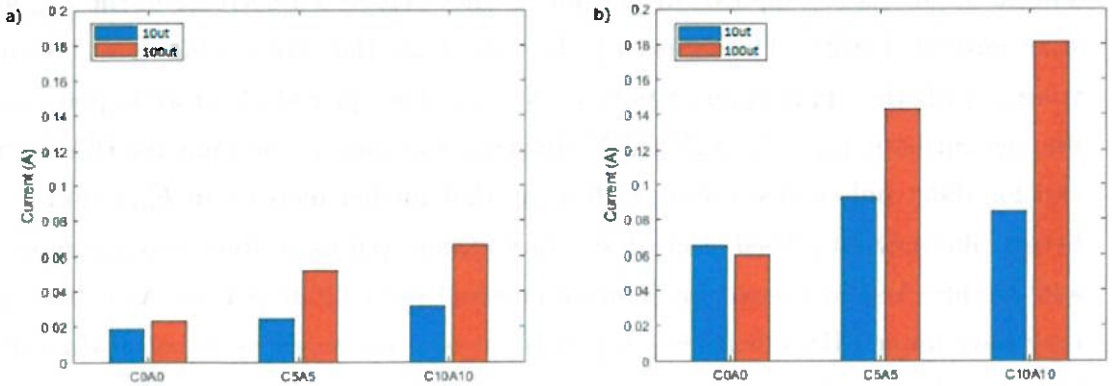


Figure 31: Mean current, $i_{total}$, for 10ut (blue) and 100ut (orange), at a)$\eta$=0.6V, b)$\eta$=0.7V

When there is a forced flow (figures 29d and 29f) $i_{total}$ is higher for 100ut for all the potential interval. Furthermore, increasing electrolyte flow increases mean current, as can be seen comparing the current values for a fixed overpotential (eg. 1V) in figures 29b, 29d, and 29f.

As a conclusion, lower pulse widths (10ut) cause higher $i_{on}$ and higher $i_{off}$. $i_{total}$ was higher for 10ut only at natural convection and $\eta > 0.6$, in all the other cases, $i_{total}$ was always higher for 100ut.

Comparing now the mean current for C10A10 (figure 32b) and its power (figure 32d), for $E_{on}$ from 1.83V-2.23V, it can be seen that both increase with the increase of $E_{on}$, for pulsed electrolysis. However, the increase in mean current is more significant than the increase in power. As a result, LHV efficienct increases with $E_{on}$, as can be seen in figure 32c. This conclusion shows that, on contrast to DC electrolysis, increasing voltage increases efficiency. Furthermore, as in DC electrolysis, increasing voltage increases production rate (mean current). This means that pulsed electrolysis permits the hydrogen production rate and efficiency to increase together and without compromise, at least in the setup and voltage range presented here. The values from DC electrolysis shown in figure 32 comes from the cyclic voltammetry, thus, they are an approximation dependent on the scan rate. In the next experiment, DC electrolysis will be performed during a 20 minutes test at a fixed voltage. It can be seen, in figure 32a, that pulsed electrolysis presents higher on-currents than DC electrolysis and $i_{on}$ increases with frequency, confirming the conclusion obtained by Tseung & Vassie (1976) and Ghoroghichian & Bockris (1985) when they say that current increases by the application of potential pulses. When Vincent et al. (2018) applied current pulses, they achieved a decrease in the $E_{on}$ for constant current density. This is exactly the same logic that gives a higher $i_{on}$ at constant voltage with the application of pulses. Nevertheless, pulsed electrolysis presents lower average currents, $i_{total}$. At 2.2V, LHV efficiency was almost the same for DC electrolysis and for 100ut pulsed electrolysis, indicating that further increase in $E_{on}$ could lead to a better efficiency for pulsed electrolysis. In addition, pulses at 10ut consume more power and produce less hydrogen (lower mean current) than 100ut pulses. As a consequence, they have lower LHV efficiency. A possible reason for pulses with an off-time of 100ut to have a better efficiency than pulses with 10ut can be that in the former case there is sufficient time for the bubbles to detach from electrode surface. Nevertheless, LHV efficiency was calculated here under the assumption of 100% Faraday efficiency, meaning that $V = Q/(nF)$, with V the volume and Q the charge. This is an hypothesis and will be tested in the next experiment, in which hydrogen will be collected. There, we will see that a Faraday efficiency of a hundred is a good approximation.

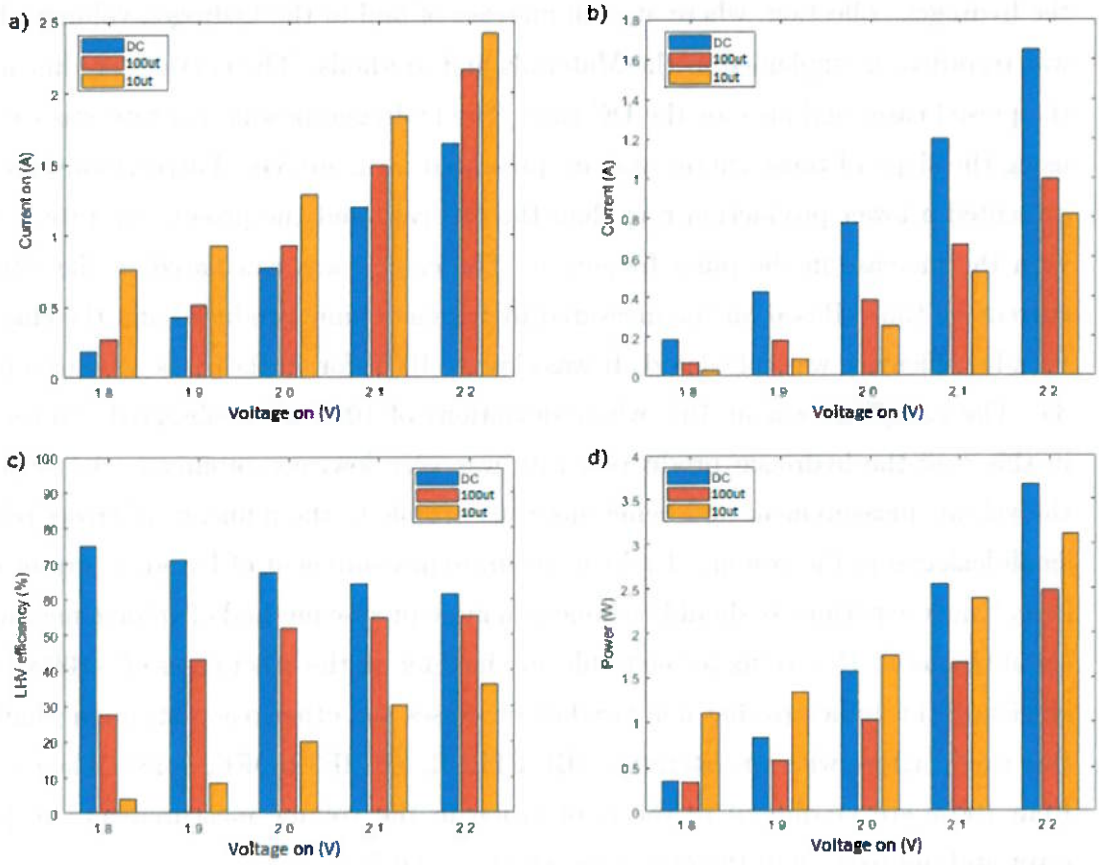


Figure 32: Results from pulsed chronoamperometry varying potential, C10A10: a) Mean values for on-current, $i_{on}$ (A); b) Mean current, $i_{total}$ (A); c) LHV efficiency; d) Power (W). DC (blue); 100ut (orange); 10ut (yellow)

## 5.2 Pulsed chronoamperometry with fixed potential and hydrogen collection

Based on the results obtained in the previous experiment, an overpotential of 0.7V was chosen, since at lower overpotentials, the mean current was practically null, as can be seen in figures 29b, 29d, and 29f. An overpotential of 0.7V means an $E_{on}$=1.93V.

To analyse the effects of the pulses, the case of C5A5 is presented. All the other cases have shown the same behaviour regarding pulses. The results can be seen in figure 33. As observed before, when pulses are applied, higher $i_{on}$ currents are observed, however the negative $i_{off}$ reduces the average current, as can be seen in figure 34b. The higher $i_{on}$ and $i_{off}$ can be seen comparing figures 33a, 33b, 33c, and 33d. In the latter figure, it can be seen that at 1ut, the voltage takes some time to arrive in 1.93V and that current arrives at a maximum of 2.33A. This maximum is limited by the potentiostat. Figure 33e shows the curves hydrogen volume vs time. This curve was plotted from the analysis of

the hydrogen collection, where at each increase of 5ml in the hydrogen volume, the time was recorded, as explained in the Materials and Methods. The curves were linear for all the pulsed cases and also for the DC case. The hydrogen production rate was calculated using the slope of those curves and are presented in figure 34a. Furthermore, the pulses presented a lower production rate than the DC case and the production rate decreased with the increase in the pulse frequency. The charge was calculated as the integral of current by time. Based on the measured hydrogen volume produced and the charge, the Faraday efficiency was calculated. It was close to 100% for all the cases, as shown in figure 35. The exception was at 1ut, where deviations of 100% were observed. Nevertheless, in this case the hydrogen production rate was very low, compromising the accuracy of the volume measurement and being more susceptible to the influence of errors related to small leakages in the system. To do an accurate measurement of Faraday current for this case, longer experiments should be done or a more precise method of volume measurement should be used. Returning to the result obtained for all the other cases of ~100% Faraday efficiency, this indicates that non faradaic processes and other reactions are negligible and this result agrees with the literature (BUTTLER; SPLIETHOFF, 2018). The deviations from 100% are attributed to the imprecision in the volume measurement, by parallax error and imprecision of the graduated cylinder, ±0.5mL.

In the case of the LHV efficiency, it was approximately 72.1%, 40.9%, 7.3%, and 0.2% for DC, 100ut, 10ut, and 1ut, respectively (figure 34c). The results for DC agrees with the literature. Buttler & Spliethoff (2018) estimate a LHV efficiency between 55-75% for DC alkaline water electrolysis. The decrease in efficiency when pulses are applied is a consequence of the power consumption when E=$E_{off}$. In this situation, the reaction goes backwards, consuming electricity and products. As a result, energetically, it was not favorable to introduce pulses. To avoid the negative currents produced when E=$E_{off}$, a diode could be placed in the system, as done by Shaaban (1994), Ghoroghichian & Bockris (1985), Shimizu, Hotta, Sekiya, & Oda (2006), Vincent et al. (2018), and Vanags et al (2012). However, the use of a diode will increase the $E_{off}$ and so, can cause other consequences in the electrolysis process. To sum up, it was not advantageous to introduce pulses, since the energetic efficiency and the production rate had been decreased.

Examining now the effects of a forced flux, one can see that it increases the hydrogen production rate and the average current, as shown in figure 34a and figure 34b, respectively, especially for DC. As observed previously, LHV efficiency decreases with the

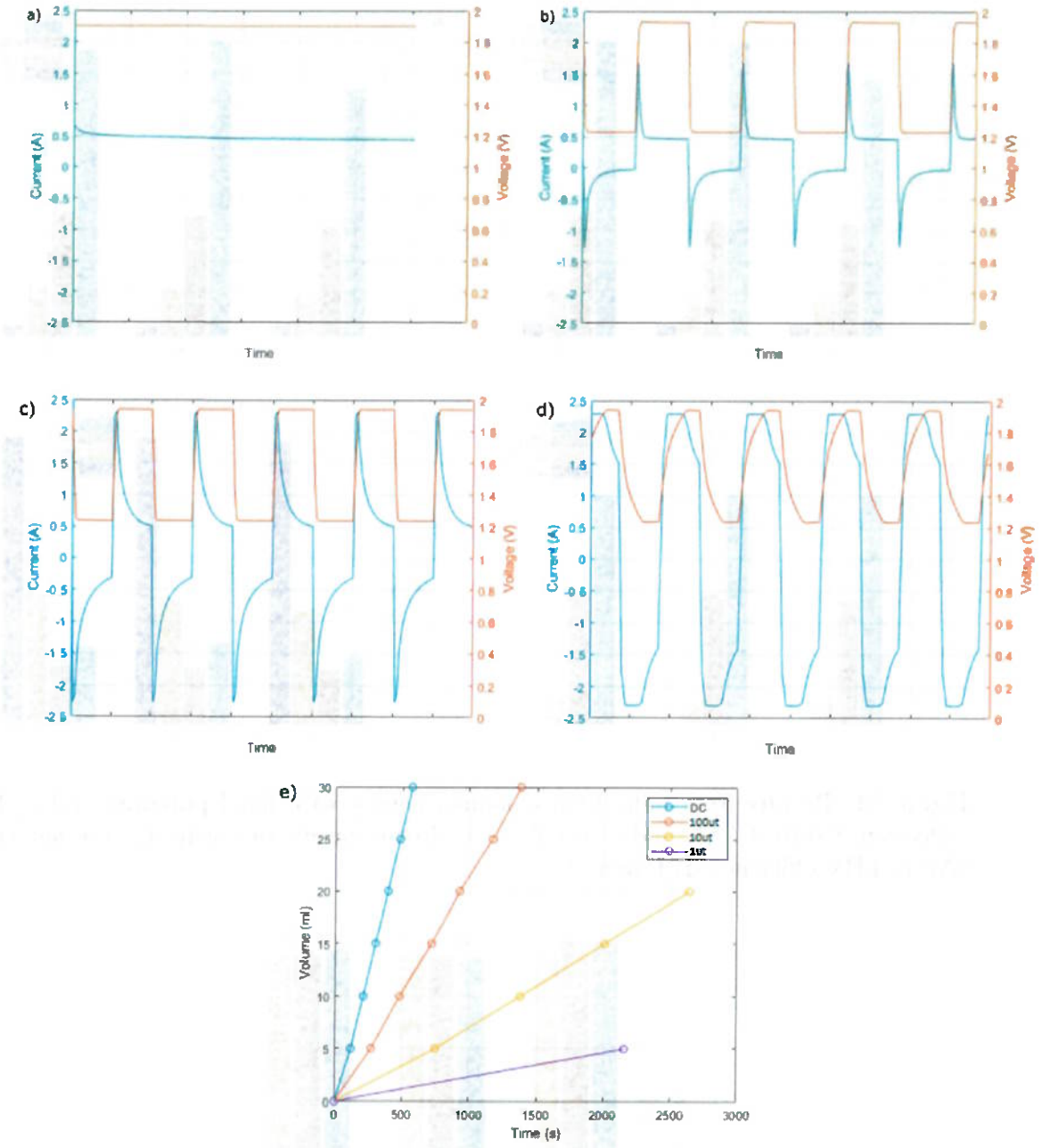


Figure 33: Results from pulsed chronoamperometry with fixed potential and hydrogen collection, C5A5: a) Current-time behaviour for DC; b) Current-time behaviour for 100ut pulses; c) Current-time behaviour for 10ut pulses; d) Current-time behaviour for 1ut pulses; e) Produced hydrogen volume vs time. The values of time in the x-axis of a), b), c) and d) were purposely removed due to confidentiality reasons

introduction of pulses (figure 34c) and with their frequency. The effects of the forced flow were minor compared to the effects of the pulses. Nevertheless, LHV efficiency slightly increases with the increase of forced flux, especially in pulsed electrolysis. For DC, the efficiency hardly changed, while for 100ut pulses, it went from 39.0% at natural convection

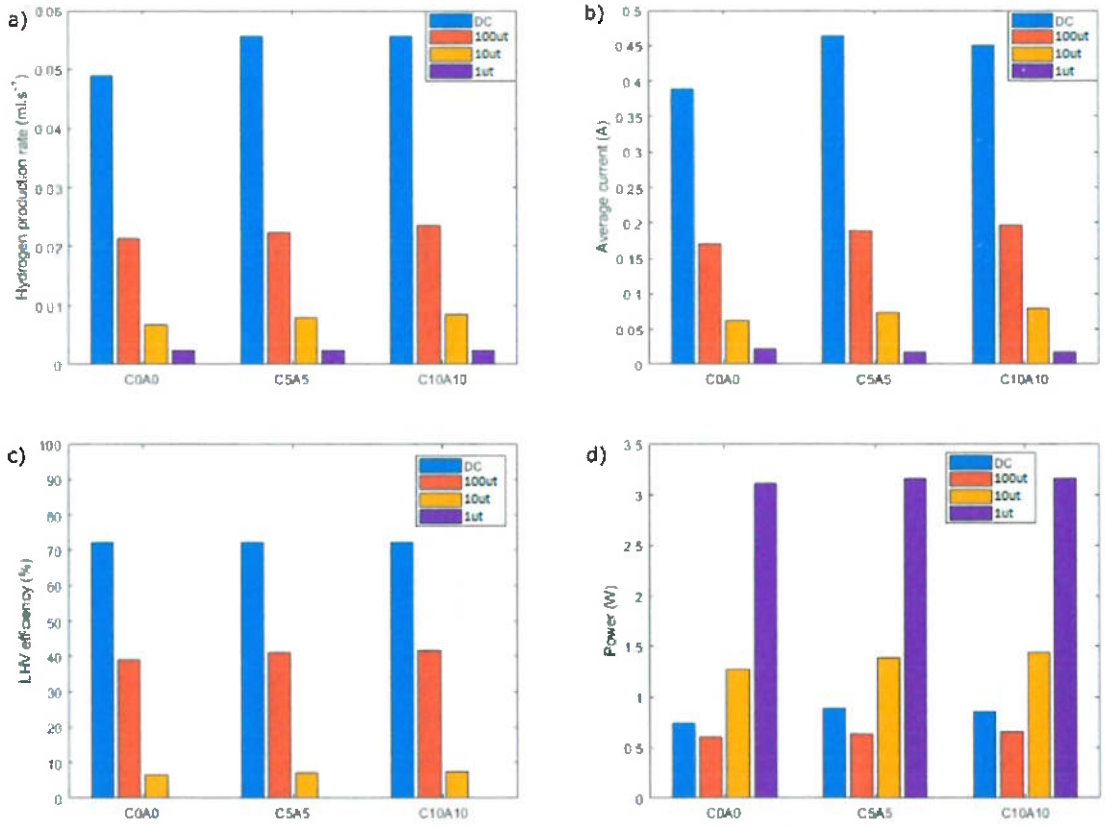


Figure 34: Results from pulsed chronoamperometry with fixed potential and hydrogen collection, C0A0, C5A5, and C10A10: a) hydrogen production rate; b) Average current (A); c) LHV efficiency d) Power (W)

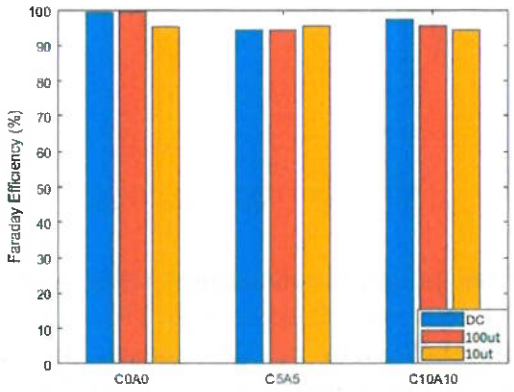


Figure 35: Faraday efficiency for C0A0, C5A5, C10A10. DC (blue); 100ut (red); 10ut (yellow)

to 41.6% at maximum flux. This change was from 6.7% to 7.6% at 10ut. At 1ut, LHV efficiency has shown no significant variations with flow.

Concluding, the results presented here have shown that pulsed water electrolysis is a less efficient process and has lower production rate. The main cause of that is the high negative current when E=$E_{off}$, which cancels the effects of the higher $i_{on}$ current. The lower efficiency of water electrolysis with the pulses' application agrees with the results from Shaaban (1994) and Dobó & Palotás (2016a). Comparing the pulses, 100ut pulses presented the highest efficiency and the highest production rate. The results contradict Shimizu, Hotta, Sekiya & Oda (2006), Ghoroghchian & Bockris (1985), and Demir, Kaya & Albawabiji, since in their cases the hydrogen production rate and/or the efficiency were not improved using pulses. This may be because, in the experiment performed here, $E_{on}$ was too low, the width was too high or the duty cycle was too high compared to those studies. These were some of the differences between the experiment presented here and the cited studies. In addition, there is strong evidence that a further increase in $E_{on}$ would lead to an increase in LHV efficiency. Nevertheless, Dobó & Palotá (2016) used pulses with $E_{on}$ in the same range as done here, the same duty cycle and the same width, however, the results were not the same. The authors concluded that for average voltage values higher than 1.8V any pulse provokes a decrease in efficiency. Here, in the case where $E_{on}$=1.93V, the average voltage was 1.55V. A possibility is that, in the set-up used here, the electrolyzer is already in the voltage range of decreasing efficiency in the pulse's presence.

## 5.3 Model fitting

When looking at the fitting results for $k_f$ (figures 36a and 36b), one sees that $k_f$ increases with $E_{on}$ and with pulse frequency. This is normal since $k_f$ is intimately related to current $i_{on}$ and that this latter increases with $E_{on}$ and with pulse frequency. Another observation is that $k_f$ apparently increases with flux. This could be an effect of the bubbles' removal: when bubbles are dragged, the electrode active surface increases. Since the current density remains unchanged, an increase in electrode area means an increase in current, what apparently gives a higher value for $k_f$.

Using the equation 3.29, one expects that a plot ln(kf) vs $\eta$ should be a line with a slope equal to -$\alpha$.f and an y-intercept equals to ln($k_0$). However, the results did not present lines, as can be seen in figures 36a and 36b. This happened because the voltage range was not narrow and this behaviour was predicted by Bard et al. (1980) and

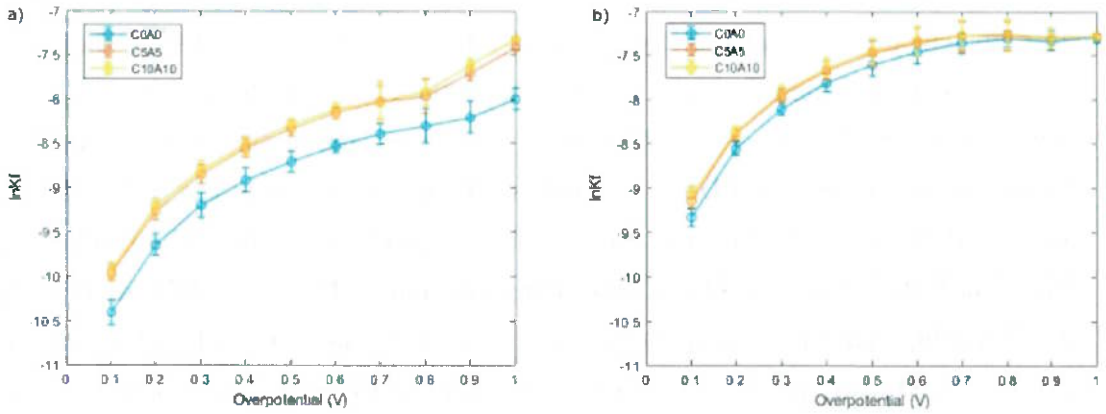


Figure 36: Coefficients resulting from the fitting for C0A0 (blue), C5A5 (red), and C10A10 (yellow): a) $\ln(k_f)$ vs overpotential for 100ut pulses; b) $\ln(k_f)$ vs overpotential for 10ut pulses.

Compton e Banks (2011), and was commented in section A.0.2. However these plots can be considered as lines for small voltage change. This means that the value of $\alpha$ changes with $E_{on}$, from 0.3 at 100ut and low potentials to 0.15 at 100ut and higher voltages. In the case of 10ut, it was changed from 0.36 at low overpotentials to practically zero at high overpotentials. However, at high overpotentials the system is in the diffusion limited regime, hence, it is normal that $k_f$ does not increase with further voltage increasing. This explains an $\alpha$ virtually equal to zero at high voltages. In reality, there is no sense to talk about alpha in this range of potential.

Knowing the values of $k_f$ and H, equation 3.32 can be used to calculate the diffusion coefficient, $D_o$. Nonetheless, in order to estimate the diffusion coefficient, the experiment should be done without the effects of convection and migration. It was not the case here, since a forced flux was imposed and even when it was not, the movement of bubbles creates itself convection. Besides, there are two reactions happening and without a reference electrode, it is impossible to establish the overpotential values for each reaction. It could be stated that the calculated diffusion coefficient is the one from the hydroxide ion, as it does not make sense to talk about diffusion coefficient of water in water. However, since the equation is considering the sum of two overpotentials, it is difficult to interpret the physical meaning of the coefficients. Because of that, the values of $D_o$ will not be shown here. The values changed with potential, which is a non expected behaviour, even if in some cases it was close to the values found in literature.

In conclusion, the model has proven to work and to present a good fit of the experimental data. However, in order to use and interpret the coefficients resulting from the fitting, the use of a reference electrode is compulsory. In this way, the voltage measured would be the voltage for which the model was projected: the electrode potential. Furthermore, a specific reaction would be analysed and the coefficients would be more meaningful. Anyway, the results presented here show the applicability of the model to fit experimental data and its power to predict reaction behavior, since the decay predicted by the model was similar to the one observed experimentally. Most importantly, this trial of fitting shows that the use of the fitting in a configuration containing a reference electrode is promising and should be done in the next researches.

# 6 CONCLUSIONS AND RECOMMENDATIONS

Hydrogen has a key role to play in the creation of a more sustainable future because it is a sustainable way to store energy coming from renewable sources, such as solar photovoltaics and windmills. The energy surplus produced by these sources can be used in water electrolysis to split water molecules, producing hydrogen and oxygen. The produced hydrogen can then be burned, depending on the demand, to produce heat and then electricity, without emission of green house gases. Alternatively, it could be used in fuel cells to recuperate energy. Nowadays, most of the hydrogen produced comes from non-renewable sources that pollute the environment with carbon dioxide. The challenge for water electrolysis is to be competitive with the other hydrogen production technologies. For that, several improvements in the electrolyzer should be made. Encouraging studies indicated that the introduction of potential pulses could improve electrolysis efficiency and production rate. In addition, there are some reasons to support this conclusion, namely the detachment of bubbles and the incomplete formation of the Nernst diffusion layer. Other authors claim to have achieved better electrolysis performance by the disturbance of the electric double layer. Following the analysis of the results of this work, the conclusions were:

1. Unlike DC electrolysis, LHV efficiency increases with voltage ($E_{on}$) for pulsed electrolysis. In addition, as in DC electrolysis, the increase in voltage increases the current and consequently, the production rate. Therefore, there may be a $E_{on}$ (higher than 2.2V) where the LHV efficiency is the same (or even higher) as that of DC, but with higher production rate;

2. $i_{on}$ is higher than the current obtained from DC and increases with frequency;

3. Hydrogen production starts for pulses at $E_{on}$ equal or higher than 1.93V, meaning an overpotential of 0.7V;

4. Even if $i_{on}$ and $i_{off}$ increase their absolute values with the decrease of pulse width

(increase of pulse frequency), $i_{total}$, is higher for higher pulse widths (lower pulse frequencies). This is the reason for the higher production rate at 100ut;

5. When pulses with $E_{on}$=1.93V were introduced, both the hydrogen production rate and the LHV efficiency were decreased in comparison with DC;
6. If $E_{on}$ is fixed at 1.93V, the efficiency increases with $E_{off}$, even if the efficiency was always lower than efficiency at DC;
7. Both the LHV efficiency and the hydrogen production rate increase with the increase of electrolyte flow;

In light of this research, there are several recommendations for the next studies. The first is to use a diode, as done by Shaaban (1994), Ghoroghichian & Bockris (1985), Shimizu, Hotta, Sekiya, & Oda (2006), Vincent et al. (2018), and Vanags et al (2012). In this way, there will be no more the counter current when the voltage is off. On the other hand, it is expected that, with a diode, the voltage $E_{off}$ will have a minimum value, maybe not arriving at 1.23V, which is not necessarily bad, since it was seen that higher $E_{off}$ promotes higher efficiency. Alternatively, current pulses could be applied, ensuring $i_{off} \geq 0$. Furthermore, the experiment should be made at higher $E_{on}$, lower pulse widths and higher duty cycle, since these were some of the differences between the experiment presented here and the experiments that achieved higher efficiencies and/or production rate. In order to achieve a higher $E_{on}$, the potentiostat must be substituted by one capable of reaching higher voltages. Alternatively, a power booster could be used. The same can be said about pulse frequency: to achieve higher frequencies, the potentiostat must be changed to one capable of arriving at pulse widths lower than 1ut. Another recommendation is related to the creation of a set-up which includes a reference electrode. In this case, the fitting would be made more accurately, without adaptations and hopefully, the coefficients such as $\alpha$ and $D_O$ would be more meaningful. Finally, one last recommendation is to use a precise method to measure the volume of hydrogen produced, which does not rely on the imprecision of a graduated cylinder or on the human eye. A possibility would be to use a barometer and with the variation in pressure, calculate the produced volume, as done by Dobó & Palotás (2016a) and Dobó & Palotás (2016b) . This barometer could be digital and automatically record the pressure at defined time intervals. With this method, the Faraday efficiency could be measured precisely, and minimum variations could be identified.

The experiments with pulses presented in this work did not achieve higher LHV efficiencies nor hydrogen production rates. However, it reveals that contrary to DC electrolysis, the increase in voltage increases efficiency. As a result, further research will very probably achieve higher efficiencies and higher hydrogen production rates. In addition, this research was important to identify recommendations for further studies and to better understand the pulse behaviour, contributing to the pulse literature.

# REFERENCES


ATKINS, P.; JONES, L. *Chemical principles.* [S.l.]: Macmillan, 2009.

ATKINS, P.; PAULA, J. D.; KEELER, J. *Atkins' physical chemistry.* [S.l.]: Oxford university press, 2018.

BARD, A. J. et al. *Electrochemical methods: fundamentals and applications.* [S.l.]: wiley New York, 1980. v. 2.

BOCKRIS, J.; POTTER, E. The mechanism of the cathodic hydrogen evolution reaction. *Journal of The Electrochemical Society*, The Electrochemical Society, v. 99, n. 4, p. 169–186, 1952.

BREEZE, P. The hydrogen economy. In: _____. [S.l.: s.n.], 2017. p. 71–75. ISBN 9780081010440.

BUTTLER, A.; SPLIETHOFF, H. Current status of water electrolysis for energy storage, grid balancing and sector coupling via power-to-gas and power-to-liquids: A review. *Renewable and Sustainable Energy Reviews*, v. 82, p. 2440–2454, 2018.

CHAMBERS, S. B. *Process and apparatus for the production of fuel gas and the enhanced release of thermal energy from such gas.* 2002. US 6419815B1.

COMPTON, R. G.; BANKS, C. E. *Understanding voltammetry.* [S.l.]: World Scientific, 2011.

DAVID, M.; OCAMPO-MARTÍNEZ, C.; SÁNCHEZ-PEÑA, R. Advances in alkaline water electrolyzers: A review. *Journal of Energy Storage*, v. 23, p. 392 – 403, 2019. ISSN 2352-152X. Disponível em: ⟨http://www.sciencedirect.com/science/article/pii/S2352152X18306558⟩.

DEMIR, N.; KAYA, M. F.; ALBAWABIJI, M. S. Effect of pulse potential on alkaline water electrolysis performance. *International Journal of Hydrogen Energy*, v. 43, n. 36, p. 17013 – 17020, 2018. ISSN 0360-3199. Disponível em: ⟨http://www.sciencedirect.com/science/article/pii/S0360319918322602⟩.

DOBÓ, Z.; PALOTÁS, A. Impact of the current fluctuation on the efficiency of alkaline water electrolysis. *International Journal of Hydrogen Energy*, 2016a.

DOBÓ, Z.; PALOTÁS, Á. B. Impact of the voltage fluctuation of the power supply on the efficiency of alkaline water electrolysis. *International Journal of Hydrogen Energy*, v. 41, n. 28, p. 11849 – 11856, 2016b. ISSN 0360-3199. Disponível em: ⟨http://www.sciencedirect.com/science/article/pii/S0360319915301774⟩.

FERRERO, R. et al. Simplified model for evaluating ripple effects on commercial pem fuel cell. *International Journal of Hydrogen Energy*, Elsevier, v. 37, n. 18, p. 13462–13469, 2012.

GABE, D. The centenary of tafel's equation. *Transactions of the IMF*, Taylor & Francis, v. 83, n. 3, p. 121–124. 2005.

GHOROGHCHIAN, J.; BOCKRIS, J. Use of a homopolar generator in hydrogen production from water. *International Journal of Hydrogen Energy*, v. 10, n. 2, p. 101 – 112, 1985. ISSN 0360-3199. Disponível em: ⟨http://www.sciencedirect.com/science/article/pii/0360319985900424⟩.

GUILLET, N.; MILLET, P. Alkaline water electrolysis. In: _____. [S.l.: s.n.], 2015. p. 117–166. ISBN 9783527333424.

HORVATH, S. *Electrolysis apparatus*. 1976. US 3954592.

HUANG, C. Solar hydrogen production via pulse electrolysis of aqueous ammonium sulfite solution. *Solar Energy*, v. 91, p. 394 – 401, 2013. ISSN 0038-092X. Disponível em: ⟨http://www.sciencedirect.com/science/article/pii/S0038092X12003337⟩.

IBL, N. Some theoretical aspects of pulse electrolysis. *Surface Technology*, v. 10, n. 2, p. 81 – 104, 1980. ISSN 0376-4583. Disponível em: ⟨http://www.sciencedirect.com/science/article/pii/0376458380900564⟩.

ITO, K.; LI, H.; HAO, Y. M. Alkaline water electrolysis. In: _____. [S.l.: s.n.], 2016. p. 137–142. ISBN 978-4-431-56040-1.

JONGE, R. D. et al. Gas bubble behaviour and electrolyte resistance during water electrolysis. *International Journal of Hydrogen Energy*, Elsevier, v. 7, n. 11, p. 883–894, 1982.

KOTHARI, R.; BUDDHI, D.; SAWHNEY, R. Comparison of environmental and economic aspects of various hydrogen production methods. *Renewable and Sustainable Energy Reviews*, v. 12, n. 2, p. 553 – 563, 2008. ISSN 1364-0321. Disponível em: ⟨http://www.sciencedirect.com/science/article/pii/S1364032106001158⟩.

KREUTER, W.; HOFMANN, H. Electrolysis: The important energy transformer in a world of sustainable energy. *International Journal of Hydrogen Energy*, v. 23, n. 8, p. 661 – 666, 1998. ISSN 0360-3199. Disponível em: ⟨http://www.sciencedirect.com/science/article/pii/S0360319997001092⟩.

LEE, J. D. *Concise inorganic chemistry*. [S.l.]: John Wiley & Sons, 2008.

LIN, M.-Y.; HOURNG, L.-W. Effects of magnetic field and pulse potential on hydrogen production via water electrolysis. *International Journal of Energy Research*, v. 38, n. 1, p. 106–116, 2014. Disponível em: ⟨https://onlinelibrary.wiley.com/doi/abs/10.1002/er.3112⟩.

LIPMAN, T. E. *What will power the hydrogen economy? Present and future sources of hydrogen energy*. [S.l.], 2004.

LUBERT, K.-H.; KALCHER, K. History of electroanalytical methods. *Electroanalysis*, v. 22, n. 17-18, p. 1937–1946, 2010. Disponível em: ⟨https://onlinelibrary.wiley.com/doi/abs/10.1002/elan.201000087⟩.

MARBÁN, G.; VALDÉS-SOLÍS, T. Towards the hydrogen economy? *International Journal of Hydrogen Energy*, v. 32, n. 12, p. 1625 – 1637, 2007. ISSN 0360-3199. Disponível em: ⟨http://www.sciencedirect.com/science/article/pii/S0360319906006276⟩.

MATSUSHIMA, H.; IIDA, T.; FUKUNAKA, Y. Observation of bubble layer formed on hydrogen and oxygen gas-evolving electrode in a magnetic field. *Journal of Solid State Electrochemistry*, v. 16, n. 2, p. 617–623, 02 2012. ISSN 1433-0768. Disponível em: ⟨https://doi.org/10.1007/s10008-011-1392-x⟩.

MAZLOOMI, K. et al. Analysis of the frequency response of a water electrolysis cell. *Int. J. Electrochem. Sci*, v. 8, n. 3, p. 3731–3739, 2013.

MCNAUGHT, A. D.; MCNAUGHT, A. D. *Compendium of chemical terminology*. [S.l.]: Blackwell Science Oxford, 1997. v. 1669.

MEYER, S. A. *Gas generator voltage control circuit*. 1989. US 4798661A.

MEYER, S. A. *Process and apparatus for the production of fuel gas and the enhanced release of thermal energy from such gas*. 1992. US 5149407A.

MONK, N.; WATSON, S. Review of pulsed power for efficient hydrogen production. *International Journal of Hydrogen Energy*, v. 41, n. 19, p. 7782 – 7791, 2016. ISSN 0360-3199. Special Issue on Progress in Hydrogen Production and Applications (ICH2P-2015), 3-6 May 2015, Oshawa, Ontario, Canada. Disponível em: ⟨http://www.sciencedirect.com/science/article/pii/S0360319915027664⟩.

NEWMAN, J.; BONINO, C. A.; TRAINHAM, J. A. The energy future. *Annual Review of Chemical and Biomolecular Engineering*, v. 9, n. 1, p. 153–174, 2018. PMID: 29879382. Disponível em: ⟨https://doi.org/10.1146/annurev-chembioeng-060817-084300⟩.

OLDHAM, K.; MYLAND, J.; BOND, A. *Electrochemical science and technology: fundamentals and applications*. [S.l.]: John Wiley & Sons, 2011.

PRICES, D. M. *Daily Metal Prices*. 2019. Disponível em: ⟨https://www.dailymetalprice.com/⟩.

PUHARICH, H. K. *Method and apparatus for splitting water molecules*. 1983. US 4394230A.

PUIPPE, J. C.; IBL, N. Influence of charge and discharge of electric double layer in pulse plating. *Journal of Applied Electrochemistry*, v. 10, n. 6, p. 775–784, 11 1980. ISSN 1572-8838. Disponível em: ⟨https://doi.org/10.1007/BF00611281⟩.

RASHID, M. et al. Hydrogen production by water electrolysis: A review of alkaline water electrolysis, pem water electrolysis and high temperature water electrolysis. *International Journal of Engineering and Advanced Technology*, ISSN, p. 2249–8958, 02 2015.

ROBERT, E.; TOBIAS, C. W. On the conductivity of dispersions. *Journal of the Electrochemical Society*, The Electrochemical Society, v. 106, n. 9, p. 827–833, 1959.

SHAABAN, A. Pulsed dc and anode depolarization in water electrolysis for hydrogen generation. p. 77, 08 1994.

SHIMIZU, N. et al. A novel method of hydrogen generation by water electrolysis using an ultra-short-pulse power supply. *Journal of Applied Electrochemistry*, v. 36, n. 4, p. 419–423, 04 2006. ISSN 1572-8838. Disponível em: ⟨https://doi.org/10.1007/s10800-005-9090-y⟩.

TARASCON, P. J.-M. *Filière hydrogène: de la production au stockage*. Disponível em: ⟨https://www.college-de-france.fr/media/jean-marie-tarascon/UPL58650_hydrogenecollege.pdf⟩.

TRASATTI, S. Work function, electronegativity, and electrochemical behaviour of metals: Iii. electrolytic hydrogen evolution in acid solutions. *Journal of Electroanalytical Chemistry and Interfacial Electrochemistry*, Elsevier, v. 39, n. 1, p. 163–184, 1972.

TSEUNG, A.; VASSIE, P. A study of gas evolution in teflon bonded porous electrodes—iii. performance of teflon bonded pt black electrodes for h2 evolution. *Electrochimica Acta*, v. 21, n. 4, p. 315 – 318, 1976. ISSN 0013-4686. Disponível em: ⟨http://www.sciencedirect.com/science/article/pii/0013468676800266⟩.

ULLEBERG Øystein. Modeling of advanced alkaline electrolyzers: a system simulation approach. *International Journal of Hydrogen Energy*, v. 28, n. 1, p. 21 – 33, 2003. ISSN 0360-3199. Disponível em: ⟨http://www.sciencedirect.com/science/article/pii/S0360319902000332⟩.

VANAGS, M.; KLEPERIS, J.; BAJARS, G. Water electrolysis with inductive voltage pulses. In: *Electrolysis*. [S.l.]: IntechOpen, 2012.

VINCENT, I.; BESSARABOV, D. Low cost hydrogen production by anion exchange membrane electrolysis: A review. *Renewable and Sustainable Energy Reviews*, Elsevier, v. 81, p. 1690–1704, 2018.

VINCENT, I. et al. Pulsed current water spliting electrochemical cycle for hydrogen production. *A review, Renewable and Sustainable Energy Reviews*, v. 43(22), p. 10240–10248, 2018.

WANG, M. et al. The intensification technologies to water electrolysis for hydrogen production. *A review, Renewable and Sustainable Energy Reviews*, v. 29, p. 573–588, 2014.

WEAST, R. C. et al. *CRC handbook of chemistry and physics*. [S.l.]: CRC press Boca Raton, FL, 2004. v. 84.

WENDT, H.; KREYSA, G. *Electrochemical engineering: science and technology in chemical and other industries*. [S.l.]: Springer Science & Business Media, 2013.

WHITE, R.; BOCKRIS, J.; CONWAY, B. *Modern Aspects of Electrochemistry, No. 15*. [S.l.]: Springer, 1983.

WILBERFORCE, T. et al. Water electrolysis technology. In: _____. [S.l.: s.n.], 2018. ISBN 9780128035818.

ZENG, K.; ZHANG, D. Recent progress in alkaline water electrolysis for hydrogen production and applications. *Progress in Energy and Combustion Science*, v. 36, p. 307–326, 2010.

# APPENDIX A – KINETICS

## A.0.1 Kinetics for homogeneous reactions

Before the considerations of the heterogeneous processes, it is important to remember some key concepts from the homogeneous processes. Consider the following reversible reaction occurring in a homogeneous medium (BARD et al., 1980):

$$aA \rightleftharpoons bB \qquad \text{[H]}$$

The single average rate of the reaction is calculated as follows (ATKINS; JONES, 2009):

$$r = -\frac{1}{a}\frac{dC_A}{dt} = \frac{1}{b}\frac{dC_B}{dt} \qquad \text{(A.1)}$$

Where $C_A$ and $C_B$ are the concentrations of A and B (mol/L), respectively; a and b are the stoichiometric coefficients; and t is the time (ATKINS; JONES, 2009). According to the rate law, the rate of the forward process for elementary reactions is given by:

$$r_f = k_f(C_A)^a \qquad \text{(A.2)}$$

With $k_f$ the rate constant for the forward reaction ($s^{-1}$). (BARD et al., 1980), which is unique for each reaction. An elementary reaction is the one at which there is only one step and a single transitional state (MCNAUGHT; MCNAUGHT, 1997). If the reaction is non-elementary, the reaction rate will be approximated by the rate of the slowest step (ATKINS; JONES, 2009). In the case of the backward process, the same logic is applied (BARD et al., 1980):

$$r_b = k_b(C_B)^b \qquad \text{(A.3)}$$

With $k_b$ the rate constant for the backward reaction. The net rate of reaction is so given by the subtraction of the forward and the backward rates:

$$r_{net} = r_f - r_b = k_f(C_A)^a - k_b(C_B)^b \tag{A.4}$$

At equilibrium, $r_{net}$=0, meaning that $r_f$=$r_b$, hence:

$$\frac{k_f}{k_b} = K_{eq} = \frac{(C_{Beq})^b}{(C_{Aeq})^a} \tag{A.5}$$

The ratio of the two rate constants ($k_f$ and $k_b$), gives another constant ($K_{eq}$), known as the equilibrium constant, since it is related to the ratio of the concentrations at equilibrium (BARD et al., 1980).

For a reaction to take place, the reactants need to collide. In addition, this collision needs to have sufficient energy to activate the reaction (activation energy). This happens because in between the reactant and the product, there is a transitional state, also called activated complex. This state is more energetic than both reactants and products (ATKINS; JONES, 2009). That said, some energy is needed for the specimens to go from the reactant state to the activated complex state. Once there, the reaction continues very quickly, forming products. As a consequence of this energy barrier, it is expected that the reaction rate is dependent on the probability of the reactants of surmounting the barrier and on the frequency of reactants collisions. As expected, the rate constant follows the so-called Arrhenius equation (BARD et al., 1980) (COMPTON; BANKS, 2011):

$$k = \breve{A}.exp\left(\frac{-\Delta G}{RT}\right) \tag{A.6}$$

Where $\breve{A}$ is the frequency factor; $\Delta$G is the activation energy; T is the temperature; and R the gas constant. While $\breve{A}$ is related to the frequency, the exponential term is related to the probability(BARD et al., 1980). The energy of activation, $\Delta$G, is defined as the difference in potential energy between the activated complex and the reactants. A representation of the different potential energies in a reaction is seen in figure 37.

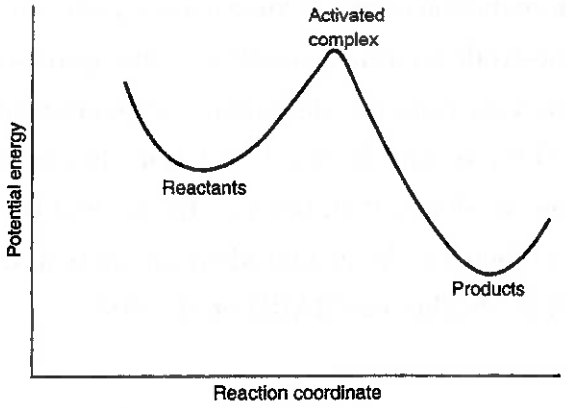


Figure 37: Schematic representation of potential changes during an elementary reaction (BARD et al., 1980)

### A.0.2 Kinetics for heterogeneous reactions

By contrast with homogeneous reactions, heterogeneous reactions occur at an interface. The focus here will be reactions at electrochemical cells, specially electrolysis. An electrochemical cell is a device capable of either generating electricity from spontaneous chemical reaction or using electricity to conduct non-spontaneous chemical reactions. In the former case, it will be called galvanic cells and in the latter case, electrolytic cell. An example of a process which occur in electrolytic cells is the electrolysis, where chemical compounds are decomposed by the use of electric energy. In both these processes, the reactions occur at the interface electrode/solution. An electrode is defined as being an electron conductor, meaning that the charge is carried by the movement of electrons. The electrochemical cell is consisted of two electrodes separated by one or more electrolyte phases. The electrolyte is an ionic conductor: the charge is carried by the movement of ions. Between these two electrodes, a difference in electric potential is applied. This difference is called cell potential. It can be measured with the help of a voltmeter with high internal resistance to prevent current from flowing through it, which would change the sample's potential. The unit for potential is the volt (V) and its physical meaning is the energy in Joule (J) available to drive 1 Coulomb (C) of charge between the electrodes (BARD et al., 1980).

The energy of electrons at an electrode can be raised by connecting it to a power supply that drives its electrical potential to a more negative value. This increase in the electrons' energy can result in an electron transfer from the metal electrode (energetic state) to a vacant molecular orbital in the electrolyte, in a process called reduction. The

electrode at which reduction occurs is known as cathode. In the opposite case, driving the potential of the electrode to a more positive value decreases the energy of the electrons and can cause a transfer from the electrolyte to the electrode. In this case, the electrode is called anode and the process is called oxidation. Regarding the point of view of kinetics, some reactions are slower than others. To increase the rate of reaction (forward or backward), one can increase the magnitude of the potential, since rate and potential are related as one will see further on (BARD et al., 1980).

In most studies the interest is in just one half-reaction occurring in one electrode, called working electrode. The other is known as the counter electrode. To analyze the current and the potential only in the working electrode, a third electrode must be introduced: the reference electrode. It is an electrode that maintains a virtually invariant potential under the experimental conditions, and that allows the measurement of the potential of the working electrode (MCNAUGHT; MCNAUGHT, 1997).

The most well-known reference electrode is the standard hydrogen electrode (SHE), also called normal hydrogen electrode (NHE) (BARD et al., 1980). It consists of a platinum black electrode, used as catalyst, in a solution of hydrochloric acid and with hydrogen gas being bubbled over the surface of the electrode, creating the following equilibrium (COMPTON; BANKS, 2011): $H^+_{aq} + e^-_{(m)} = \frac{1}{2}H_{2(g)}$. Where (m) indicates that the source of electrons is the metal electrode and aq indicates an aqueous medium (COMPTON; BANKS, 2011). The SHE can be represented as (BARD et al., 1980): $Pt/H_2/H^+_{aq}$. Where the activity of all components are unit (BARD et al., 1980).

However, the SHE is not very convenient for experiments. As a consequence, another used reference electrode is the saturated calomel electrode (SCE). It is composed of a column of liquid mercury, contacting calomel (di-mercury (I) chloride: $Hg_2Cl_2$). This column is surrounded by an aqueous solution of saturated KCl or another source of chloride ion. The equilibrium is established at the three-phase boundary (COMPTON; BANKS, 2011):

$$\frac{1}{2}Hg_2Cl_{2(s)} + e^-_{(m)} = Hg_{(l)} + Cl^-_{(aq)} \tag{A.7}$$

It can be represented as: $Hg/Hg_2Cl_2/KCl$. Its potential is 0.242V in comparision with SHE (BARD et al., 1980). Finally, another known reference electrode is the sil-

ver/silver chloride one. It is comprised of a silver wire coated with a porous layer of silver chloride dipped into a KCl solution. The equilibrium established is (COMPTON; BANKS, 2011): $AgCl_s + e^-_{(m)} = Ag_{(}s) + Cl^-_{aq}$. Its potential is of 0.197V vs SHE and its electrochemical cell is represented as: Ag/AgCl/KCl (BARD et al., 1980). For convenience, henceforth, the potential will be shown respectively to the standard hydrogen electrode (SHE). As stated above, when the SHE is connected to another electrode, a voltmeter can be used to measure the cell potential. If the activity coefficients of all the components are unit, the measured cell potential is called standard electrode potential, $E^0$. To exemplify, consider the following system:

$$Pt/H_2(a=1)/H^+(a=1)//Ag^+(a=1)/Ag$$

The left part represents the SHE and the right part represents the working electrode. For this system, the cell potential is +0.799V (WEAST et al., 2004). Thus, the standard electrode potential of the reaction $Ag^+ + e^- \rightleftharpoons Ag$ is $E^0$=+0.799VV vs SHE. The positive sign indicates that, in this case, the forward reaction (reduction of $Ag^+$) is the spontaneous one. With the standard electrode values, it is possible to predict the standard cell potential of a system:

$$E^0_{cell} = E^0_{highest} - E^0_{lowest} \tag{A.8}$$

With $E^0_{highest}$ the highest standard electrode potential measured with the SHE, and $E^0_{lowest}$ the lowest one. To illustrate, we can imagine an alkaline elctrolysis cell. The equilibrium at the cathode is given by(WEAST et al., 2004):

$$2H_2O + 2e^- \rightleftharpoons H_2 + 2OH^-, E^0 = -0.8227(V)$$

While for the anode it is(WEAST et al., 2004):

$$O_2 + 2H_2O + 4e^- \rightleftharpoons 4OH^-, E^0 = +0.401(V)$$

Hence, the standard cell potential is given by:

$$E^0_{cell} = E^0_{highest} - E^0_{lowest} = 0.401 - (-0.8227) = 1.2287(V)$$

This means that at standard conditions (activity coefficients equals to unit), the minimum difference in potential needed to produce hydrogen by water electrolysis is 1.23V. However, due to kinetic reasons, the real value to start hydrogen production lies between 1.8-2V. To understand better the kinetics at electrodes, consider the following redox reaction:

$$O + ne^- \rightleftharpoons R \qquad \text{[I]}$$

Where species O and R are dissolved in a solution and the electron comes from a metal electrode. As in the homogeneous case, the rate of reaction depends on a rate constant and on the concentration of reactants. Nevertheless, other information can be added: the current. An electric current is also a means to measure reaction rate in an electrode since current is the passage of a charge by a unit of time and the charge depends on the reaction. For example, for 1 mol of O reduced, n mol of electrons reacted (stoichiometry). n mol of electrons has a charge of approximately n.96500C (Faraday constant). Because of that, if the current (charge/time) is divided by the Faraday constant (F) and by the stoichiometric coefficient n, one has the rate of reaction in mol of O per unit of time. As the reaction occurs at an interface, the larger the interface, the higher the rate. In order to compare different systems, one needs to normalize this rate by the interface area. Hence (BARD et al., 1980):

$$r_f = k_f.C_O = \frac{i_f}{nFA} \qquad \text{(A.9)}$$

And

$$r_b = k_b.C_R = \frac{i_b}{nFA} \qquad \text{(A.10)}$$

Where i is the current, A is the area of the electrode, the indexes f and b, indicates forward and backward reactions, respectively, and n is the stoichiometric electron coefficient. As for a homogeneous process, the net rate will be given by the difference between the forward (cathodic) and the backward (anodic) reactions (BARD et al., 1980):

$$r_{net} = k_f.C_O - k_b.C_R = \frac{i_f}{nFA} - \frac{i_b}{nFA} \qquad \text{(A.11)}$$

Since it is often easier to measure the current, it is more interesting to rearrange the

previous equation as follows:

$$i = i_f - i_b = nFA(k_f.C_O - k_b.C_R) \tag{A.12}$$

Since the reaction occurs on a surface, $C_O$ and $C_R$ are the concentrations at the interface. In 1905, a Swiss scientist published two papers summarising a considerable amount of electrochemical data and showing that a logarithmic relationship between overpotential and current exists:

$$\eta = a + b.ln(i) \tag{A.13}$$

Where a and b are characterizing constants, $\eta$ is the overpotential, and i is the current. This scientist, whose name was Julius Tafel, however, was not able to lay his theory in a theoretical model. This was only achieved in 1930 by Butler and Volmer, as we will see further on (GABE, 2005).

Knowing now that the current is potential dependent (equation A.13), it is clear from the equation A.12 that $k_f$ and $k_b$ are also potential dependent. If the potential in the metal electrode, $\phi_m$, becomes more negative, means that the energy of the electrons on the metal will increase. Therefore, the energy of the reactant increases, while the energy of the product remains unchanged (in reaction [I]). Maintaining $\phi_m$ constant but changing the potential of the solution, $\phi_s$, by the addition of negative ions (anions) would increase the energy of all the negative substances, which could include reactants and products. The more negative the substance, the more its energy will increase. The effects of changing potential can be seen in figure 38. The figure illustrates these effects in the reaction $Fe^{3+} + e^- \rightleftharpoons Fe^{2+}$. If $\phi_m$ becomes more negative, the energy of the reactants increases while the energy of products is kept constant. If $\phi_s$ becomes more positive, energy of both reactants and products increases, but the increase in the energy of reactants is greater than the increase in the energy of the products (COMPTON; BANKS, 2011).

Imagine now a system at its standard electrode potential, $E^0$. If the potential is changed by $\Delta$E (E-$E^0$), the energy of the electrons (hence the reactant's energy) will be changed by -F$\Delta$E. Here, E is the actual potential. The energy of the activated complex changes, but in a fraction $\beta$ of the -F$\Delta$E value: $\Delta E_{complex}$=-$\beta$F$\Delta$E. The variable $\beta$ is defined as being $\beta$=1-$\alpha$, where $\alpha$ is the transfer coefficient. Its value (as $\beta$ value) is

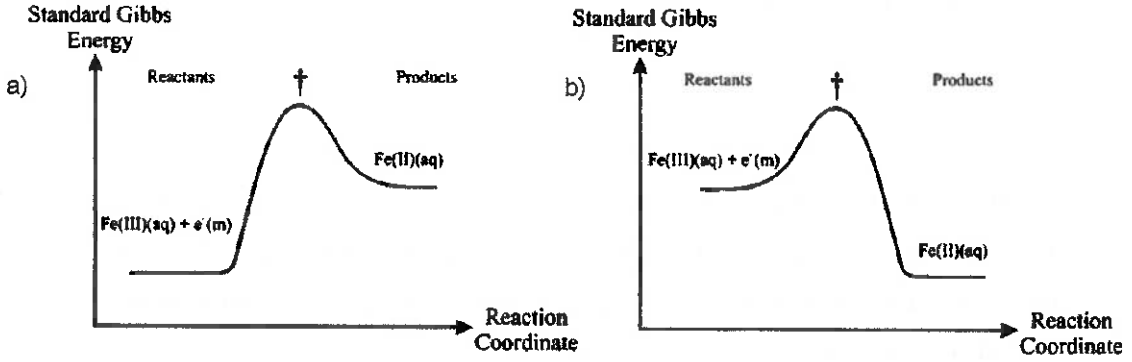


Figure 38: Effects of the change in potential in electrode reactions. a) $\phi_m$ relatively positive and/or $\phi_s$ relatively negative; b) $\phi_m$ relatively negative and/or $\phi_s$ relatively positive. Adapted from (COMPTON; BANKS, 2011)

commonly between 0 and 1. Because of this change in the energy of the reactants and in the energy of the activated complex, the activation energy will also be changed (BARD et al., 1980):

$$\Delta G_f = \Delta G_{0f} + F\Delta E - \beta F\Delta E = \Delta G_{0f} + \alpha F\Delta E \tag{A.14}$$

$$\Delta G_b = \Delta G_{0b} - \beta F\Delta E = \Delta G_{0b} - (1-\alpha)F\Delta E \tag{A.15}$$

With $\Delta G_{0f}$ and $\Delta G_{0b}$ the activation energies at E=$E^0$ of the forward and the backward reactions, respectively. The changes in energy due to a change in the potential of the electrode ($\phi_m$) can be seen in figure 39. It can be seen that the energy of the reactants (O and $e^-$) was decreased by F$\Delta$E and the energy from the activated complex was decreased by $\beta$F$\Delta$E. Finally, combining equation A.6 with equations A.14 and A.15, one has:

$$k_f = \breve{A}_f.exp\left(\frac{-\Delta G_{0f}}{RT}\right) exp(-\alpha f\Delta E) \tag{A.16}$$

$$k_b = \breve{A}_b.exp\left(\frac{-\Delta G_{0b}}{RT}\right) exp[(1-\alpha)f\Delta E] \tag{A.17}$$

With f=$\frac{F}{RT}$. The value $\Delta$E is measured in comparison to the standard electrode potential $E^0$: $\Delta$E=E-$E^0$=$\eta$, where $\eta$ is called overpotential. The terms $\breve{A}_f.exp(\frac{-\Delta G_{0f}}{RT})$ and the term $\breve{A}_b.exp(\frac{-\Delta G_{0b}}{RT})$ are called standard rate constant, $k_{0f}$ and $k_{0b}$, since it represents the rate constant when E=$E^0$ (standard potential). Hence (BARD et al., 1980):

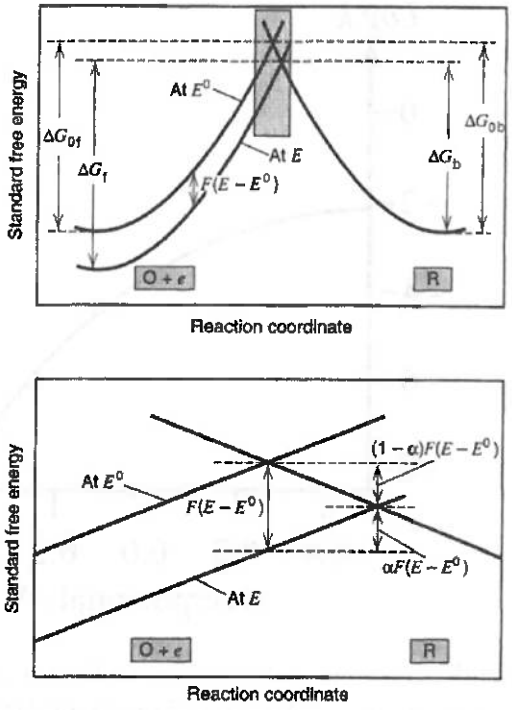


Figure 39: Change in the standard free energy caused by a change in the electrode potential (BARD et al., 1980)

$$k_f = k_{0f} exp(-\alpha f \eta) \tag{A.18}$$

$$k_b = k_{0b} exp[(1-\alpha) f \eta] \tag{A.19}$$

Now, substituting these equations in equation A.12, one has:

$$i = nFA\{k_{0f} exp(-\alpha f \eta).C_O - k_{0b} exp[(1-\alpha) f \eta.C_R]\} \tag{A.20}$$

This current-potential relation is known as the Butler-Volmer formulation. The standard rate constant , $k_0$, indicates the facility of a reaction in terms of kinetics. The higher the $k_0$, the faster the reaction. Its value is commonly between 1-10 cm/s even if values lower than $10^{-9}$ cm/s have been reported. The transfer coefficient ($\alpha$) lies between 0.3-0.7, with 0.5 the most common value. Its value is potential-dependent, but it can be considered constant if the potential range is narrow enough (BARD et al., 1980). If not, Tafel plots will be curved as can be seen in figure 40 (COMPTON; BANKS, 2011). According to Bockris & Potter (1952) (BOCKRIS; POTTER, 1952), $\alpha$=0.5 for the hydrogen evolution reaction in Nickel alkaline solutions.

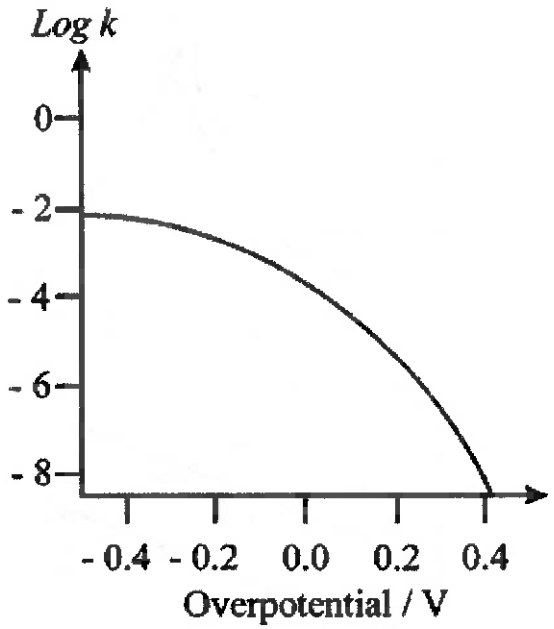


Figure 40: The dependence of the rate constant of the reaction of $Fe^{3+} + e^- \rightarrow Fe^{2+}$ in 1 M $HClO_4$ on the overpotential. Adapted from (COMPTON; BANKS, 2011)

At equilibrium, the total current (given by equation A.20) is zero, since by definition, $r_{net}$=0. Additionally, the concentrations are the same on the surface of the electrode and on the bulk. As a consequence, the concentrations at equilibrium can be shown as a function of the bulk's concentration, $C_O^*$ and $C_R^*$. Hence:

$$i = i_f - i_b = 0 \tag{A.21}$$

$$nFAk_{0f}exp(-\alpha f\eta).C_O^* = nFAk_{0b}exp[(1-\alpha)f\eta].C_R^* \tag{A.22}$$

Hence,

$$E = E^0 + \frac{1}{f}ln\left(\frac{C_R^*}{C_O^*} + \frac{1}{f}ln\left(\frac{k_{0b}}{k_{0f}}\right)\right) \tag{A.23}$$

Years before the development of equation A.23, a German scientist called Walther Nernst formulated in his post-doctoral thesis an equation for reactions occurring on electrodes at equilibrium (LUBERT; KALCHER, 2010):

$$E = E^0 + \frac{1}{f} ln \left( \frac{C_R^*}{C_O^*} \right) \tag{A.24}$$

This equation is only valid if the reaction is electrochemically reversible, meaning that if a perturbation is applied, the time for the system to reach equilibrium is lower than the measurement time (BARD et al., 1980). When equation A.23 is compared with the Nernst equation, it can be seen that $k_{0b}$ is equal to $k_{0f}$. As a consequence, henceforth, $k_{0b}$ and $k_{0f}$ will be represented only as $k_0$ (COMPTON; BANKS, 2011). Hence:

$$nFAk_0 exp(-\alpha f\eta).C_O^* = nFAk_0 exp[(1-\alpha)f\eta].C_R^* \tag{A.25}$$

Rearranging, the concentration at equilibrium can be given as a function of the overpotential:

$$\frac{C_O^*}{C_R^*} = exp(f\eta) \tag{A.26}$$

This is exactly the same relation presented by the Nernst equation but in an exponential form. The value of the forward (or backward) current at equilibrium (when the total current is zero) is called exchange current, $i_0$. It can be calculated using the left or the right side of equation A.25. Alternatively, raising both sides of the equation A.26 by $\alpha$ power and substituting it in equation A.25 gives:

$$i_0 = nFAk_0 C_O^{*(1-\alpha)} C_R^{*(\alpha)} \tag{A.27}$$

When $C_O^*$=$C_R^*$=$C^*$:

$$i_0 = nFAk_0 C^* \tag{A.28}$$

In this case, $i_0$ and $k_0$ differ only by a constant and are proportional. Dividing A.20 by A.27, one has:

$$\frac{i}{i_0} = \frac{C_O}{C_O^*} exp(-\alpha f\eta) \left( \frac{C_O^*}{C_R^*} \right)^{\alpha} - \frac{C_R}{C_R^*} exp[(1-\alpha)f\eta) \left( \frac{C_O^*}{C_R^*} \right)^{-(1-\alpha)} \tag{A.29}$$

Evaluating $(\frac{C_O^*}{C_R^*})^{\alpha}$ and $(\frac{C_O^*}{C_R^*})^{-(1-\alpha)}$ by equation A.26, gives:

$$i = i_0 \left\{ \frac{C_O}{C_O^*}[exp(-\alpha f\eta) - \frac{C_R}{C_R^*}exp[(1-\alpha)f\eta] \right\} \quad \text{(A.30)}$$

Where $C_O$ and $C_R$ are the concentrations at the surface and at a time t; and $\eta$ is equal to E-$E^0$. This is known as the current-overpotential equation. There are some special cases at which the equation A.30 can be simplified. They will be presented now.

Case A - Well stirred solution

In this case, $C_O^*$=$C_O$ and $C_R^*$=$C_R$, hence:

$$i = i_0\{exp(-\alpha f\eta) - exp[(1-\alpha)f\eta]\} \quad \text{(A.31)}$$

And this is historically known as the Butler-Volmer equation.

Case B - Small $\eta$ ($f\eta << 1$)

If $\eta$ is small enough, exp(x)=1+x, hence:

$$i = -i_0.f.\eta \quad \text{(A.32)}$$

Case C -Large and positive $\eta$ ($\eta > 0.12$ V)

In this case, equation A.30 becomes:

$$i = -i_0 \frac{C_R}{C_R^*}exp[(1-\alpha)f\eta] \quad \text{(A.33)}$$

It is a goof approximation for anodic reactions.

Case D - Large and negative $\eta$ ($\eta <$ -0.12 V)

Following the same logic as before, one gets:

$$i = i_0 \frac{C_O}{C_O^*} exp(-\alpha f \eta) \tag{A.34}$$

Alternatively,

$$\eta = \frac{ln(i_0)}{\alpha f} - \frac{ln(i)}{\alpha f} \tag{A.35}$$

Which is exactly the Tafel equation (equation A.13) with a=$\frac{ln(i_0)}{\alpha f}$ and b=$\frac{-1}{\alpha f}$ and works well for cathodic reactions, where $\eta$ is negative (BARD et al., 1980) (ATKINS; PAULA; KEELER, 2018).

### A.0.3 Marcus theory

An electron transfer occurs at a time scale much shorter ($10^{-15}$s) than the molecule's vibration ($10^{-13}$s). Hence, when electron transfer occurs, the molecule can be considered frozen. Now, we can look at a plot of potential energy versus reaction coordinate in figure 41 (COMPTON; BANKS, 2011). Reaction coordinate is a geometric parameter that changes during the conversion of reactants into products. It can be a bond length or bond angle or a combination of both. (MCNAUGHT; MCNAUGHT, 1997). In the case presented in figure 41 it is the distance between the Fe-O bond in the reaction $Fe_2O_3 + e^- \rightarrow 2FeO + 1/2O_2$. One sees that the reactants have lower Fe-O distances than the products. At the ground state, $\upsilon$ =0, the reaction coordinate of the reactants oscillates between values that are always lower than the values from the products. For the reaction to take place, the reactants must be excited in a way that its reaction coordinate arrives at a common value with the products (represented by the dot or the intersection in figure 41). This need for a thermal agitation of the reactants is what creates the activation energy. The products formed, initially excited (with energy at the level of the activated complex), will be soon de-excited by the interactions with the neighbors solvent molecules, losing heat until reaching the ground state for products. The more different the reaction coordinates from products and reactants are, higher will be the level of excitation needed (as one can imagine separating one of the potential curves from the other). This results in a lower standard rate constant, $k_0$. Hence, reactions where O and R (from classical redox reaction [I]) are close in terms of bond length, angles, and so on, $k_0$ is high, which corresponds to a low energy barrier. The power of the Marcus theory is the simplicity to calculate the Gibbs free energy of activation by the following relation(COMPTON; BANKS, 2011):

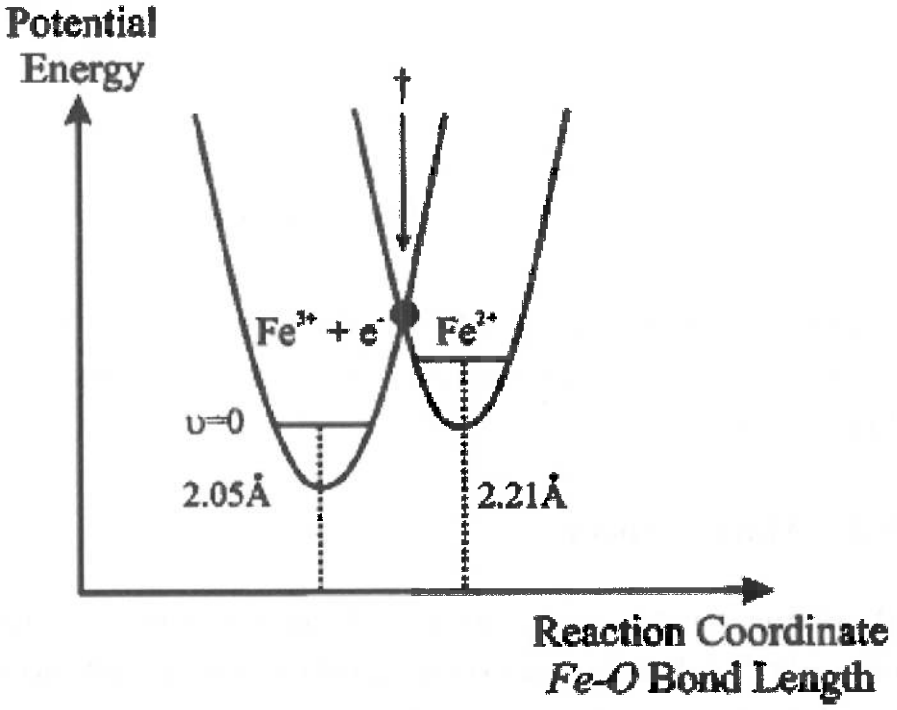


Figure 41: Schematic representation of the potential energy as a function of a reaction coordinate: Fe-O bond length. (COMPTON; BANKS, 2011)

$$k = KZexp\left(\frac{-\Delta G}{RT}\right) \tag{A.36}$$

Where k is the rate constant; K the transition probability such as K≈1 for an adiabatic process and K≪1 for a non adiabatic process; and Z is a pre-exponential term. This relation agrees with the Arrhenius law seen in equation A.6, with $KZ = \breve{A}$.

# APPENDIX B – MECHANISMS FOR OXYGEN AND HYDROGEN EVOLUTION REACTION

## B.0.1 Hydrogen evolution reaction and the volcano plot

The hydrogen evolution reaction is one of the most researched reactions, thus, there is extensive literature about it. In alkaline medium, the source of hydrogen is the water molecule, and not the $H_3O^+$ cation as in the case of acid electrolysis. Considering this, the possible reaction paths for the hydrogen evolution are (BOCKRIS; POTTER, 1952):

$$H_2O + e^- \rightarrow MH + OH^- \qquad [J]$$

Where M represents the metal electrode and MH represents an hydrogen atom adsorbed in the electrode. This raction is followed by one of these:

$$MH + MH \rightarrow H_2 + 2M \qquad [K]$$

$$H_2O + MH + e^- \rightarrow H_2 + OH^- + M \qquad [L]$$

Generally, for low potentials, electron transfer (step [J]) is not as fast as desorption and hydrogen adsorption will be the rate determining step ([K] or [L]). By contrast, if

the potential is higher, hydrogen desorption will be the rate-determining step (ZENG; ZHANG, 2010). Nevertheless, it is also possible that the metal ion, $M_1^{z+}$, present in the solution, discharge as an intermediate step of the evolution reaction, as shown below (BOCKRIS; POTTER, 1952):

$$M_1^{z+} + ze^- \rightarrow M_1 \qquad [M]$$

$$M_1 + zH_2O \rightarrow M_1H + zOH^- \qquad [N]$$

Followed by on of these:

$$M_1H + M_1H \rightarrow H_2 + 2M_1 \qquad [O]$$

$$H_2O + M_1H + e^- \rightarrow H_2 + OH^- + M_1 \qquad [P]$$

One example of a cation taking part in a reaction is the hydrogen evolution at liquid mercury cathodes in aqueous alkaline solutions. In this case (BOCKRIS; POTTER, 1952):

$$M^{z+} + ze^- \rightarrow M/Hg \qquad [Q]$$

$$M/Hg + zH_2O \rightarrow M^{z+} + zHgH + zOH^- \qquad [R]$$

Where [Q] is the fastest reaction and occurs even without appreciable overpotential and [R] is the rate limiting step. After these steps, comes the desorption of hydrogen (BOCKRIS; POTTER, 1952):

$$HgH + HgH \rightarrow H_2 + 2Hg \qquad [S]$$

$$H_2O + HgH + e^- \rightarrow H_2 + OH^- \quad [T]$$

For Nickel alkaline hydrogen evolution, the rate limiting step has one electron, and $\alpha$=0.5 (where $\alpha$ is the transfer coefficient presented in section A.0.2). In this particular case, the suggested mechanism is the following (BOCKRIS; POTTER, 1952):

$$M^{z+} + ze^- \underset{fast}{\overset{fast}{\rightleftharpoons}} M/Ni \quad [U]$$

$$M/Ni + zH_2O \rightarrow M^{z+} + zNiH + zOH^- \quad [V]$$

$$H_2O + NiH + e^- \rightarrow H_2 + OH^- \quad [W]$$

For hydrogen evolution reaction, a relation was found between the strength of the metal-H bond (in adsorption) and the exchange current density, $i_0$ (see equation A.27). A plot of $\log(i_0)$ versus M-H bond strength has a volcano shape as shown in figure 42 (TRASATTI, 1972). As can be seen, $i_0$ value for Nickel is equal to $10^{-5}$ mA cm$^{-2}$ while Platinum is at the top with a value in the range of $10^{-3}$ mA cm$^{-2}$ (TRASATTI, 1972). However, while Nickel costs \$12.94/Kg, Platinum costs \$28,807.07/Kg. The costs of Rhodium, Iridium and Gold are also in the order of ten thousand dollars per kilogram (PRICES, 2019). That is why Nickel is a popular electrode material (ZENG; ZHANG, 2010). The shape of the curve can be explained considering the mechanism [J] followed by the path [K]. For weak M-H bonds (left side of the volcano plot shown in figure 42), the first reaction is the rate determining. The activation barrier of the first step reaction tends to decrease when M-H bond strength increases, promoting an increase in the exchange current value. However, after the peak, the second reaction becomes the rate determining. As a consequence, the activation barrier increases with increasing M-H bond strength, thus, exchange current decreases. For the electrodes on the left side, $\alpha$=1/2, while in the right side, $\alpha$=3/2 (COMPTON; BANKS, 2011). According to the exchange

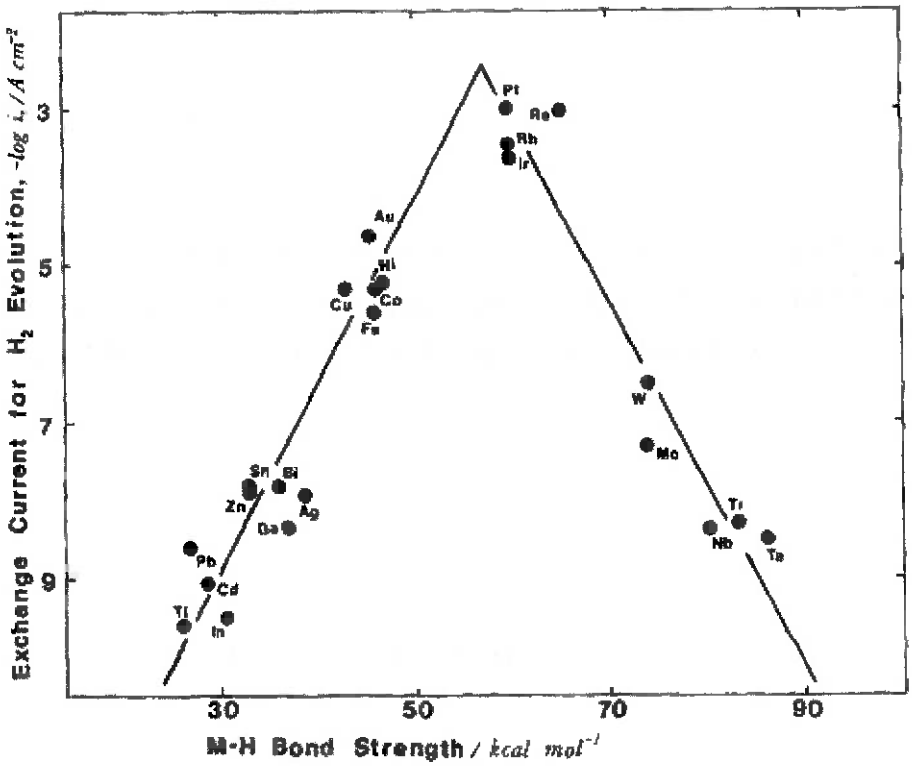


Figure 42: Volcano plot (TRASATTI, 1972)

current values, metals as cathodes can be divided as (WANG et al., 2014):

a) Metals with high overpotential: Cd, Tl, Hg, Pb, Zn, Sn, etc

b) Metals with middle overpotential: Fe, Co, Ni, Cu, Au, Ag, W, etc

c) Metals with low overpotential: Pt, Pd

### B.0.2 Oxygen evolution reaction

The mechanisms for oxygen evolution are more complex than those for hydrogen. However, the most generally accepted mechanism in an alkaline medium is the following (ZENG; ZHANG, 2010):

$$OH^-_{ads} \rightleftharpoons OH_{ads} + e^- \qquad [X]$$

$$OH^- + OH_{ads} \rightleftharpoons O_{ads} + H_2O + e^- \quad [Y]$$

$$O_{ads} + O_{ads} \rightleftharpoons O_2 \quad [Z]$$

For low temperatures, step [X] is commonly the rate determining (ZENG; ZHANG, 2010). The reduction of overpotential for oxygen evolution is more difficult than the one from hydrogen because of the complex mechanism and irreversibilities.

# APPENDIX C – MODELS OF ELECTRIC DOUBLE LAYER

The simplest model of Electric Double Layer is the Helmholtz layer model. In this model, the ions from the bulk arrange themselves around the surface of the electrode. Since these ions are dissolved, their solvent molecules (water, if aqueous medium) keep them at a specific distance from the metal. The locus of charged centers creates a plane covering the surface of the electrode at a certain distance. This plane is the outer Helmholtz plane (OHP). Since the interaction of these ions with the electrode is only long-range electrostatic forces, these ions are said to be nonspecifically adsorbed (BARD et al., 1980). For this model, the following reaction is valid (OLDHAM; MYLAND; BOND, 2011):

$$\frac{C_H}{A} = \frac{dQ}{dE} = \frac{\epsilon_H}{x_H} \tag{C.1}$$

Where $C_H$ is the capacitance of the Helmholtz layer, A is the cross-sectional area through which current flows, Q is the charge, E is the electrical potential, $x_H$ is the thickness of the OHP, and $\epsilon_H$ its permittivity. As a refinement of this model, ions that have discarded their solvating molecules and became attached to the surface by specifically adsorption will create a charged layer closer to the surface of the metal. This layer will be called the inner Helmholtz plane (IHP). Increasing even further the complexity, there is the Gouy-Chapman model of diffuse double layer. It considers the thermal motion that tends to disperse charge. In this model, the OHP is not rigid and it is not a plane, but a diffuse layer with excess of charge (ATKINS; PAULA; KEELER, 2018) (BARD et al., 1980). The capacitance in this model is predicted by the following equation (OLDHAM; MYLAND; BOND, 2011):

$$\frac{C_{GC}}{A} = \sqrt{\frac{2F^2\epsilon_{GC}C_O^*}{RT}}\cosh\left(\frac{F}{2RT}(E - E_{zc})\right) \tag{C.2}$$

Where $C_O^*$ is the bulk ionic concentration, $E_{zc}$ is the potential at zero charge, $C_{GC}$ is the capacitance in the Gout-Chapman layer, and $\epsilon_{GC}$ the permittivity. Nevertheless, a better model to represent the EDL is a combination of the Helmholtz and the Gouy-Chapman models: the Stern model.

**Universidade de São Paulo**

**Engenharia de Petróleo — Escola Politécnica**

**Número USP: 8990900**

**Data: 10/10/2019**

# Intensification of alkaline water electrolysis using forced electrolyte flow and pulsed voltage

**Fernando Saraiva Rocha da Silva**

Supervisor: Joris Proost

Artigo Sumário referente à disciplina PMI1096 — Trabalho de Formatura para Engenharia de Petróleo II
Este artigo foi preparado como requisito para completar o curso de Engenharia de Petróleo na Escola Politécnica da USP.

## 1 Introduction

Hydrogen is the most abundant element in the universe, representing 92% of the atoms in the cosmos. It is present in many compounds such as water, living matter, fossil fuels, etc. By contrast, hydrogen gas, $H_2$, is not abundant on earth Lee (2008). Most of the hydrogen atoms on earth are presented as water molecules Atkins & Jones (2009). As a result, hydrogen must be produced by several chemical reactions.

Nowadays, hydrogen is mainly produced by methods that produces significant amounts of $CO_2$. Hopefully, there is a clean method that produces very pure hydrogen without emission of greenhouse gases: water electrolysis. In this method, water is split into hydrogen and oxygen by the application of an electrical potential difference between two metals, called electrodes, immersed in an electrolytic solution Lee (2008) Kothari et al. (2008).

Hydrogen is widely considered to be the fuel of our future, since it has the highest specific enthalpy of any known fuel Atkins & Jones (2009) and unlike burning fossil fuels, burning hydrogen does not produce $SO_2$ nor $NOx$ nor $CO_2$, responsible for acid rain and the latter, for global warming. Burning hydrogen produces only water and liberates a significant amount of energy Lee (2008).

Production of hydrogen from water electrolysis allows the integration of renewable energy sources. As an example, we can imagine a photovoltaic solar panel (or a windmill) linked to a fuel cell. During day-time, part of the energy is used by customers and the surplus is used to produce hydrogen. During the night, hydrogen is consumed, supplying uninterrupted electricity. Combining water electrolysis with renewable sources is important because water electrolysis is only as clean as the method used to produce the electricity used to split water molecules Marbán & Valdés-Solís (2007). If coal was burned to produce electricity and this electricity was used in an electrolyzer, the produced hydrogen cannot be considered clean, since in the overall process, $CO_2$ was produced Zeng & Zhang (2010).

The way to reduce electrolysis cost is to achieve better electrolyzer performance. Recent and encouraging studies achieved an improvement in water electrolysis efficiency by the substitution of DC (direct current) power supply by a pulsed power supply.

## 2 Objectives

The main objective of this work is to investigate the effects of potential pulses in the efficiency and hydrogen production rate of a specific electrolyzer set-up, using an alkaline solution of 1M KOH and Nickel electrodes.

## 3 Materials and Methods

Two main experiments were carried out: pulsed chronoamperometry varying potential, and pulsed chronoamperometry with fixed potential and hydrogen collection. Different electrolyte fluxes were applied, going from natural convection (no forced flow) to maximum pump flow. Three pulse widths were analyzed: 100ut, 10ut, and 1ut, where ut means unit of time.

In the experimental setup, there were pumps to promote a forced electrolyte flow. This flux was used to drag gas bubbles from the electrode surface and to stir the solution. The electrolytic solution on each half-cell was 1 liter of potassium hydroxide 1 mol/L.

The electrodes were made of pure Nickel. Between them, there was a membrane, which only permits the passage of hydroxide ions. The membrane was used to prevent mixing between oxygen and hydrogen as well as electron migration. Before and after every cell assembly, the components were washed three times with de-ionized water.

Before running the experiment, a galvanostatic run at 2A was performed to initiate the cell. During the galvanostatic experiment, nitrogen gas was circulated in the cathode, to remove the remaining oxygen present in the cathode's drum and to avoid explosions. The galvanostatic test was also performed to evaluate the stability of the membrane and to check the maximum voltage value, since the potentiostat is limited to a maximum current of 2A. No membrane degradation was observed in the experiment time-scale. After the galvanostatic run, a Cyclic Voltammetry - CV - was applied to guarantee that the only reaction occurring was the water electrolysis. The CV was done at a rate of 0.1V/s from 1.23V to 2.23V. There were no side reactions and the water electrolysis reaction began at a voltage close to 1.7V. After the galvanostatic and the CV, the power supply imposed potential pulses in the form of squares, as shown in figure 1. A reference electrode was not used since in the chosen electrode the potential and current presents spacial variations. As a consequence, depending on the location where the reference electrode is put, the result is different. To avoid that, it was decided to work with the total current and total voltage between the cathode and the anode. All the experiments were performed at room temperature (~21°C).

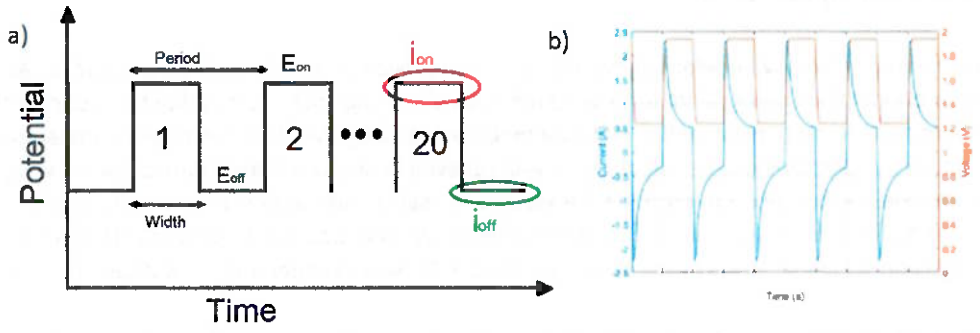


**Figure 1 – a) Representation of the applied voltage pulses, showing: $E_{on}$; $E_{off}$; Pulse period; Pulse width; b) Example of a serie of potential pulses and the corresponding current. The currents' average was calculated in the last $E_{on}$ and the last $E_{off}$, as represented here.**

### 3.1 Pulsed chronoamperometry varying potential

In this first experiment, $E_{off}$ was fixed at 1.23 V, which is the standard potential for water electrolysis, and $E_{on}$ started at 1.33 V (overpotential of 0.1 V) and 20 pulses were applied. Then, $E_{on}$ was increased to 1.43 V and 20 subsequent pulses were produced. This process continued in steps of +0.1V until reaching an overpotential of 1 V ($E_{on}$=2.23 V). Here, overpotential is defined as the difference between the actual potential and the standard cell potential of 1.23 V. The power supply limited the maximum voltage at 2.23 V. Then, the process was re-started two more times, completing three loops. Two different pulse periods were tested: 100 ut and 10 ut. Three electrolyte

flows were tested for each electrode: natural convection, middle flux, and maximum flux. The maximum is defined by the maximum power the pump could provide. The terminology C0A5 indicates natural convection in the cathode and middle velocity in the anode, while C10A10 indicates maximum flow in both. The values for the flows were measured calculating the time needed to fill a graduated cylinder.

## 3.2 Pulsed chronoamperometry with fixed potential and hydrogen collection

The setup used for this experiment was the same as in pulsed chronoamperometry varying potential. The only difference was that in this case a graduated cylinder was used to measure the volume of hydrogen produced. Even though the setup was more or less the same, the method was different. Here we kept $E_{off}$=1.23 V, however, $E_{on}$ was fixed at 1.93 V. Furthermore, this experiment took more time. To evaluate the efficiency of hydrogen production, pulses were applied for 20 minutes. The variables that were changed were: the electrolyte flow and pulse frequency. The hydrogen volumetric production was measured. For that, at each increase of 5 ml in the total hydrogen volume, the time was recorded, up to a maximum volume of 30 ml. The same combinations of fluxes as in the latter experiment were tested, going from natural convection to maximum pump power, passing through middle power. Here, three pulse widths were evaluated: 100 ut, 10 ut, and 1 ut. These pulses were compared with the results obtained from an experiment using direct current, DC, at 1.93 V.

# 4 Results and Discussion

## 4.1 Pulsed chronoamperometry varying potential

Figure 2 shows some plots of the mean current versus voltage. The mean current was calculated as a current average at the $20^{th}$ pulse for each $E_{on}$ at the third (and last) loop, as seen in figure 1, with $i_{on}$ the mean current during on-time and $i_{off}$ the mean current at off-time. The existence of a counter current $i_{off}$ confirms the results of Shaaban (1994), where a change in current polarity was also observed during the $E_{off}$ period. $i_{total}$, shown in figure 2b is the average between $i_{on}$ and $i_{off}$. No difference in the value of the pulse was observed between the loops.

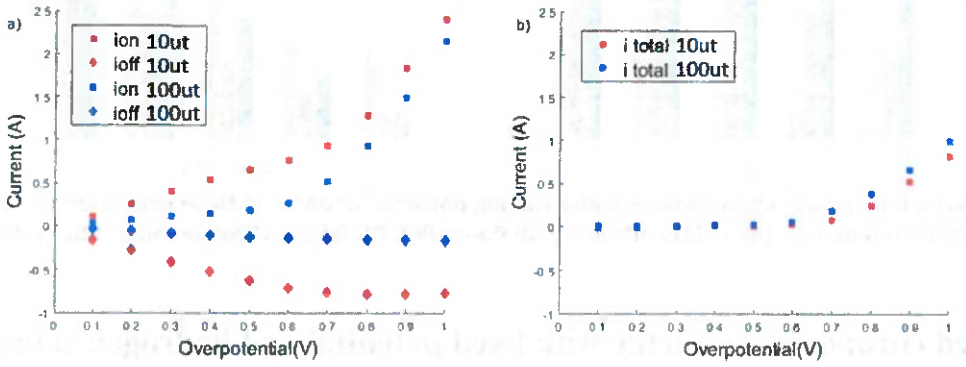


**Figure 2 – Polarization curves for 100ut pulses (blue) and 10ut pulses (red). The current displayed here is the average in a pulse for each overpotential. a) C10A10 average $i_{on}$ (square) and $i_{off}$ diamond; b) C10A10 average $i_{total}$;**

It can be seen in figure 2a that $i_{on}$ is twice as high for 10ut than for 100ut, however, the absolute value of $i_{off}$ is also much higher. As a consequence, $i_{total}$ is higher for 100ut in all the potential interval. In conclusion, lower pulse widths (10ut) cause higher $i_{on}$ and higher $i_{off}$, promotong a higher $i_{total}$ for 100ut.

Comparing now the mean current (figure 3b) and its power (figure 3d), for $E_{on}$ from 1.83V-2.23V, it can be seen that both increase with the increase of $E_{on}$, for pulsed electrolysis. However, the increase in mean current is more significant than the increase in power. As a result, energy efficiency increases with $E_{on}$, as can be seen in figure 3c. This

conclusion shows that, on contrast to DC electrolysis, increasing voltage increases efficiency. Furthermore, as in DC electrolysis, increasing voltage increases production rate (mean current). This means that pulsed electrolysis permits the hydrogen production rate and efficiency to increase together and without compromise, at least in the setup and voltage range presented here. It can be seen, in figure 3a, that pulsed electrolysis presents higher on-currents than DC electrolysis and $i_{on}$ increases with frequency. Nevertheless, pulsed electrolysis presents lower average currents, $i_{total}$. At 2.2V, energy efficiency was almost the same for DC electrolysis and for 100ut pulsed electrolysis, indicating that further increase in $E_{on}$ could lead to a better efficiency for pulsed electrolysis. In addition, pulses at 10ut consume more power and produce less hydrogen (lower mean current) than 100ut pulses. As a consequence, they have lower energy efficiency. A possible reason for pulses with an off-time of 100ut to have a better efficiency than pulses with 10ut can be that in the former case there is sufficient time for the bubbles to detach from electrode surface.

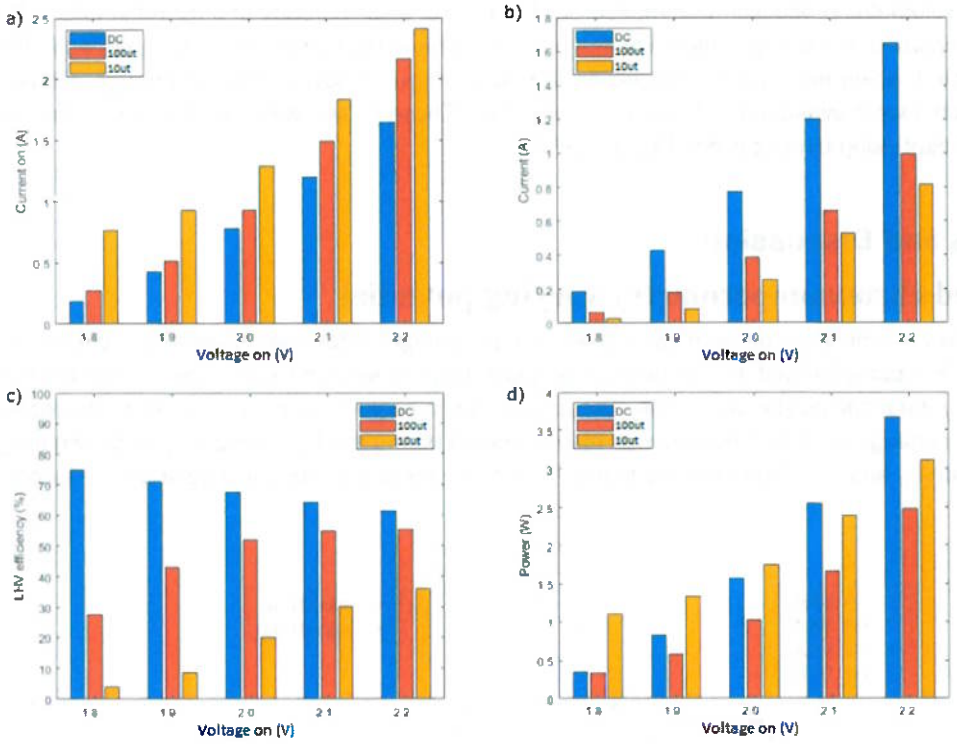


**Figure 3 – Results from pulsed chronoamperometry varying potential, C10A10: a) Mean values for on-current, $i_{on}$ (A); b) Mean current, $i_{total}$ (A); c) LHV efficiency; d) Power (W). DC (blue); 100ut (orange); 10ut (yellow)**

## 4.2 Pulsed chronoamperometry with fixed potential and hydrogen collection

Based on the results obtained in the previous experiment, an overpotential of 0.7V was chosen, since at lower overpotentials, the mean current was practically null, as can be seen in figure 2b. An overpotential of 0.7V means an $E_{on}$=1.93V.

To analyse the effects of the pulses, the case of C5A5 is presented. All the other cases have shown the same behaviour regarding pulses. The pulses presented a lower production rate than the DC case and the production rate decreased with the increase in the pulse frequency. The charge was calculated as the integral of current by time. Based on the measured hydrogen volume produced and the charge, the Faraday efficiency was calculated. It was close to 100% for all the cases. This indicates that non faradaic processes and other reactions are negligible and this result agrees with the literature Buttler & Spliethoff (2018).

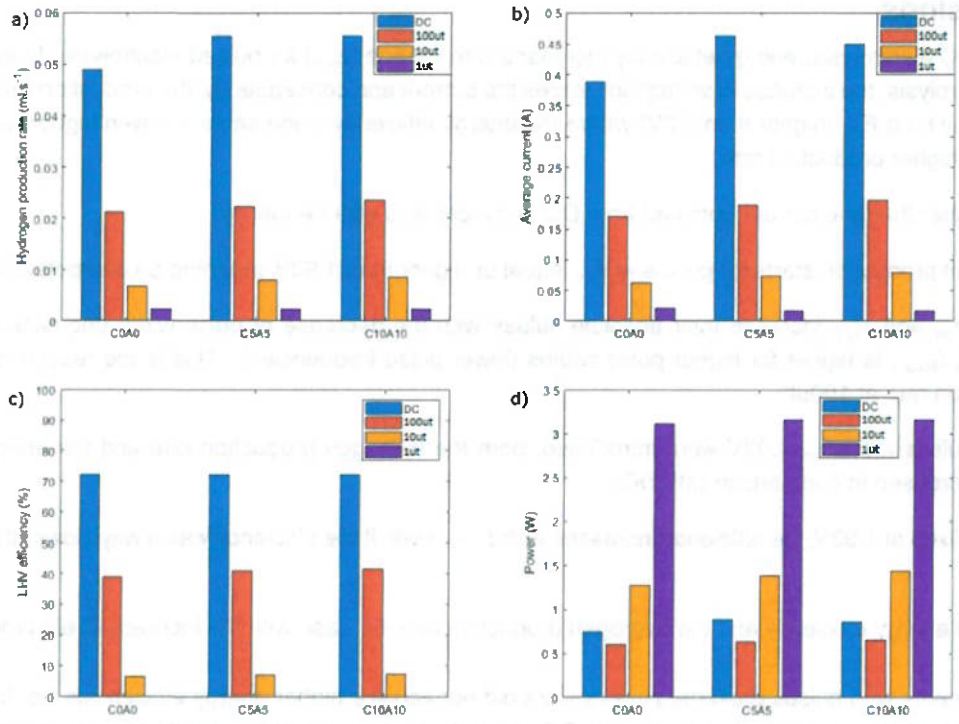


**Figure 4 – Results from pulsed chronoamperometry with fixed potential and hydrogen collection, C0A0, C5A5, and C10A10: a) hydrogen production rate; b) Average current (A); c) LHV efficiency d) Power (W)**

In the case of the energy efficiency, it was approximately 72.1%, 40.9%, 7.3%, and 0.2% for DC, 100ut, 10ut, and 1ut, respectively (figure 4c). The results for DC agrees with the literature. The decrease in efficiency when pulses are applied is a consequence of the power consumption when E=$E_{off}$. In this situation, the reaction goes backwards, consuming electricity and products. As a result, energetically, it was not favorable to introduce pulses. To avoid the negative currents produced when E=$E_{off}$, a diode could be placed in the system. However, the use of a diode will increase the $E_{off}$ and so, can cause other consequences in the electrolysis process. To sum up, it was not advantageous to introduce pulses, since the energetic efficiency and the production rate had been decreased.

Examining now the effects of a forced flux, one can see that it increases the hydrogen production rate and the average current, as shown in figure 4a and figure 4b, respectively, especially for DC. As observed previously, energy efficiency decreases with the introduction of pulses (figure 4c) and with their frequency. The effects of the forced flow were minor compared to the effects of the pulses. Nevertheless, energy efficiency slightly increases with the increase of forced flux, especially in pulsed electrolysis. For DC, the efficiency hardly changed, while for 100ut pulses, it went from 39.0% at natural convection to 41.6% at maximum flux. This change was from 6.7% to 7.6% at 10ut. At 1ut, energy efficiency has shown no significant variations with flow.

Concluding, the results presented here have shown that pulsed water electrolysis is a less efficient process and has lower production rate. The main cause of that is the high negative current when E=$E_{off}$, which cancels the effects of the higher $i_{on}$ current. Comparing the pulses, 100ut pulses presented the highest efficiency and the highest production rate. In addition, there is strong evidence that a further increase in $E_{on}$ would lead to an increase in energy efficiency.

# 5 Conclusions

1. Unlike DC electrolysis, energy efficiency increases with voltage ($E_{on}$) for pulsed electrolysis. In addition, as in DC electrolysis, the increase in voltage increases the current and consequently, the production rate. Therefore, there may be a $E_{on}$ (higher than 2.2V) where the energy efficiency is the same (or even higher) as that of DC, but with higher production rate;

2. $i_{on}$ is higher than the current obtained from DC and increases with frequency;

3. Hydrogen production starts for pulses at $E_{on}$ equal or higher than 1.93V, meaning an overpotential of 0.7V;

4. Even if $i_{on}$ and $i_{off}$ increase their absolute values with the decrease of pulse width (increase of pulse frequency), $i_{total}$, is higher for higher pulse widths (lower pulse frequencies). This is the reason for the higher production rate at 100ut;

5. When pulses with $E_{on}$=1.93V were introduced, both the hydrogen production rate and the energy efficiency were decreased in comparison with DC;

6. If $E_{on}$ is fixed at 1.93V, the efficiency increases with $E_{off}$, even if the efficiency was always lower than efficiency at DC;

7. Both the energy efficiency and the hydrogen production rate increase with the increase of electrolyte flow;

The experiments with pulses presented in this work did not achieve higher energy efficiencies nor hydrogen production rates. However, it reveals that contrary to DC electrolysis, the increase in voltage increases efficiency. As a result, further research will very probably achieve higher efficiencies and higher hydrogen production rates. In addition, this research was important to identify recommendations for further studies and to better understand the pulse behaviour, contributing to the pulse literature.

# 6 Bibliography

ATKINS, P., JONES, L. (2009). *Chemical principles*, Macmillan.

BUTTLER, A., SPLIETHOFF, H. (2018). Current status of water electrolysis for energy storage, grid balancing and sector coupling via power-to-gas and power-to-liquids: A review, *Renewable and Sustainable Energy Reviews* **82**: 2440–2454.

KOTHARI, R., BUDDHI, D., SAWHNEY, R. (2008). Comparison of environmental and economic aspects of various hydrogen production methods, *Renewable and Sustainable Energy Reviews* **12**(2): 553 – 563.
**URL:** *http://www.sciencedirect.com/science/article/pii/S1364032106001158*

LEE, J. D. (2008). *Concise inorganic chemistry*, John Wiley & Sons.

MARBÁN, G., VALDÉS-SOLÍS, T. (2007). Towards the hydrogen economy?, *International Journal of Hydrogen Energy* **32**(12): 1625 – 1637.
**URL:** *http://www.sciencedirect.com/science/article/pii/S0360319906006276*

ZENG, K., ZHANG, D. (2010). Recent progress in alkaline water electrolysis for hydrogen production and applications, *Progress in Energy and Combustion Science* **36**: 307–326.